

**LIBRARY
Michigan State
University**

This is to certify that the
thesis entitled

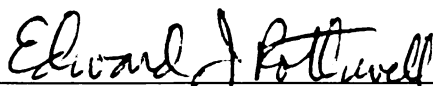
A SELF-STRUCTURING PATCH ANTENNA

presented by

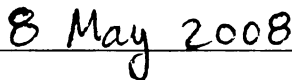
LYNN MARIE GREETIS

has been accepted towards fulfillment
of the requirements for the

Master of Science degree in Electrical and Computer Engineering



Major Professor's Signature



Date

PLACE IN RETURN BOX to remove this checkout from your record.
TO AVOID FINES return on or before date due.
MAY BE RECALLED with earlier due date if requested.

DATE DUE	DATE DUE	DATE DUE

A SELF-STRUCTURING PATCH ANTENNA

By

Lynn Marie Greetis

A THESIS

Submitted to

Michigan State University

in partial fulfillment of the requirements
for the degree of

MASTER OF SCIENCE

Electrical and Computer Engineering

2008

ABSTRACT

A SELF-STRUCTURING PATCH ANTENNA

By

Lynn Marie Greetis

This thesis introduces a new type of self-structuring antenna called the self-structuring patch antenna. The self-structuring patch antenna is a combination of the concepts of the self-structuring antenna with the geometry of a microstrip patch antenna. This is accomplished by inserting thirty-two shorting pins between the surface of the patch and the ground plane and connecting them to switches. When different combinations of these switches are turned on, the cavity field of the patch antenna is perturbed in an unpredictable way, which alters the performance characteristics of the antenna.

Results from simulations of the self-structuring patch antenna are presented. A genetic algorithm optimization is employed to efficiently search through the large number of possible switch combinations of the antenna. Both single-frequency operation and multiple-frequency operation are discussed.

Experimental measurements of a self-structuring patch antenna prototype are also presented. A discussion of the design and construction of the prototype is also included. Results from random state searches are shown, as well as results of genetic algorithm optimizations and a brief discussion of electromagnetic compatibility investigations.

Copyright by
Lynn Marie Greetis
2008

For Dante

ACKNOWLEDGMENTS

Were it not for the help of many people, this thesis never would have been completed. First, many thanks have to go to my thesis advisor, Dr. Edward J. Rothwell, for allowing me to work on this project. He has been a great friend and mentor during my time here at MSU. Thanks also are in order for Dr. Leo Kempel for supporting my studies my second year, and the team of Dr. Barbara O'Kelly and Dr. Percy Pierre for supporting me through the Sloan/Rigas program my first year.

I would also like to thank Raoul Ouedraogo for his unending help with Visual Basic code and Brian Greetis for all of his incredibly useful Python scripts for sorting through data. Without these two, I would still be going through text files line-by-line and setting switches by hand.

A thank-you is in order to my father, James P. Greetis, for laying out the antenna in AutoCAD. I also want to thank Brian Wright and the staff in the MSU ECE shop for all of their help with the antenna fabrication. Thank you also to Lori Wynants at Taconic for sending me a sample board that turned out to be exactly what I needed.

A big thanks is in order for Dr. John E. Ross, III for allowing me to use GA-FEKO for my simulations. He has always been willing to take the time to help me out when I have had a question. I would also like to thank Dr. Christopher Coleman for sending me the Matlab code to make Smith chart plots.

Most of all, I would like to thank my parents, Jim and Mariann, my brother Brian, and my fiancée Jon for their support throughout this process. Without you guys I would never be where I am today.

TABLE OF CONTENTS

LIST OF TABLES	viii
LIST OF FIGURES	ix
KEY TO SYMBOLS AND ABBREVIATIONS	xiv
CHAPTER 1	
Introduction	1
CHAPTER 2	
Background	2
2.1 History and background of the self-structuring antenna	2
2.2 Microstrip patch antennas	4
2.3 The self-structuring patch antenna	11
CHAPTER 3	
Simulation of the self-structuring patch antenna	13
3.1 Single-frequency operation	13
3.1.1 Genetic algorithm optimizations	14
3.1.2 Smith chart investigations	18
3.2 Multiple-frequency operation	21
3.3 Lower frequency simulations	25
CHAPTER 4	
Construction of a self-structuring antenna prototype and experimental results	57
4.1 Design and construction	57
4.2 Measurement of antenna voltage standing wave ratio	59
4.3 Random searches	62
4.4 Genetic algorithm optimizations	70
4.5 Electromagnetic compatibility investigations	77
CHAPTER 5	
Conclusions	151
APPENDIX A	
Visual Basic code: random searches of states of the self-structuring patch antenna	155
APPENDIX B	
Visual Basic code: genetic algorithm for the self-structuring patch antenna . . .	159

BIBLIOGRAPHY 171

LIST OF TABLES

Table 3.1	Pin locations given in sub-patch coordinates. Feed pin is placed at (6,1).	30
Table 3.2	Results of simulations of the self-structuring patch antenna. . . .	32
Table 4.1	Chromosomes for the best states found in the genetic algorithm searches.	142
Table 4.2	Bit-to-switch number reference chart.	143
Table 4.3	Results of random searches and the genetic algorithm optimizations for the self-structuring patch antenna prototype.	145

LIST OF FIGURES

Images in this thesis are presented in color.

Figure 2.1	A typical self-structuring antenna system.	12
Figure 3.1	Segmentation of the patch in FEKO.	28
Figure 3.2	Placement of shorting pins.	29
Figure 3.3	VSWR vs. frequency for the self-structuring patch antenna. . . .	31
Figure 3.4	Return loss for the traditional patch antenna resonant at 4.768 GHz.	33
Figure 3.5	Return loss for the self-structuring patch antenna optimized at 4.768 GHz.	34
Figure 3.6	Comparison of the return losses of the traditional patch antenna and the self-structuring patch antenna optimized at the same frequency.	35
Figure 3.7	Radiation pattern of the traditional patch antenna in the $y - z$ plane.	36
Figure 3.8	Radiation pattern of the self-structuring patch antenna in the $y - z$ plane.	37
Figure 3.9	Smith chart showing the impedances of 1000 random states at 2 GHz.	38
Figure 3.10	Smith chart showing the impedances of 1000 random states at 3 GHz.	39
Figure 3.11	Smith chart showing the impedances of 1000 random states at 3.5 GHz.	40
Figure 3.12	Smith chart showing the impedances of 1000 random states at 4.3 GHz.	41
Figure 3.13	Smith chart showing the impedances of 1000 random states at 5 GHz.	42
Figure 3.14	Smith chart showing the impedances of 1000 random states at 6.2 GHz.	43
Figure 3.15	Smith chart showing the impedances of 1000 random states at 7.4 GHz.	44
Figure 3.16	Smith chart showing the impedances of 1000 random states at 8 GHz.	45
Figure 3.17	Smith chart showing the impedances of 1000 random states at 9.2 GHz.	46
Figure 3.18	Return loss for the self-structuring patch antenna optimized at 5.0 GHz and 6.0 GHz.	47

Figure 3.19	Return loss for the self-structuring patch antenna optimized at 5.0 GHz and 5.2 GHz.	48
Figure 3.20	Return loss for the self-structuring patch antenna optimized at 5.0 GHz, 5.1 GHz, and 5.2 GHz.	49
Figure 3.21	Return loss for the self-structuring patch antenna optimized at 5.0 GHz, 5.2 GHz, and 5.4 GHz.	50
Figure 3.22	Return loss for the self-structuring patch antenna optimized at 4.8 GHz, 5.0 GHz, 5.2 GHz, and 5.4 GHz.	51
Figure 3.23	Return loss for the self-structuring patch antenna optimized at 3.0 GHz, 4.0 GHz, 5.0 GHz, and 6.0 GHz.	52
Figure 3.24	Return loss for the self-structuring patch antenna with no shorting pins with a 1.575 mm thick board.	53
Figure 3.25	Return loss for the self-structuring patch antenna with no shorting pins with a 3.175 mm thick board.	54
Figure 3.26	Return loss for the self-structuring patch antenna with no shorting pins with a 5.0 mm thick board.	55
Figure 3.27	Return loss for the self-structuring patch antenna optimized at 670 MHz.	56
Figure 4.1	Top of self-structuring antenna circuit board as laid out in AutoCAD. All dimensions given in inches.	80
Figure 4.2	Bottom of self-structuring antenna circuit board as laid out in AutoCAD. All dimensions given in inches.	81
Figure 4.3	Diagram of shorting pin connections.	82
Figure 4.4	Photograph of one of the switches on the self-structuring patch antenna.	83
Figure 4.5	Schematic of the control board.	84
Figure 4.6	Photograph of the surface of the self-structuring patch antenna.	85
Figure 4.7	Photograph of the ground plane of the self-structuring antenna with switches and control lines.	86
Figure 4.8	Photograph of the control board.	87
Figure 4.9	Return loss plot for the self-structuring patch antenna with all switches disconnected.	88
Figure 4.10	Block diagram of the experimental setup.	89
Figure 4.11	Photograph of the National Instruments ribbon cable splitting into a BNC cable and a 10-line ribbon cable.	90
Figure 4.12	Photograph of the connection between the two ribbon cables.	91

Figure 4.13	Photograph of the experimental setup.	92
Figure 4.14	Number of states per VSWR, showing all states with VSWR under 50 at 200 MHz.	93
Figure 4.15	Number of states per VSWR, showing all states with VSWR under 2 at 200 MHz.	94
Figure 4.16	Number of states per VSWR, showing all states with VSWR under 50 at 285 MHz.	95
Figure 4.17	Number of states per VSWR, showing all states with VSWR under 50 at 330 MHz.	96
Figure 4.18	Number of states per VSWR, showing all states at 380 MHz. . . .	97
Figure 4.19	Number of states per VSWR, showing all states at 400 MHz. . . .	98
Figure 4.20	Number of states per VSWR, showing all states with VSWR under 2 at 400 MHz.	99
Figure 4.21	Number of states per VSWR, showing all states with VSWR under 50 at 417 MHz.	100
Figure 4.22	Number of states per VSWR, showing all states with VSWR under 2 at 417 MHz.	101
Figure 4.23	Number of states per VSWR, showing all states with VSWR under 50 at 450 MHz.	102
Figure 4.24	Number of states per VSWR, showing all states with VSWR under 2 at 450 MHz.	103
Figure 4.25	Number of states per VSWR, showing all states with VSWR under 50 at 473 MHz.	104
Figure 4.26	Number of states per VSWR, showing all states with VSWR under 2 at 473 MHz.	105
Figure 4.27	Number of states per VSWR, showing all states with VSWR under 50 at 513 MHz.	106
Figure 4.28	Number of states per VSWR, showing all states with VSWR under 2 at 513 MHz.	107
Figure 4.29	Number of states per VSWR, showing all states with VSWR under 50 at 555 MHz.	108
Figure 4.30	Number of states per VSWR, showing all states with VSWR under 2 at 555 MHz.	109
Figure 4.31	Number of states per VSWR, showing all states at 597 MHz. . . .	110
Figure 4.32	Number of states per VSWR, showing all states with VSWR under 50 at 635 MHz.	111

Figure 4.33	Number of states per VSWR, showing all states with VSWR under 2 at 635 MHz.	112
Figure 4.34	Number of states per VSWR, showing all states with VSWR under 50 at 670 MHz.	113
Figure 4.35	Number of states per VSWR, showing all states with VSWR under 2 at 670 MHz.	114
Figure 4.36	Number of states per VSWR, showing all states at 695 MHz. . . .	115
Figure 4.37	Number of states per VSWR, showing all states with VSWR under 2 at 695 MHz.	116
Figure 4.38	Number of states per VSWR, showing all states at 715 MHz. . . .	117
Figure 4.39	Number of states per VSWR, showing all states with VSWR less than 50 at 770 MHz.	118
Figure 4.40	Number of states per VSWR, showing all states with VSWR less than 50 at 840 MHz.	119
Figure 4.41	Number of states per VSWR, showing all states with VSWR less than 50 at 900 MHz.	120
Figure 4.42	VSWR vs. frequency for all randomly searched states.	121
Figure 4.43	Sample proportion of states with a VSWR below 3 for each randomly searched frequency.	122
Figure 4.44	Sample proportion of states with a VSWR below 2 for each randomly searched frequency.	123
Figure 4.45	Sample proportion of states with a VSWR below 1.5 for each randomly searched frequency.	124
Figure 4.46	Proportion of states with a VSWR below 3 for each randomly searched frequency. Error bars are 95% confidence intervals.	125
Figure 4.47	Proportion of states with a VSWR below 2 for each randomly searched frequency. Error bars are 95% confidence intervals.	126
Figure 4.48	Proportion of states with a VSWR below 1.5 for each randomly searched frequency. Error bars are 95% confidence intervals.	127
Figure 4.49	Return loss for a state with VSWR of 1.0088 at 200 MHz.	128
Figure 4.50	Return loss for a state with VSWR of 2.588 at 285 MHz.	129
Figure 4.51	Return loss for a state with VSWR of 2.56 at 330 MHz.	130
Figure 4.52	Return loss for a state with VSWR of 7.06 at 380 MHz.	131
Figure 4.53	Return loss for a state with VSWR of 1.027 at 400 MHz.	132
Figure 4.54	Return loss for a state with VSWR of 1.013 at 417 MHz.	133
Figure 4.55	Return loss for a state with VSWR of 1.0076 at 450 MHz.	134

Figure 4.56	Return loss for a state with VSWR of 1.0186 at 473 MHz.	135
Figure 4.57	Return loss for a state with VSWR of 1.008 at 513 MHz.	136
Figure 4.58	Return loss for a state with VSWR of 1.0094 at 555 MHz.	137
Figure 4.59	Return loss for a state with VSWR of 1.443 at 597 MHz.	138
Figure 4.60	Return loss for a state with VSWR of 1.027 at 670 MHz.	139
Figure 4.61	Return loss for a state with VSWR of 1.0065 at 695 MHz.	140
Figure 4.62	Return loss for a state with VSWR of 1.59 at 715 MHz.	141
Figure 4.63	Switch numbers on the self-structuring antenna prototype.	144
Figure 4.64	Comparison of lowest VSWRs found in the random search and the genetic algorithm optimizations.	146
Figure 4.65	Block diagram of experimental setup for electromagnetic compati- bility testing.	147
Figure 4.66	Amplitude vs. Frequency of conducted emissions with switching frequency set to 150 Hz.	148
Figure 4.67	Amplitude vs. Frequency of conducted emissions with switches idle.	149
Figure 4.68	Amplitude vs. Frequency of conducted emissions with switching frequency set to 150 Hz and a 455 μ H blocking inductor in series with the ground wire.	150

KEY TO SYMBOLS AND ABBREVIATIONS

SSA: Self-Structuring Antenna

VSWR: Voltage Standing Wave Ratio

GA: Genetic Algorithm

WLAN: Wireless Local Area Network

MAX: Measurement and Automation Software

EMC: Electromagnetic Compatibility

CHAPTER 1

INTRODUCTION

This thesis introduces a new type of self-structuring antenna, the self-structuring patch antenna. Self-structuring antennas are a class of antennas with the ability to change their electrical configuration in response to environmental factors. Microstrip patch antennas are a widely used type of resonant antenna. The self-structuring patch antenna combines the concept of the self-structuring antenna with the geometry of a microstrip patch antenna.

A short history of the self-structuring antenna and a review of the research in both self-structuring antennas and microstrip patch antennas relevant to the self-structuring patch antenna is given in Chapter 2. Additionally, Chapter 2 includes a brief introduction to the self-structuring patch antenna.

Chapter 3 includes a discussion of the simulations that were run on the self-structuring patch antenna. This includes both single-frequency simulations and multiple-frequency simulations. Many of these simulations used a genetic algorithm optimization, though some random search simulations are also discussed.

The self-structuring patch antenna prototype is presented in Chapter 4. An overview of its design and construction is given, along with specifications about the experimental setup. The random searches that were run are detailed. The chapter concludes with a discussion of the genetic algorithm optimizations that were carried out for the antenna and a section on electromagnetic compatibility investigations.

Chapter 5 is the conclusion to this thesis. Possibilities for future research on the self-structuring patch antenna are discussed.

CHAPTER 2

BACKGROUND

The self-structuring patch antenna represents a union between the self-structuring antenna (SSA) and the traditional microstrip patch antenna. As such, a great deal of research has been done in both of these areas. A brief history of the self-structuring antenna is given in Section 2.1. Section 2.2 covers the previous research in the area of microstrip patch antennas that relates to the self-structuring patch antenna. Finally, a short overview of the self-structuring patch antenna is given in Section 2.3.

2.1 History and background of the self-structuring antenna

Self-structuring antennas are a class of antennas that have the ability to change their configuration in response to environmental factors [1]. This makes SSAs useful in a variety of situations where designing an antenna would traditionally be very difficult. The SSA was developed at Michigan State University (MSU) by Dr. Edward J. Rothwell in 1997, and U.S. Patent no. 6,175,723 was awarded to MSU in January of 2001. The work was then continued by Dr. Christopher Coleman for his Ph.D. dissertation [2] and by Dr. Bradley Perry for his M.S. thesis [3]. Dr. John Ross was also involved in the early SSA research, and was ultimately responsible for writing the genetic algorithm optimization program GA-FEKO (<http://www.johnross.com>) that has been essential to the success of the SSA. More recently, Joachim Jessberger and Raenita Fenner have continued SSA research at MSU.

Until recently, the SSA was only implemented on planar circuit boards [4],[5]. The original block diagram of the SSA is shown in Figure 2.1 [2]. N switches are placed on the circuit board and connected by wires. These switches are also connected to a microcontroller, or a computer, that can optimize a certain operational parameter, such as voltage standing wave ratio (VSWR), input impedance, received signal strength,

or any other fitting parameter. A receiver is then used to measure the chosen operational parameter of the SSA in a given state. Since each switch can be either open or closed, there are 2^N possible states, or configurations of switches. The switches and wires were arranged on the original SSA template in such a way as to eliminate repeated states, thereby maximizing the number of possible states for the antenna. The number of states can quickly become very large, so an intelligent algorithm such as simulated annealing, ant colony optimization, or a genetic algorithm is used to search through the possible states [6],[7]. The SSA is different from other types of antennas because the performance parameters of the system are unknown at the time of the antenna design.

Extensive research has been done in the past on a variety of topics relating to the SSA. One of the original applications for the SSA was as an automobile antenna [8],[9]. The SSA is a natural choice for a vehicle because of its ability to adapt to its surroundings, since a vehicle's environment is constantly changing. It also has the potential to replace the numerous antennas currently in use on any given vehicle with its ability to operate at several different frequencies. Since the SSA has many switches, studies were also done to determine the effects of switch failures [10],[11]. Depending on the location of the failed switch, the SSA is able to compensate to varying degrees for a switch failure. The closer that the failed switch is to the antenna feed, the more impact this switch failure has on overall performance. The SSA was also considered for use as a television antenna [12].

In 2005, Joachim Jessberger investigated the near-field properties of the self-structuring antenna [13]. His work was done to find out if the near-zone electric field could be concentrated into a small region using the SSA. He found that the field could be concentrated in certain cases. In 2007, Raenita Fenner developed a new type of SSA that was to function as a body-worn antenna vest [14]. This was the first time that the SSA left its planar circuit board. She found that incorporating the SSA into

a vest was a good choice for a body-worn antenna due to its ability to work at many different frequencies. This gave the antenna vest a very broad range of frequencies that it was able to be used at, which made it very useful for the military application for which it was intended. The SSA has come a long way since its inception in 1997, and SSA research continues at Michigan State University to find new types and applications of the SSA.

2.2 Microstrip patch antennas

Microstrip patch antennas have been in existence for nearly half a century. It would seem that the first patch antenna was introduced by Watkins in 1969 [15]. This first patch antenna was simply a circular conducting disk suspended over a ground plane. Watkins analytically derived the radiated fields of this resonant structure. He also calculated the Q of the dominant resonant mode of the disk and found it to be very high due to the low dissipation losses of the system, which leads to low bandwidths.

The patch antenna next made an appearance in a paper presented by Howell at the IEEE Group on Antennas and Propagation International Symposium in December of 1972 [16]. This paper investigated microstrip-fed rectangular patch antennas and found that the fundamental resonant frequency of the patch is primarily determined by the length of the side of the patch that is parallel to the microstrip feed line. Howell was the first to mention that patch antennas are analytically similar to cavities, where the patch antenna has magnetic walls at the edges of the patch. Like a cavity, his patch had a very low bandwidth: less than 1% at 1.727 GHz. Howell followed with a journal paper in 1975 [17]. In this paper, he again discussed edge-fed patches but also expanded his discussion to probe-fed patches. He was quick to recognize how useful patch antennas could be due to their ease of construction, low cost, low profile, and durability. Howell was also the first to develop equations to predict the fundamental

resonant frequency of a patch. For square and rectangular patches,

$$f_0 = \frac{c}{2d\sqrt{\epsilon_r}} \quad (2.1)$$

where d is “the distance from the feed point to the opposite side of the antenna” [17].

For a circular patch,

$$f_0 = \frac{1.841c}{2a\pi\sqrt{\epsilon_r}} \quad (2.2)$$

where a is the radius of the circular patch. In addition to his theoretical analysis, he also measured the resonant frequencies of several patches, and found these patches to have resonant frequencies ranging from 378 MHz to 6.04 GHz. In each case, Howell found the measured resonant frequencies to be slightly lower than the resonant frequencies predicted by (2.1) and (2.2). He continued to see low bandwidths, with 3:1 VSWR bandwidths ranging from 0.9% up to 3.5%.

With his paper in 1979, Lo and his colleagues at the University of Illinois Electromagnetics Laboratory soon moved to the forefront of patch antenna research [18]. They were the first to develop the cavity model for patch antenna analysis. The cavity model assumes that the field structure of the patch is similar to that of a cavity, and from this one can compute input admittance, radiation pattern, and radiated power at any feed point. In their paper, wavefunctions are developed for many different patch antenna geometries: rectangular, circular, wedge-shaped, circular with a slot, triangular, circular rings, circular ring segments, and elliptical. In addition to these wavefunctions, they analytically derive the fields for a rectangular edge-fed patch by both expansion of resonant modes and modal matching. They then use Huygen’s principle to calculate the radiated power and input impedance. Furthermore, these theoretical predictions are then compared to measured results, and the two show good agreement. Lo’s paper represented the most comprehensive study into microstrip patch antennas to that date.

While this early research into patch antennas discovered many useful characteristics, it also uncovered some shortcomings. The most notable of these are the patch antenna's single-frequency operation and small bandwidth, and it was only a matter of time before research moved toward making up for these shortcomings. Researchers found many ways to tackle these problems, but only those papers where shorting posts were used will be covered in this thesis. The first to use shorting posts were Schaubert et al. in 1981 [19]. By adding shorting posts along the centerline of the long dimension of a rectangular probe-fed patch, the operating frequency could be tuned and the polarization could be changed. Adding two posts gave a frequency tuning range of approximately 20%. Adding more posts can give a greater tuning range, up to 50%. Schaubert and his colleagues only added posts along the centerlines of the patch. Adding these posts did not significantly change the radiation patterns of the patches, and bandwidths remain near 1% regardless of operating frequency. This represented the first time that a patch antenna could be tuned without changing the size of the patch or the feed location, but this patch antenna still could only operate at one frequency at a time.

By 1983 Lo and his colleagues had found a way to use a single patch antenna to achieve dual-band operation, once again using shorting posts [20]. By placing these shorting posts at fixed locations on the patch, they were able to excite two different resonant modes of the patch. Between one and six shorting posts were used, with more shorting posts moving the two frequencies of operation closer together. Low-band frequencies ranged from 613 MHz and 891 MHz, with a 3:1 VSWR bandwidth of 2%, while high-band frequencies were between 1861 MHz and 1874 MHz, with a 3:1 VSWR bandwidth of 8%. At the time, this was as close together as the low-band and high-band frequencies could get.

In order to move the two frequencies of operation even closer together, in 1984 Lo et al. added a slot to the patch with shorting posts where the magnetic field

of the higher-order mode had a maximum [21]. This served to lower the high-band frequency. Again using the cavity model, they derived the fields for a probe-fed patch with a slot. To calculate the input impedance and radiation patterns of this patch, the patch is treated as a two-port network. The probe is one port and is fed with an electric current. The slot is the second port and is fed with a magnetic current. By using this approach, the Z-parameters of this network can be calculated. Lo and his colleagues found that their experimental results matched up very well with this theory, where in general the shorting posts raise the low-band frequency and the slot lowers the high-band frequency. The radiation patterns of these patches are not significantly affected by either the shorting posts or the slot. By using up to six posts and up to three slots, the ratio of the high-band center frequency to the low-band center frequency can be varied between 3.02 and 1.31.

In 1985, Lan and Sengupta applied the concepts from Schaubert's earlier paper to probe-fed circular patches [22]. They developed a transmission-line theory for analyzing the patch, where the shorting posts were treated as purely inductive impedance loads. The authors used up to four shorting posts to create his frequency-tunable patch. They found that in general, the patch's frequency of operation increases as the shorting posts are moved closer to the edge of the patch.

By 1995, trends in technology had started to move toward miniaturization, and patch antennas were not immune to this revolution. Due to their resonant structure, patch antenna dimensions could approach half a wavelength, which at low frequencies can quickly become very large. Waterhouse used a single shorting post on a probe-fed circular patch in order to attempt to reduce the size of the patch [23]. He first designed a patch with a radius of $0.14\lambda_0$, but without a shorting post. By adding a shorting post, the patch radius was reduced to $0.047\lambda_0$, while maintaining the same frequency of operation. The smaller patch did suffer a small reduction in bandwidth, down to 1.2% from 1.8%.

Another widely used form of the patch antenna is the cavity-backed patch antenna. In 1996, Zavosh and Aberle investigated multiple ways to improve the shortcomings of these cavity-backed patches [24]. The authors used high-permittivity superstrates (layers of dielectric above the surface of the patch) to achieve frequency agility. By changing ϵ_r from 1.006 to 20, the frequency of operation drops from 3.6 GHz all the way down to less than 1.5 GHz. However, as the relative permittivity is increased, the bandwidth decreases. Using shorting posts to improve the performance of the cavity-backed patch is also discussed. As the number of posts is increased (up to six shorting posts), the frequency of operation can be varied from 2.6 GHz up to 3.6 GHz. These posts can also be used to widen the bandwidth. By adding these shorting posts, bandwidth was improved on one antenna from 6.7% to 10%. Another way the authors present to rectify the bandwidth issues is to use a stacked-patch structure. For a single patch, bandwidths are near 3%, while the stacked patches give a bandwidth near 15%. To achieve this wide bandwidth, the stacked patches are designed in such a way that their two resonances are very close together, and start to merge into one resonance. The authors note that if the sizes of the stacked patches were changed, this structure could be used for a dual-mode patch with two separate resonances rather than a single combined resonance.

Bandwidth enhancement investigations continued with Waterhouse et al.'s paper in 1998 [25]. This paper compared circular patch antennas with different numbers of shorting posts. With one post, the bandwidth of the patch was 6.8%, while with two posts the bandwidth was 7.9%. In both of these cases the shorting posts were close together and close to the feed of the antenna. If the two shorting posts were moved farther apart, bandwidth could be improved to 10%. However, each of these improvements in bandwidth came at the cost of a larger antenna size.

More investigations into dual-mode patches were done by Chakravarty and De in 1999 [26]. They analytically derived fields for a circular probe-fed patch where

shorting posts were arranged on a circle concentric with the edge of the patch. Two theories were developed: symmetric, where the posts were evenly spaced around the circle, and asymmetric, where they were not. The symmetrically loaded antenna was used for frequency-tunable modes, where up to four shorting posts were used to excite different modes of the antenna. The asymmetrically loaded antenna was used for dual-band operation. Only one shorting post was used, and the authors were able to achieve a ratio of the high-band center frequency to the low-band center frequency as low as 1.05.

By 2000, research in patch antennas was starting to move toward antennas that had novel shapes. The first of these papers was by Kan and Waterhouse [27]. Their patch had a single shorting post and “wings,” where the intent of these wings was to reduce the size of the antenna. An advantage of this geometry is that it is not necessary for the shorting post to be in close proximity to the feed, as in previous cases. By adding the wings, the overall size of the antenna was reduced by a factor of 26, making it a suitable size for cell phone applications. However, these modifications did reduce the bandwidth to 6.9%, down from 10% for a standard rectangular edge-fed patch at the same frequency.

In 2001, Zhao and Raman used shorting posts and a GaAs substrate to reduce patch size down to a size feasible for wireless local area network (WLAN) applications [28]. The gallium arsenide (GaAs) substrate has an ϵ_r of 12.9, and the shorting posts are all arranged along one edge of the square patch. These modifications reduced the patch size from 53 mm on a side to 3.72 mm on a side. The bandwidth of this patch is only 1-2% and the radiation efficiency is also low, but the authors state that for short-range, low-power communications, this may be acceptable performance for WLAN.

Also in 2001, Shackleford et al. developed a square probe-fed patch with one shorting post and two triangular notches [29]. These serve to reduce the patch size

by about 75%. By changing the dimensions of these two identically sized notches, dual-band performance can be achieved and bandwidths can also be varied. In this paper, the low-band resonance occurs between 472 MHz and 530 MHz, and the high-band resonance between 1.02 GHz and 1.31 GHz. For single-band operation, bandwidth was 13.2%, and for dual-band operation, bandwidths varied between 6.1% and 9.6%.

In 2005, Fang et al. developed a dual-band patch for use with WLAN applications [30]. This circular patch had arc-shaped slots cut into it along with a single shorting post. By adding pairs of slots (up to eight slots total), they were able to achieve bandwidths of 5% at 2.44 GHz and 3.9% at 5.3 GHz, which are acceptable bandwidths for WLAN applications.

Kan and his colleagues also used slots in a patch antenna in a 2005 conference paper [31]. Their antenna was a rectangular probe-fed antenna with eight large slots cut into it and one shorting post placed close to the feed. The measured bandwidth for this antenna was 8.1%, though the authors note that this large bandwidth may be due to the fact that the ground plane only extends 1 mm beyond the edges of the patch on all sides. The authors also investigate a dual-frequency stacked patch, where the low-frequency antenna is stacked on top of the high-frequency antenna with a layer of foam in between. The high-frequency layer of stacked patch is the antenna with the large slots, where the low-frequency layer of the patch is an antenna shaped more like a rectangular ring. Both antennas have shorting posts connecting them to the ground plane. The antennas have fairly low bandwidths, 1.6% at 1.8 GHz and 2% at 2.6 GHz.

In 2006, Bonefacic et al. developed the first patch antenna that can electronically switch between two bands [32]. This pin-fed rectangular patch had a shorting wall along one edge and four shorting posts. These shorting posts are connected to the ground plane using PIN diode switches. When the PIN diodes are reverse biased, the patch operates at 2 GHz. When the PIN diodes are forward biased, the patch operates

at 4 GHz. This patch represents the first dual-band patch that can electronically switch between the two bands without altering the geometry of the patch in any way.

Patch antenna research has come a long way since patches were first introduced in 1969. From multiple-frequency operation to miniaturization, patch antennas have proven to be far more versatile than they first appeared to be.

2.3 The self-structuring patch antenna

The self-structuring patch antenna is a combination of the concepts of the original SSA with the geometry of a microstrip patch antenna. An array of shorting pins is added to the traditional patch antenna. These shorting pins, unlike the posts mentioned in the research above, are not static. Rather, they are connected to switches, and each can be in one of two states: closed, where the pin connects the ground plane to the surface of the patch, or open, where the pin does not connect the ground plane to the surface of the patch. These shorting pins connected to the switches serve the purpose that the switches alone did in the original SSA.

Like the original SSA, the pins are arranged on the patch in such a way as to minimize repeated states. When one of the shorting pins connects the surface of the patch to the ground plane, it perturbs the cavity field of the patch antenna in an unexpected manner. By opening and closing different combinations of shorting pins, the field can be perturbed in many different ways, leading to many different states. As with the SSA, for N shorting pins there will be 2^N states of the antenna. Simulation and experimental results for the self-structuring patch antenna are presented in the following chapters.

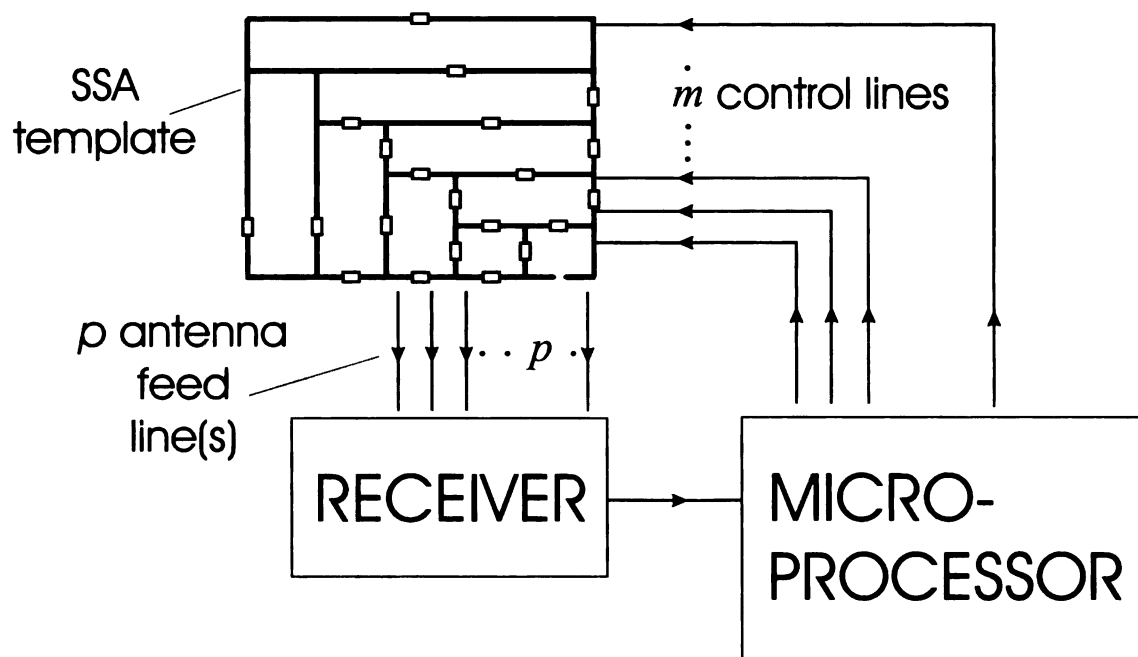


Figure 2.1. A typical self-structuring antenna system.

CHAPTER 3

SIMULATION OF THE SELF-STRUCTURING PATCH ANTENNA

This chapter details the simulations that were run for the self-structuring patch antenna. All simulations in this chapter were done using the electromagnetic simulation program FEKO [33] and the genetic algorithm optimizer GA-FEKO (<http://www.johnross.com>). Section 3.1 discusses simulations where the antenna was optimized for one frequency at a time, as well as presenting some Smith charts for random searches at the same frequencies. Multiple-frequency operation is examined in Section 3.2. In Section 3.3, a larger patch that is designed to work at lower frequencies is discussed. A Dell Dimension 8500 desktop computer with a 2.4 GHz Pentium 4 processor and 1 GB of RAM was used to run all simulations in this chapter.

3.1 Single-frequency operation

The first simulations that were run on the self-structuring patch antenna were to optimize the voltage standing wave ratio (VSWR) of the antenna at one frequency at a time. The dimensions of the simulated antenna are 46 mm (x -direction) by 30 mm (y -direction), with a substrate thickness of 2.87 mm and a relative permittivity of 2.2. This size was chosen to be the same size as a patch used in a FEKO example that was resonant near 3 GHz. For these simulations, the maximum length of a triangle edge was set to $\lambda/10$, where λ is calculated from

$$\lambda = \frac{c}{f\sqrt{\epsilon_r}}. \quad (3.1)$$

The maximum wire segment length was also set to $\lambda/10$. A picture of the segmentation of the patch at 5 GHz is shown in Figure 3.1.

To set up the simulation of the self-structuring patch antenna in FEKO, the patch

was first manually divided into sub-patches. The x -direction of the patch was divided into 12 sub-patches and the y -direction of the patch was divided into 7 sub-patches. This gives each sub-patch dimensions of 3.833 mm by 4.286 mm. As the simulation frequency increased, FEKO would divide these sub-patches into smaller and smaller triangles for segmentation purposes. Thirty-two shorting pins were then arranged on the patch as shown in Figure 3.2, where each pin is placed at a corner where four sub-patches meet. The pins are arranged on the patch in such a way as to eliminate repeated states. The exact locations of the pins, given in sub-patch coordinates, are given in Table 3.1. Since the shorting pins are a binary system, they provide 2^{32} or 4.3 billion possible states for the antenna. The shorting pins are modeled as wire segments between the top surface of the patch and the ground plane. When a switch is closed, the wire segment has a length that is the same as the height of the dielectric layer, effectively shorting the surface of the patch and the ground plane together. When a switch is open, the wire segment has a length 0.1 mm shorter than the height of the dielectric, and therefore does not have the shorting effect. The self-structuring patch antenna was simulated in FEKO with all of the switches open and was found to have fundamental resonant frequencies of 3.06 GHz and 4.12 GHz.

3.1.1 Genetic algorithm optimizations

Due to the large number of states, running an exhaustive or random search to find a state with the desired operation parameters could be very time-consuming and inefficient. For this reason, the genetic algorithm optimization program GA-FEKO was used to optimize the VSWR of the antenna. Genetic algorithms are a set of evolutionary algorithms that mimic the behavior of a population of organisms in nature. The program was run to determine if a state exists with a VSWR less than 1.1 (relative to 50 ohms). The genetic algorithm parameters were set as follows: population size was set at 70 members, with a crossover probability of 0.7, a mutation probability of 0.01, and a generation gap of 0.95. These parameters were kept the

same for all simulations discussed in this thesis. The program was set to run for a maximum of 200 generations, after which it would stop if the VSWR did not meet the target optimization value. When the program ran for the maximum number of generations, run times were typically about 36 hours. Higher frequencies required longer run times due to the smaller triangle size that had to be used in FEKO, with one simulation that reached 200 generations without finding a state with VSWR less than 1.1 taking nine days to complete. If a state was found with a VSWR of less than 1.1, the optimization program would stop. This does not necessarily mean that states with lower VSWRs do not exist. To find a state with a lower VSWR, one could simply change the target optimization parameter to a lower VSWR value. However, the lower the VSWR target optimization value that is chosen, the longer the run time of the simulations are.

Nine optimization frequencies were arbitrarily chosen between 2 GHz and 9.2 GHz and simulated one frequency at a time. Below 2 GHz and above 9.2 GHz, GA-FEKO failed to find a state with a VSWR below 1.1 after 200 generations. The lowest VSWR at 1 GHz was 51, and at 10.6 GHz the lowest VSWR after 200 generations was 1.34. The frequencies chosen were 2.0 GHz, 3.0 GHz, 3.5 GHz, 4.3 GHz, 5.0 GHz, 6.2 GHz, 7.4 GHz, 8.0 GHz, and 9.2 GHz. At each frequency a state with a VSWR of no larger than 1.087 was found, as shown in Figure 3.3. This corresponds to a return loss of at least -28 dB. However, this does not represent the lower limit of the VSWR for the self-structuring patch antenna. In this frequency range, VSWR values as low as 1.002 were found using GA-FEKO's genetic algorithm optimization.

Since microstrip patch antennas traditionally have a very narrow bandwidth, the -10 dB ($\text{VSWR} = 2$) bandwidth was calculated for each frequency simulated above. To do this, the antenna state was fixed and FEKO was used to find the VSWR across a band centered on the resonant frequency. Table 3.2 shows the VSWR, return loss, bandwidths, and input impedances for the above frequencies. While the bandwidth in

GHz goes up as the frequency goes up, the percentage bandwidth remains relatively constant at each of the nine frequencies. When the self-structuring patch antenna is operating below one of its natural resonant frequencies of 3.06 GHz, the percentage bandwidth is lower than when the antenna is operating at higher frequencies. The percentage bandwidth begins to drop again when the self-structuring patch antenna is operating at frequencies much higher than its natural resonant frequency.

To compare the performance of the self-structuring patch antenna to that of a traditional microstrip patch antenna, a traditional patch antenna was designed to operate at 5 GHz. The antenna was chosen to be a square patch, with dimensions given by

$$L = \frac{0.49\lambda}{\sqrt{\epsilon_r}} \quad (3.2)$$

where L is the length of one side of the patch [34]. For a relative permittivity of 2.2 and a center frequency of 5.0 GHz, (3.2) gives the patch dimensions of 19.8 mm by 19.8 mm. The feed pin was placed 6.6 mm from the left edge of the antenna and 6.6 mm from the bottom edge of the antenna. The height of the dielectric layer is the same as the self-structuring patch antenna described previously in this chapter. When the traditional patch antenna was simulated in FEKO, it was found to have a fundamental resonance at 4.768 GHz, with a return loss of -33 dB. This corresponds to a VSWR of 1.05. The fact that the simulated resonant frequency is slightly lower than the resonant frequency predicted by (3.2) is consistent with Howell's findings in his original journal paper [17]. The return loss for the traditional patch antenna is shown in Figure 3.4. From this plot, one can see that the traditional patch antenna has a bandwidth of 0.26 GHz (5.5%). This bandwidth is consistent with or even slightly greater than the bandwidths of traditional patch antennas examined earlier in this thesis [17],[18].

GA-FEKO was then run to optimize the VSWR of the self-structuring patch

antenna with the frequency set to 4.768 GHz. The optimization VSWR was set to 1.001 to push GA-FEKO to find a state with a very low reflection coefficient. A state was found with a VSWR of 1.001, which is equivalent to a return loss of -52 dB. The return loss of the self-structuring patch antenna as a function of frequency is shown in Figure 3.5. The bandwidth is 0.15 GHz (3.1%). From the return loss plots one can see that the self-structuring patch antenna is capable of achieving a better VSWR value at this particular frequency than the traditional microstrip patch antenna, though the percentage bandwidth is decreased by almost a factor of two. A direct comparison of the return losses is shown in Figure 3.6. The return loss of the traditional patch antenna is shown by the dashed line, and the return loss of the self-structuring patch antenna is shown by the solid line. The self-structuring patch clearly achieves a better return loss, but this comes at the price of lower bandwidth. However, the bandwidth of the self-structuring patch antenna is not terribly low when compared to other traditional patch antennas presented earlier in this thesis.

A brief comparison of the far-field radiation patterns of the traditional and self-structuring patch antennas was also carried out. All patterns shown here are in the $y - z$ plane, where y corresponds to the direction along the short dimension of the self-structuring patch antenna and the right and left edges of the traditional patch antenna. The radiation pattern of the traditional patch antenna is well-known [34]. It is very symmetric and appears nearly circular, with nulls in the plane of the patch. The antenna simulated here shows the expected pattern, as shown in Figure 3.7. The radiation pattern of the self-structuring patch antenna optimized at 4.768 GHz shown in Figure 3.8 shows no significant departure from the radiation pattern of the traditional patch antenna operating at the same frequency.

The self-structuring patch antenna has shown capability of operating over a greater than 4:1 frequency range for single-frequency operation, as well as operating below its fundamental resonant frequency. At the frequency of comparison, the self-structuring

patch antenna was able to achieve a lower VSWR value than the traditional patch antenna, while maintaining an acceptable bandwidth and a radiation pattern that is not markedly different than the radiation pattern of the traditional patch antenna.

3.1.2 Smith chart investigations

In addition to using the genetic algorithm to find a state with an optimized VSWR, additional simulations were run to see the distribution of impedances of antenna states on a Smith chart. GA-FEKO was still used, but instead of using its genetic algorithm, the initial population size was set to 1000 members and only this initial population was run. This essentially evaluates 1000 random states of the antenna. The frequencies at which these 1000 random states were evaluated are the same nine frequencies at which the genetic algorithm optimization was run.

The first frequency investigated was 2 GHz. The Smith chart for these states is shown in Figure 3.9. At this frequency there are no states anywhere near an impedance of 50Ω . Most of the states are clustered at the very top of the Smith chart, with very low resistance values and inductive reactance values in the range of 25 to 50Ω . GA-FEKO found a state with a VSWR value of 1.037 after 34 generations. It is not surprising that it took the genetic algorithm this long to find a good state with the absence of any good states in these 1000 random looks.

Figure 3.10 shows the Smith chart for states at 3 GHz. At this frequency, the states are clustered at the top of the Smith chart. For the most part, these states have very low resistances and moderately high inductive reactances. The few states that do have a capacitive reactance show a higher resistance. While there are no states with an impedance very close to 50Ω in the center of the Smith chart, GA-FEKO was able to find a state with a VSWR of 1.087 after only 8 generations.

The Smith chart for states at 3.5 GHz is shown in Figure 3.11. Like the previous frequency, there are many states clumped near the top of the Smith chart. Once again, these states have low resistances, but even higher inductive reactances than

the previous frequency. However, unlike the previous frequency, we now see several states with impedances very near to 50Ω in the center of the Smith chart. There are also many more states with higher resistance values. Interestingly, even though it would appear there are more good states at this frequency, it took GA-FEKO 20 generations to find a state with a VSWR of 1.082.

Figure 3.12 shows the Smith chart for the states at 4.3 GHz. At this frequency, the states are scattered over a much wider area of the Smith chart. Generally, the states still have high inductive reactance values, but they are spread over a larger range of resistances. There appear to be a good number of states with impedances near 50Ω in the center of the Smith chart. This was verified by GA-FEKO, as it found a state with a VSWR of 1.079 after only 4 generations.

The Smith chart for states at 5 GHz is shown in Figure 3.13. The impedances seem to cluster near the upper right corner of the chart, but there are still many good states near 50Ω in the center of the Smith chart. This shows that the states continue to have high inductive reactance over a spread of resistance values. When GA-FEKO was run at this frequency, it was able to find a state with a VSWR of 1.058 in only 3 generations. This makes sense since one would assume if more states were plotted on this Smith chart, there would be even more states clustered around 50Ω .

Figure 3.14 shows the Smith chart for the 1000 random states run at 6.2 GHz. This Smith chart looks very similar to the one at 5 GHz. States are again somewhat concentrated in the upper right corner of the chart. However, these states appear to be almost evenly spread over resistance and inductive reactance values. There are no states with the low resistances that we saw at lower frequencies. GA-FEKO found a member with a VSWR of 1.054 in the first generation when it was run. Again, seeing the large number of states near 50Ω in the center of the Smith chart, this makes sense.

The Smith chart for states at 7.4 GHz, shown in Figure 3.15, looks considerably different than previous frequencies. Here we see a strong tendency of the states to

clump together in the upper right region of the chart. These states are often quite close to a 50Ω resistance, but have very high inductive reactance values. There are no states at this frequency with a capacitive reactance. Surprisingly, even with the very few states near 50Ω at the center of the Smith chart, GA-FEKO found a state with a VSWR of 1.087 in 13 generations.

Like the Smith chart for 7.4 GHz, the Smith chart for states at 8 GHz shows the same clumping tendency, as shown in Figure 3.16. While the states are not as closely clumped, they are still much closer together than at lower frequencies. These states have moved away from the 50Ω resistance value that we saw at the previous frequency and are now closer to 100Ω . Again we see very few states near the center of the Smith chart. When GA-FEKO was run at this frequency, a state with a VSWR of 1.078 was found after 21 generations.

Figure 3.17 shows the Smith chart for states at 9.2 GHz. These states are still clumped, though not nearly as closely as for some lower frequencies. Nearly all of these states have a high resistance value and a low reactance value. However, unlike previous frequencies, there are an almost equal number of capacitive reactances as there are inductive reactances. In fact, many of these states have reactances very close to zero. On the chart we can see that there is only one state with an impedance very close to 50Ω in the center of the Smith chart. When GA-FEKO was run at this frequency, it found a state with a VSWR of 1.061 after 8 generations.

While these Smith charts show a lot of useful information about the distribution of impedances at a particular frequency, there are only 1000 points plotted on each chart. The reason that only 1000 points are plotted is simply because the higher frequency simulations were taking too much time (over 26 hours for the 1000 points). If more points were plotted, the likelihood of finding more states with impedances near 50Ω would increase. However, the states would most likely still exhibit the same clumping tendencies that the plots with 1000 points show. These Smith charts are a

good tool to show how useful the genetic algorithm is. Each of the charts shows 1000 random states of the antenna. Since the population size in GA-FEKO was set to 70, and for most of the frequencies discussed above less than 15 generations were needed to find a good state, the genetic algorithm usually looked at less than 1000 states. When compared with the fact that on the Smith charts, there are very few states with low VSWRs, it shows how efficient a search method using a genetic algorithm can be.

3.2 Multiple-frequency operation

The self-structuring patch antenna also has the ability to operate at multiple frequencies at once. As many as four frequencies at a time have been simulated. The simulated antenna in this section has the same dimensions and characteristics as the antenna simulated for single-frequency operation, and all genetic algorithm parameters were kept the same except the target VSWR value. Typical run times of multiple-frequency simulations were much longer than single-frequency simulations, with the shortest run times around 48 hours and the longest taking up to six days. Run times increased as the number of operation frequencies was increased.

The first multiple-frequency simulations were done to optimize the self-structuring patch antenna at two frequencies at a time. The first frequencies picked were 5.0 GHz and 6.0 GHz. The optimization VSWR in GA-FEKO was set to 2.2. This VSWR was chosen because for multiple-frequency simulations, GA-FEKO adds together the VSWR value from each frequency of interest to come up with one total VSWR for all frequencies. Unlike the single-frequency optimization, this does not necessarily make it possible for each state to have a VSWR of less than 1.1. A state was found with a VSWR of 1.09 at 5.0 GHz and 1.13 at 6.0 GHz. These correspond to return losses of -27 dB and -24 dB, respectively. The return loss plot for these two optimization frequencies is shown in Figure 3.18, clearly showing two resonances. The -10 dB

bandwidth at 5.0 GHz is 0.31 GHz (6.2%), and the bandwidth at 6.0 GHz is 0.18 GHz (3.0%).

Compared to other dual-mode patches discussed earlier in this thesis, these two bandwidths fall somewhere in the middle. They are greater than the bandwidths achieved by Lo and his colleagues [20], whose 3:1 VSWR bandwidths were between 2% and 8%. The bandwidth of the dual-mode self-structuring antenna is less than the bandwidth seen by both Zavosh and Aberle [24] (10%) and Waterhouse et al. [25] (between 6.8% and 10%). However, this may be due to several key differences between the antennas. Zavosh and Aberle's antenna was a cavity-backed patch, and Waterhouse et al.'s antenna was a circular patch. Both sets of researchers were also using far fewer shorting posts than were used with the self-structuring patch antenna. Zavosh and Aberle used up to six posts while Waterhouse et al. only used two. Since the shorting posts perturb the cavity field of the patch antenna in unexpected ways, this may be contributing to the loss of bandwidth for the self-structuring patch antenna.

More bandwidth comparisons can be made between the self-structuring patch antenna and other patch antennas mentioned in Chapter 2 with unusual geometries. Shackelford et al.'s notched patch antenna [29] had dual-band bandwidths of between 6.1% and 9.6%, which are certainly greater than the self-structuring patch antenna's 3.0% and 6.2%. No return loss information was provided in that paper, so no comparisons between return losses can be drawn. Fang et al.'s patch with arc-shaped slots cut into it [30] had bandwidths of 3.9% and 5%, which are very similar to those of the self-structuring patch antenna. However, their patch had return losses that were not as low as those of the self-structuring patch antenna, with a return loss of -22 dB for the lower frequency and a return loss of -17 dB for the upper frequency. The self-structuring patch does show greater bandwidth than Kan et al.'s stacked patches with slots [31], where the two antennas have bandwidths of only 1.6% and 2.0%. Once

again, the self-structuring patch showed better return losses than this patch, which has a return loss of about -16 dB at the lower frequency and about -12 dB at the upper frequency. However, drawing any meaningful conclusions from these bandwidth comparisons would be difficult, because the geometry of the self-structuring patch antenna is so different than any of the other patch antennas mentioned here.

The next two-frequency simulation was done at 5.0 GHz and 5.2 GHz. A state was found that has a VSWR of 1.13 at 5.0 GHz and 1.07 at 5.2 GHz. This corresponds to return losses of -33 dB and -36 dB, respectively. The return loss plot is shown in Figure 3.19. Once again, there are two resonances. However, with the two optimization frequencies so close together, the combined bandwidth increases to 0.44 GHz, or approximately 8.6%. This is an improvement over any single-frequency operation bandwidth previously simulated in this thesis as well as nearly double the bandwidth of the traditional patch antenna simulated in Section 3.1. Since one major drawback of using patch antennas is their narrow bandwidth, the fact that the self-structuring patch antenna can work at multiple frequencies at once and hence broaden the bandwidth may make them a desirable choice among antenna options. Zavosh and Aberle saw a similar phenomenon with their stacked-patch structure [24], where they were able to achieve a bandwidth of nearly 15%. While this bandwidth is greater than that of the self-structuring patch, their stacked-patch structure only gives the option of combining two resonances. As we will see below, the self-structuring patch antenna has the ability to combine more than two resonances together for the purpose of bandwidth enhancement.

Since optimizing the antenna at two frequencies that are close together helped to increase the -10 dB bandwidth of the antenna, the next simulation that was run was at three frequencies that are even closer together: 5.0 GHz, 5.1 GHz, and 5.2 GHz. The intent of optimizing at three frequencies close together was to combine all three resonances to expand the bandwidth even further. The optimization VSWR was set

to 3.3. GA-FEKO found a state that has a VSWR of 1.11 at 5.0 GHz, 1.43 at 5.1 GHz, and 1.08 at 5.2 GHz. As shown in the return loss plot in Figure 3.20, there is no appreciable difference in the return loss or bandwidth from optimizing at 5.0 GHz and 5.2 GHz. This may be due to the fact that the optimization frequencies are too close together.

The next step to continue trying to enhance the bandwidth was to optimize at three frequencies slightly farther apart: 5.0 GHz, 5.2 GHz, and 5.4 GHz. A state was found with a VSWR of 1.10 at 5.0 GHz, 1.14 at 5.2 GHz, and 1.22 at 5.4 GHz. The return loss plot of this state is shown in Figure 3.21. The bandwidth of this state is 0.65 GHz, or 12.5%. Optimizing at three frequencies slightly farther apart shows another improvement in -10 dB bandwidth over a two-frequency optimization. This is nearly three times the percentage bandwidth of the self-structuring patch antenna in single-frequency mode from Section 3.1.

To continue the investigation into bandwidth enhancement, the antenna was next optimized at four frequencies: 4.8 GHz, 5.0 GHz, 5.2 GHz, and 5.4 GHz. The VSWR in GA-FEKO was set to 4.4. A state was found with a VSWR of 1.2 at 4.8 GHz, 1.61 at 5.0 GHz, 1.23 at 5.2 GHz, and 1.39 at 5.4 GHz. The bandwidth of this state increased to 0.78 GHz, or approximately 15.3%. The return loss for the four-frequency optimization is shown in Figure 3.22. While this state only has one strong resonance, its large bandwidth is very desirable for a patch antenna. This state's bandwidth is comparable to or greater than the largest bandwidth of any patch antenna discussed in this thesis, which was Zavosh and Aberle's cavity-backed stacked patch structure [24]. While none of the individual optimization frequencies of this state have a VSWR as low as the VSWR of the traditional patch antenna's resonant frequency, the percentage bandwidth of this state is nearly three times the percentage bandwidth of the traditional patch antenna from Section 3.1. These results show promise for even further bandwidth enhancement using even more frequencies. However, due to the

long simulation time for these multiple-frequency simulations, further investigations into broadening the bandwidth were postponed until a prototype could be built.

One more four-frequency simulation was run, this time at frequencies that are farther apart to make sure the antenna could be optimized to have several distinct resonances as well. The chosen frequencies were 3.0 GHz, 4.0 GHz, 5.0 GHz, and 6.0 GHz. A state was found that has a VSWR of 1.31 at 3.0 GHz, 1.08 at 4.0 GHz, 1.35 at 5.0 GHz, and 1.16 at 6.0 GHz. Figure 3.23 shows that this state actually has five fundamental resonances, with one resonance at each of the optimization frequencies and an additional resonance near 5.25 GHz. While this state does not show the broad bandwidth that the four-frequency state with the frequencies closer together does, there is reason to believe that a patch antenna with the ability to work at several distinct frequencies could be desirable as well. Investigations into more than four frequencies were not done at this time due to time constraints.

The self-structuring patch antenna has shown the ability to operate at two, three, or four frequencies at once. These frequencies can be placed somewhat far apart to give distinct resonances, or placed closer together in order to enhance the bandwidth at any one frequency. Bandwidths have been shown to be up to three times greater than that of the traditional patch antenna simulated earlier in this thesis.

3.3 Lower frequency simulations

In preparation for the construction of the self-structuring patch antenna prototype to be used in the experimental part of this thesis, a larger self-structuring patch designed to work at lower frequencies was simulated. This antenna has dimensions of 22.9 cm by 38.1 cm (9 inches by 15 inches). Three different dielectric thicknesses were simulated: 1.575 mm, 3.175 mm, and 5 mm. These thicknesses were chosen because they correspond to standard thicknesses of Rogers Duroid 5880 circuit boards (1.575 mm and 3.175 mm) and the thickness of a sample TLY-5 circuit board that was

received from Taconic (5 mm).

The antennas were first simulated in FEKO without shorting pins to find the fundamental resonant frequency for each thickness. The feed pin was placed 7.5 inches from the left edge of the patch surface and 1.2857 inches from the bottom edge of the patch surface. The 1.575 mm thick board had four resonances, at 428 MHz (-12.5 dB), 501 MHz (-12.6 dB), 526 MHz (-13.3 dB), and 679 MHz (-12.6 dB). The bandwidth of the resonance at 526 MHz was only 1.6%, which is slightly lower than bandwidths discussed earlier in this thesis [17]. The return loss plot for this board thickness is shown in Figure 3.24. The 3.175 mm thick board also had four resonances: 414 MHz (-14.6 dB), 490 MHz (-14.9 dB), 512 MHz (-19 dB), and 665 MHz (-17.7 dB). At the 512 MHz resonance the bandwidth was 2%. The return loss plot for this board thickness is shown in Figure 3.25.

The 5 mm thick board was simulated next. Without any shorting pins, this antenna has a fundamental resonance of -19.7 dB at 527 MHz. The bandwidth of this antenna without shorting pins is 6.19 MHz or 1.2%. This is somewhat low, but that is to be expected because the dielectric layer is still thin compared to a wavelength. The return loss plot for this board thickness is shown in Figure 3.26. This thickness was chosen because it was equivalent to the thickness of the actual circuit board to be used to construct the antenna. The thickest possible board was chosen in order to potentially have the largest possible bandwidths, since bandwidth is proportional to the thickness of the dielectric layer [35].

The 32 shorting pins were arranged on the patch in the same pattern as the smaller antenna simulated earlier in this chapter. GA-FEKO was run to find a state at an arbitrarily chosen frequency of 670 MHz. A state was found that has a VSWR of 1.05. This state has a low bandwidth of only 0.8%, as shown in Figure 3.27. Since these simulations were only run to make sure that the larger self-structuring patch antenna prototype would work at the frequencies of interest, no further low-frequency

simulations were run.

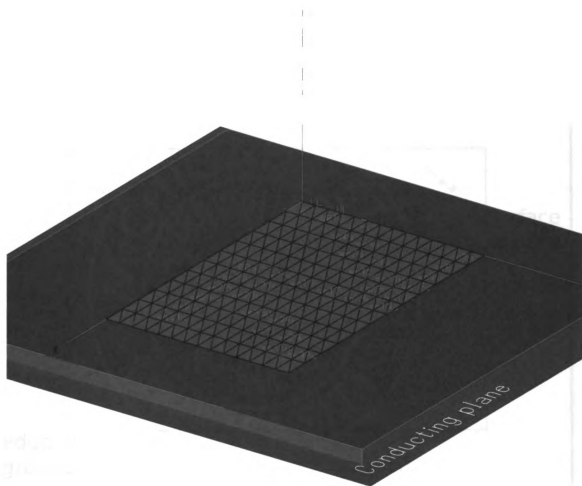


Figure 3.1. Segmentation of the patch in FEKO.

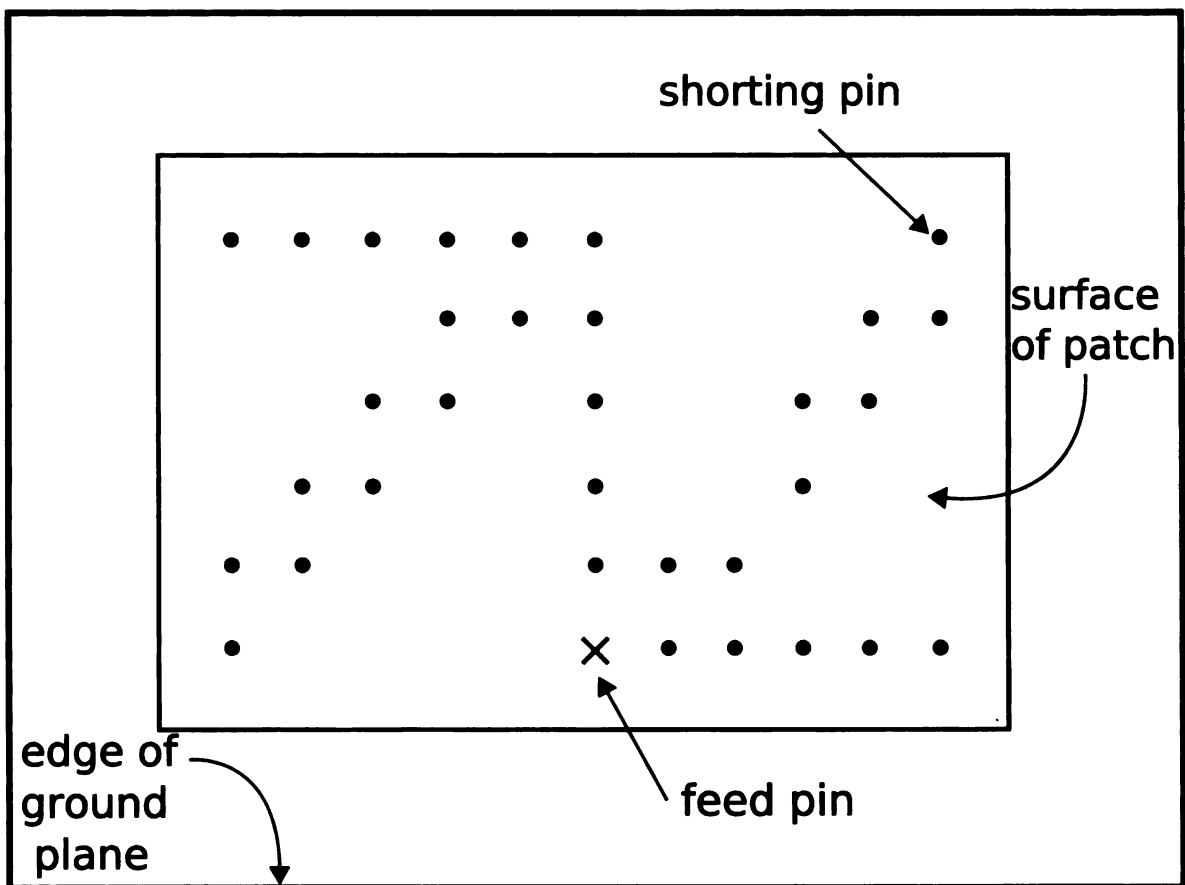


Figure 3.2. Placement of shorting pins.

Table 3.1. Pin locations given in sub-patch coordinates. Feed pin is placed at (6,1).

Pin Number	Location	Pin Number	Location
1	(1,1)	17	(6,4)
2	(1,2)	18	(6,5)
3	(1,6)	19	(6,6)
4	(2,2)	20	(7,1)
5	(2,3)	21	(7,2)
6	(2,6)	22	(8,1)
7	(3,3)	23	(8,2)
8	(3,4)	24	(9,1)
9	(3,6)	25	(9,3)
10	(4,4)	26	(9,4)
11	(4,5)	27	(10,1)
12	(4,6)	28	(10,4)
13	(5,5)	29	(10,5)
14	(5,6)	30	(11,1)
15	(6,2)	31	(11,5)
16	(6,3)	32	(11,6)

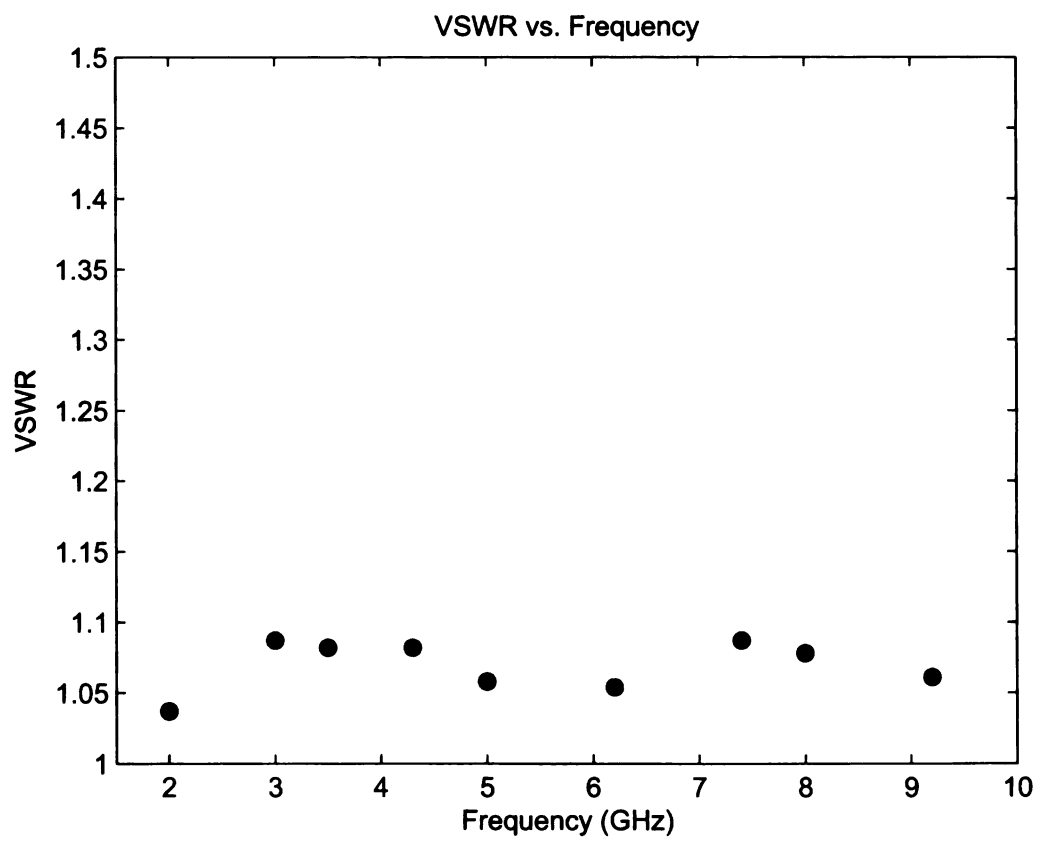


Figure 3.3. VSWR vs. frequency for the self-structuring patch antenna.

Table 3.2. Results of simulations of the self-structuring patch antenna.

Freq. (GHz)	VSWR	Return Loss (dB)	Bandwidth (GHz)	Bandwidth (%)	Input Impedance (Ohms)
2.0	1.037	-35	0.04	2	51.78-j0.44
3.0	1.087	-27.6	0.12	4	53.26-j2.9
3.5	1.082	-28.2	0.14	4	54.10+j0.42
4.3	1.079	-28.4	0.21	4.9	49.33+j3.85
5.0	1.058	-31.2	0.18	3.6	51.77-j2.27
6.2	1.054	-31.8	0.2	3.2	48.06-j1.68
7.4	1.087	-27.8	0.24	3.2	53.33+j2.74
8.0	1.078	-28.6	0.24	3	53.0-j2.44
9.2	1.061	-30.7	0.26	2.8	47.11-j0.12

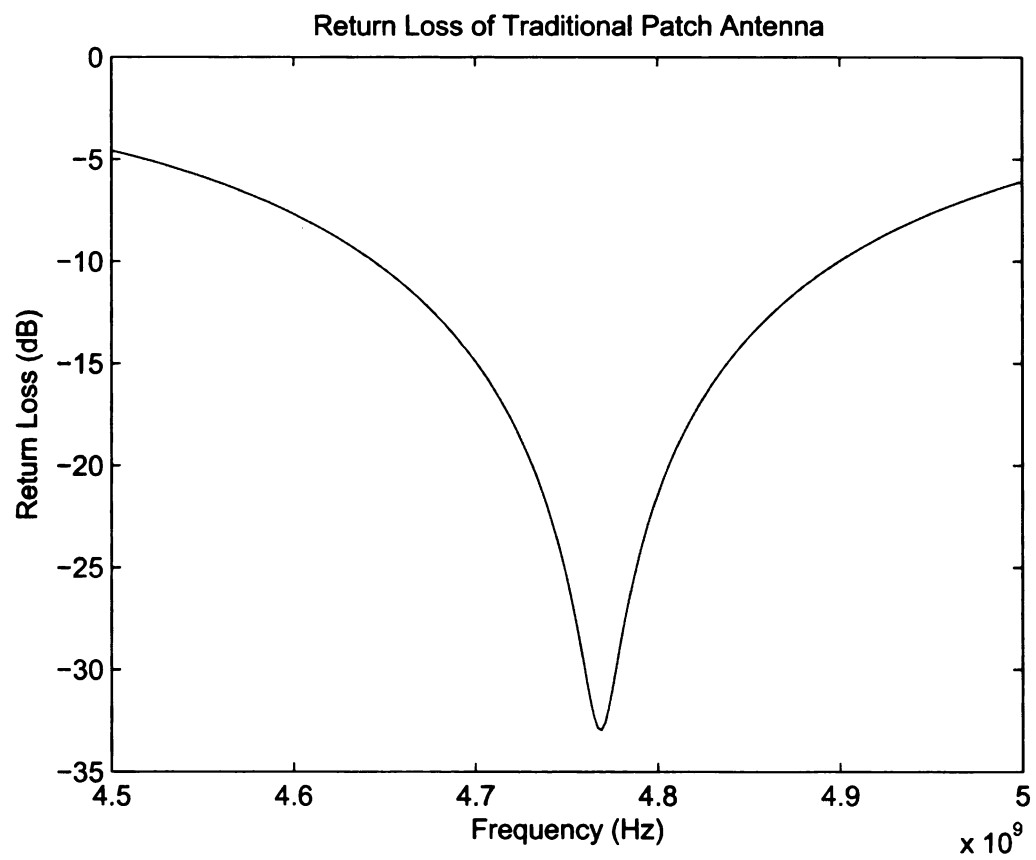


Figure 3.4. Return loss for the traditional patch antenna resonant at 4.768 GHz.

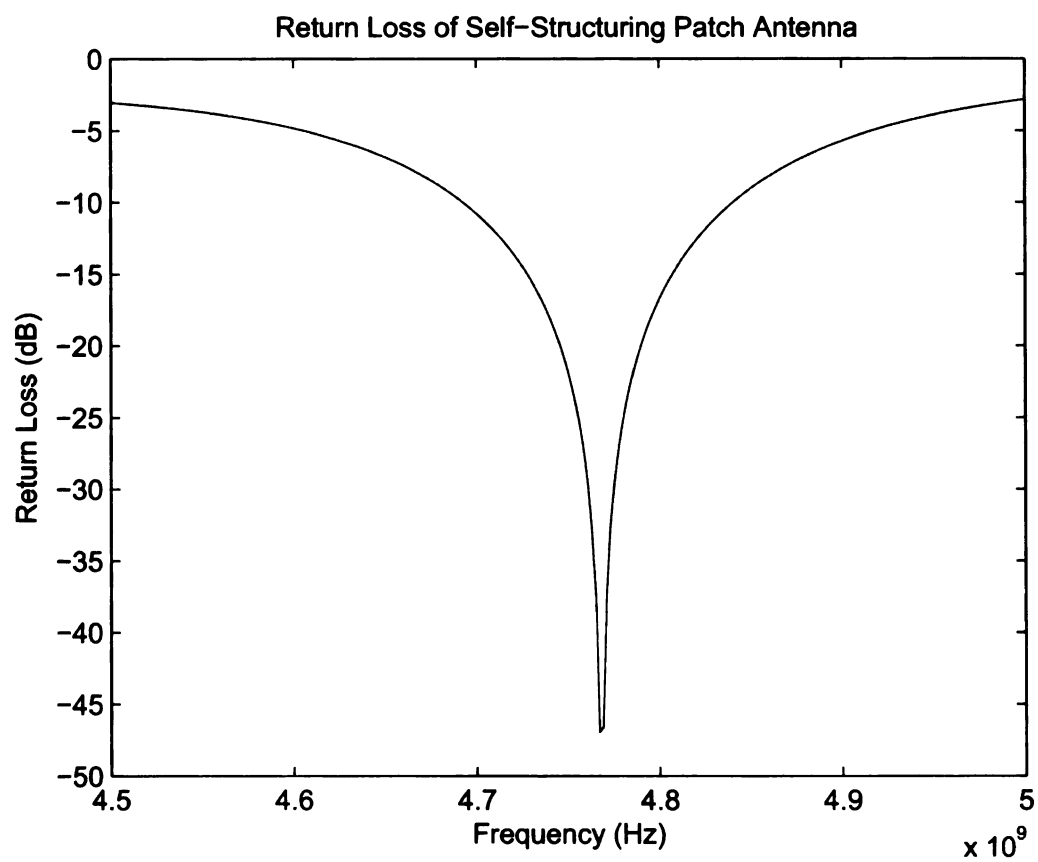


Figure 3.5. Return loss for the self-structuring patch antenna optimized at 4.768 GHz.

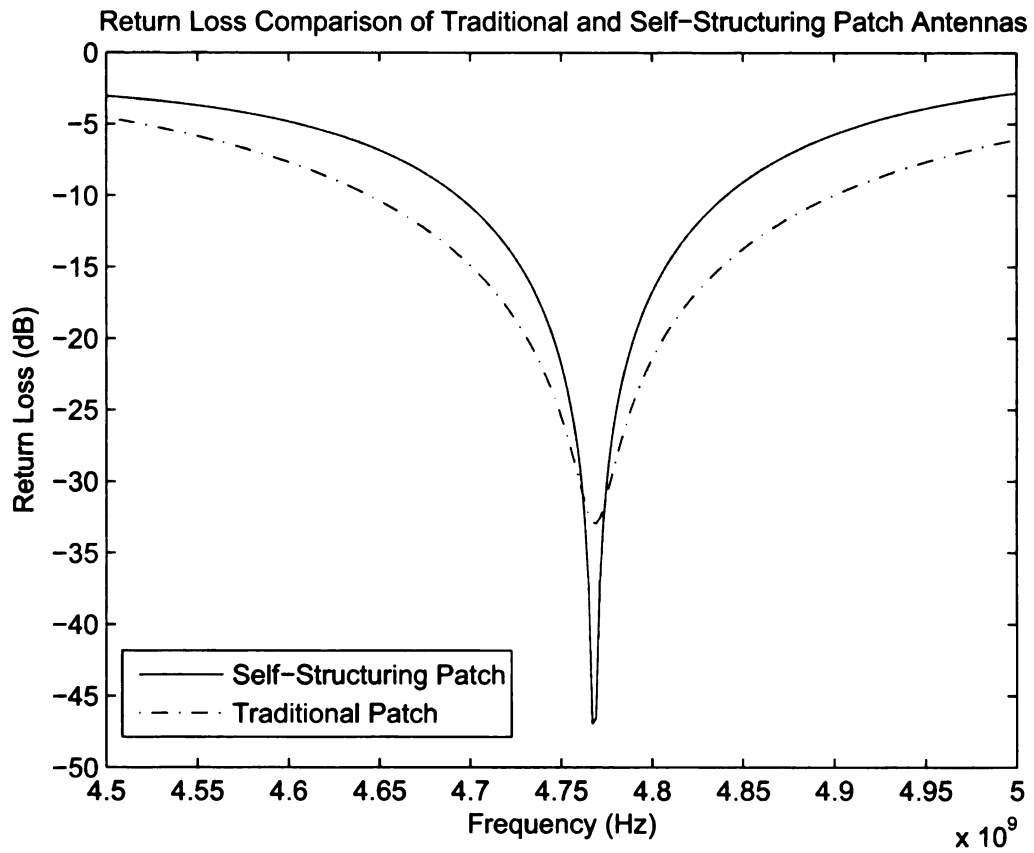


Figure 3.6. Comparison of the return losses of the traditional patch antenna and the self-structuring patch antenna optimized at the same frequency.

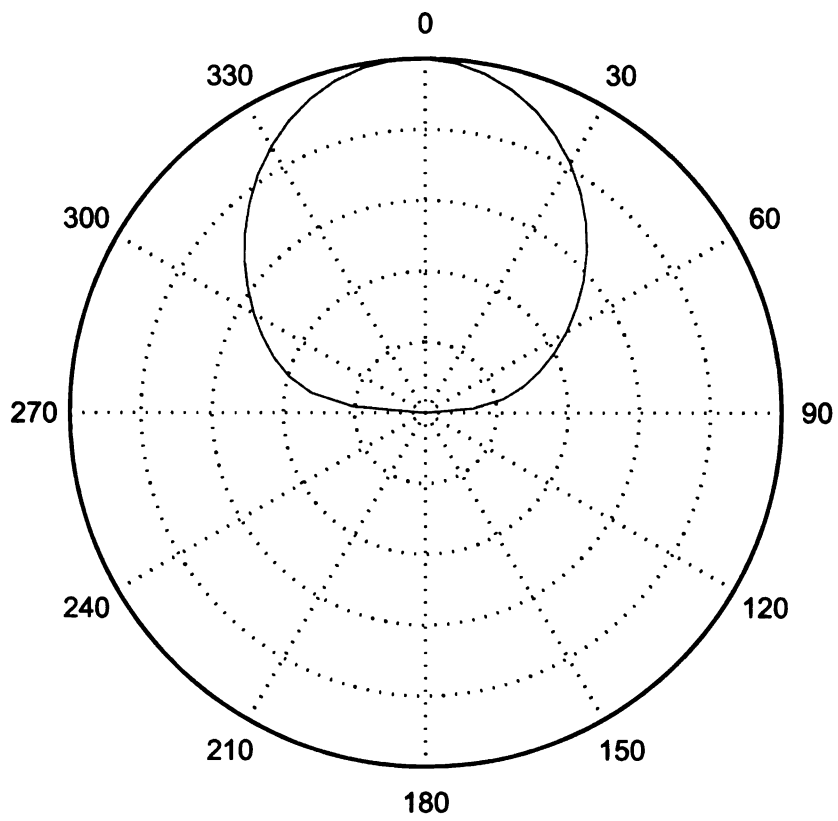


Figure 3.7. Radiation pattern of the traditional patch antenna in the $y - z$ plane.

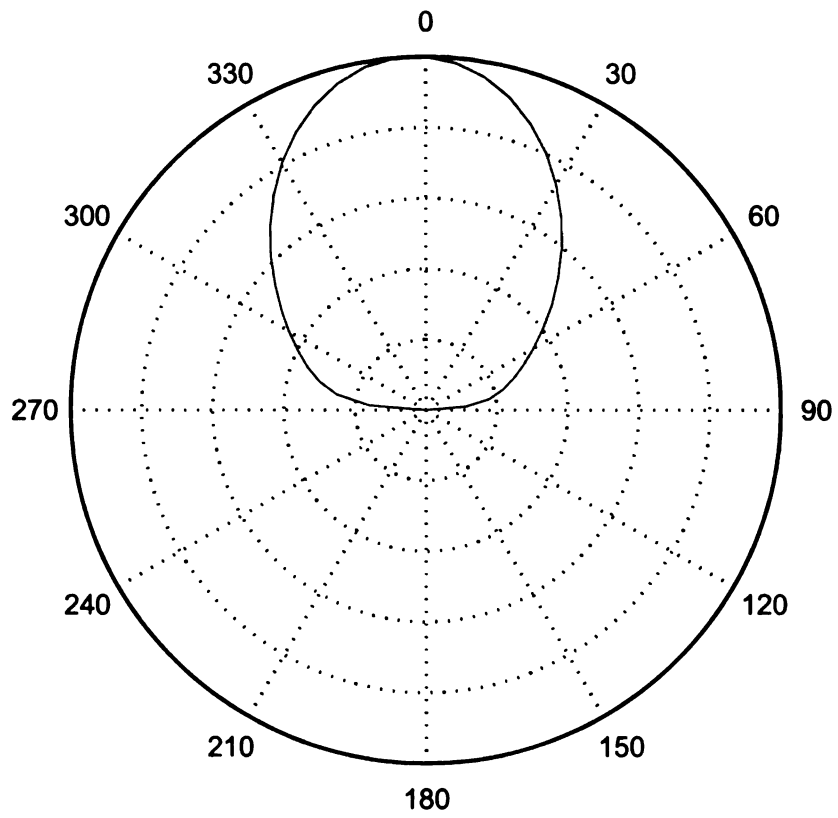


Figure 3.8. Radiation pattern of the self-structuring patch antenna in the $y-z$ plane.

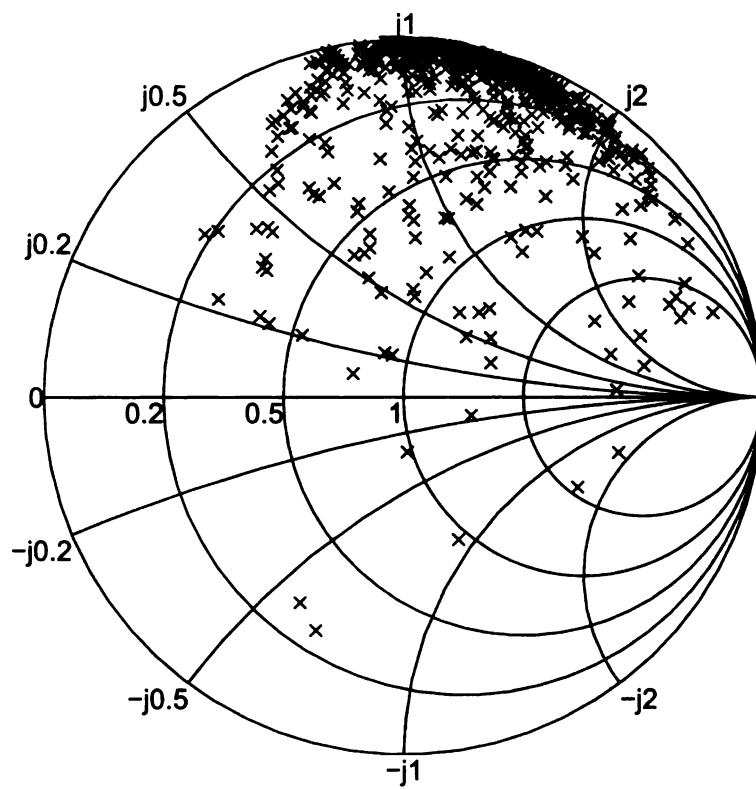


Figure 3.10. Smith chart showing the impedances of 1000 random states at 3 GHz.

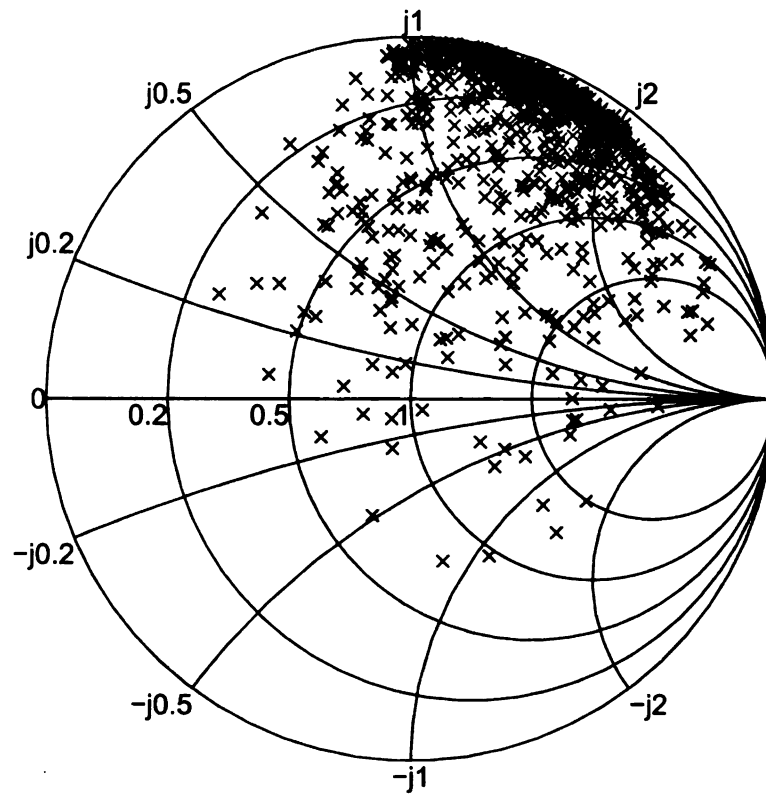


Figure 3.11. Smith chart showing the impedances of 1000 random states at 3.5 GHz.

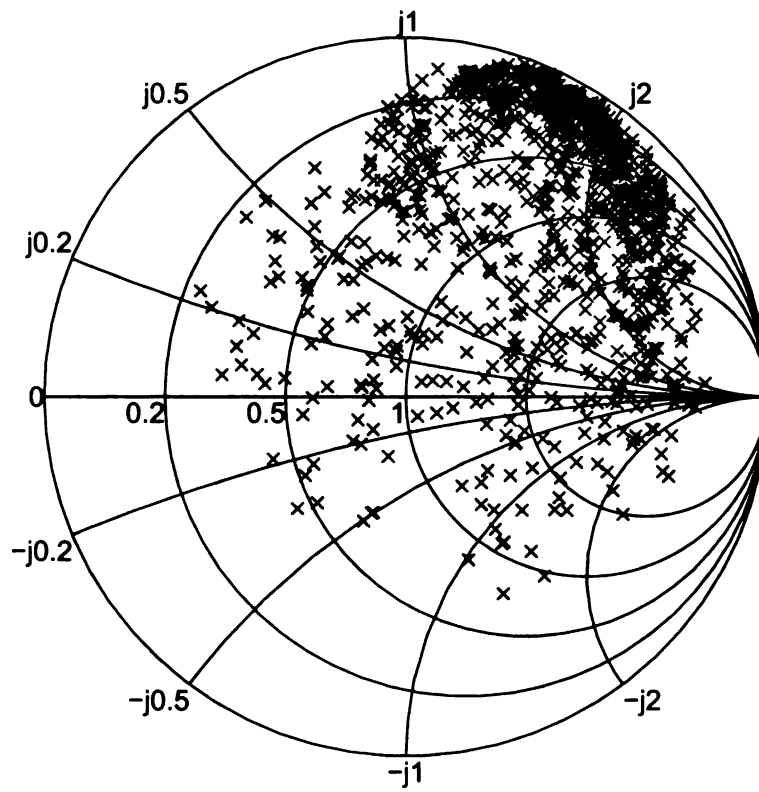


Figure 3.12. Smith chart showing the impedances of 1000 random states at 4.3 GHz.

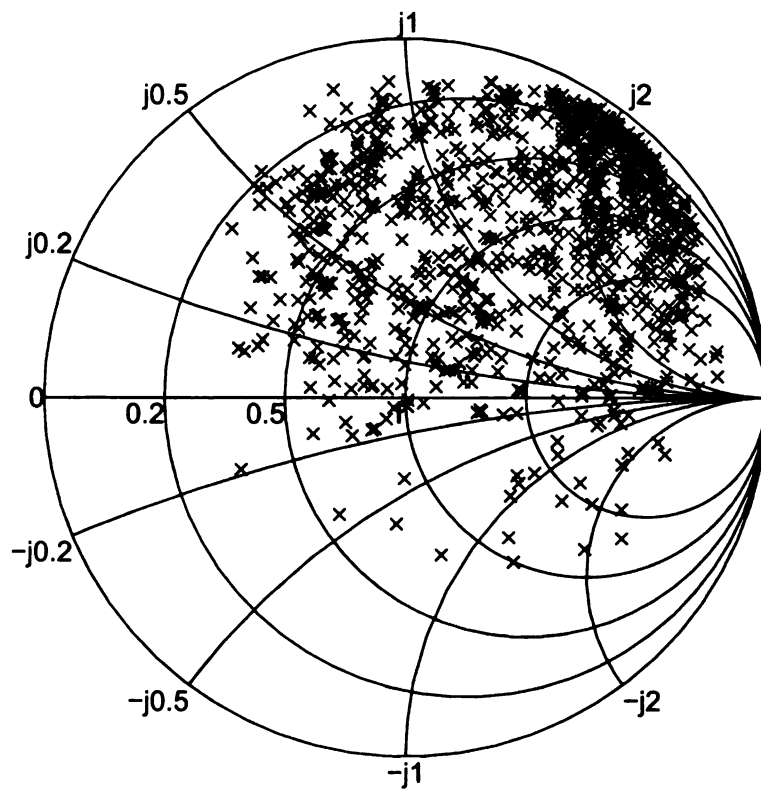


Figure 3.13. Smith chart showing the impedances of 1000 random states at 5 GHz.

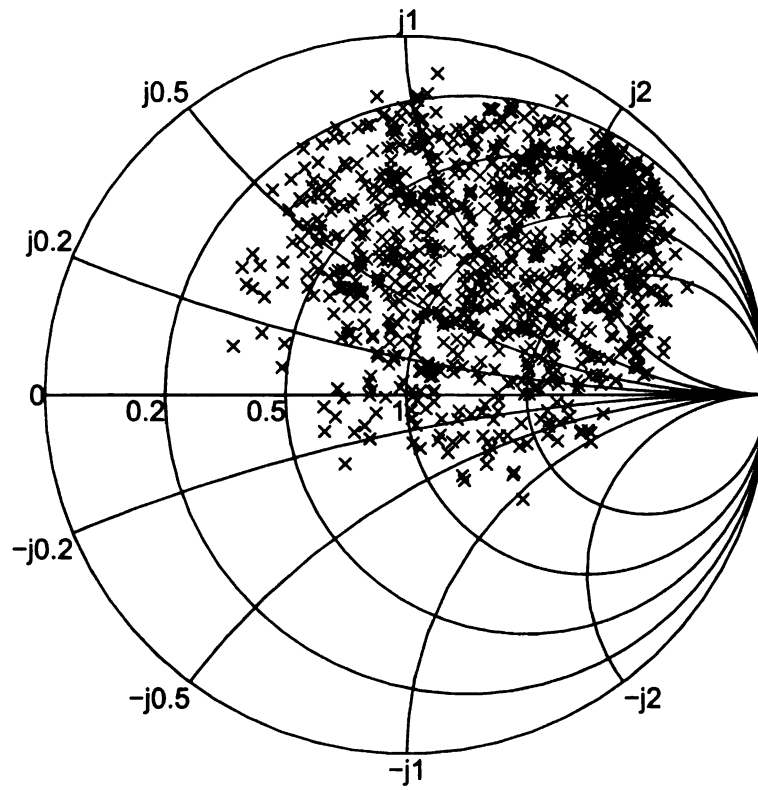


Figure 3.14. Smith chart showing the impedances of 1000 random states at 6.2 GHz.

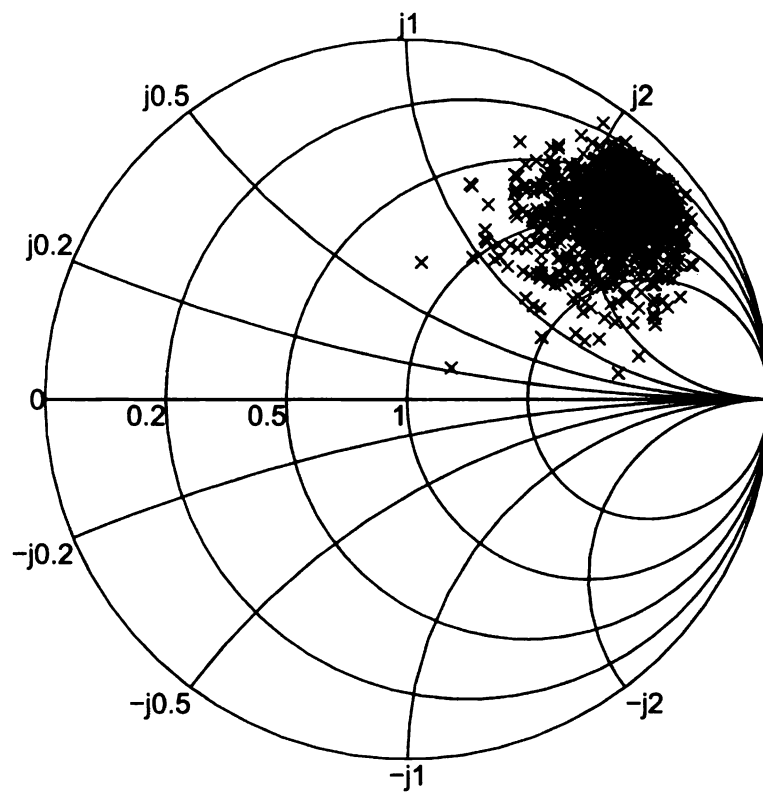


Figure 3.15. Smith chart showing the impedances of 1000 random states at 7.4 GHz.

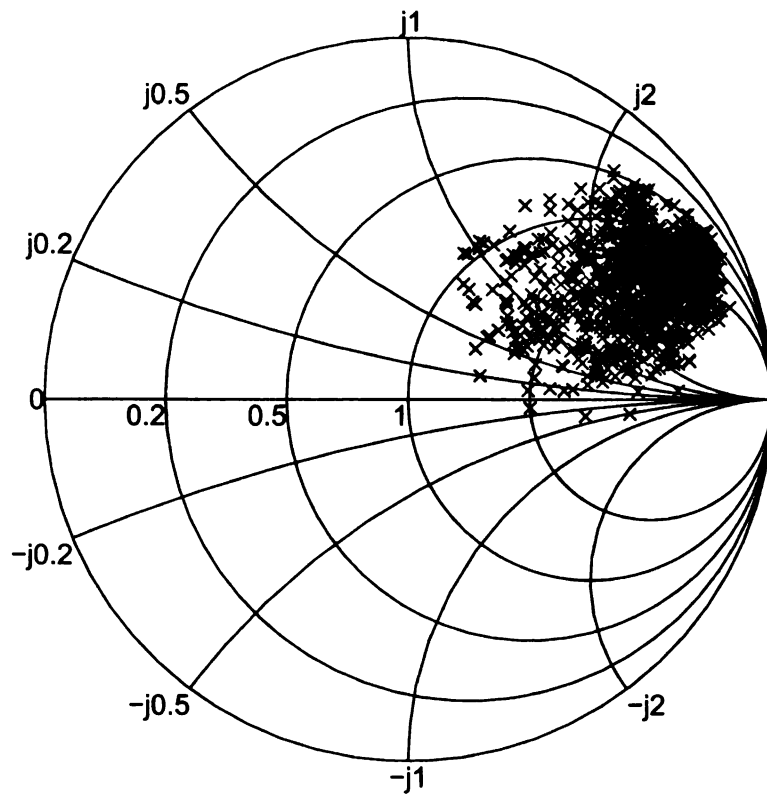


Figure 3.16. Smith chart showing the impedances of 1000 random states at 8 GHz.

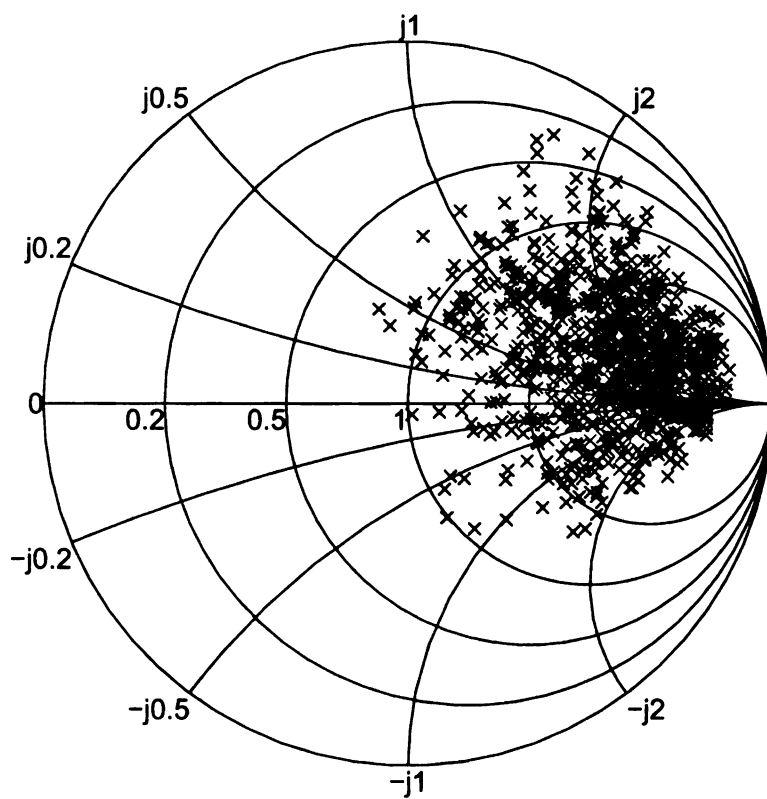


Figure 3.17. Smith chart showing the impedances of 1000 random states at 9.2 GHz.

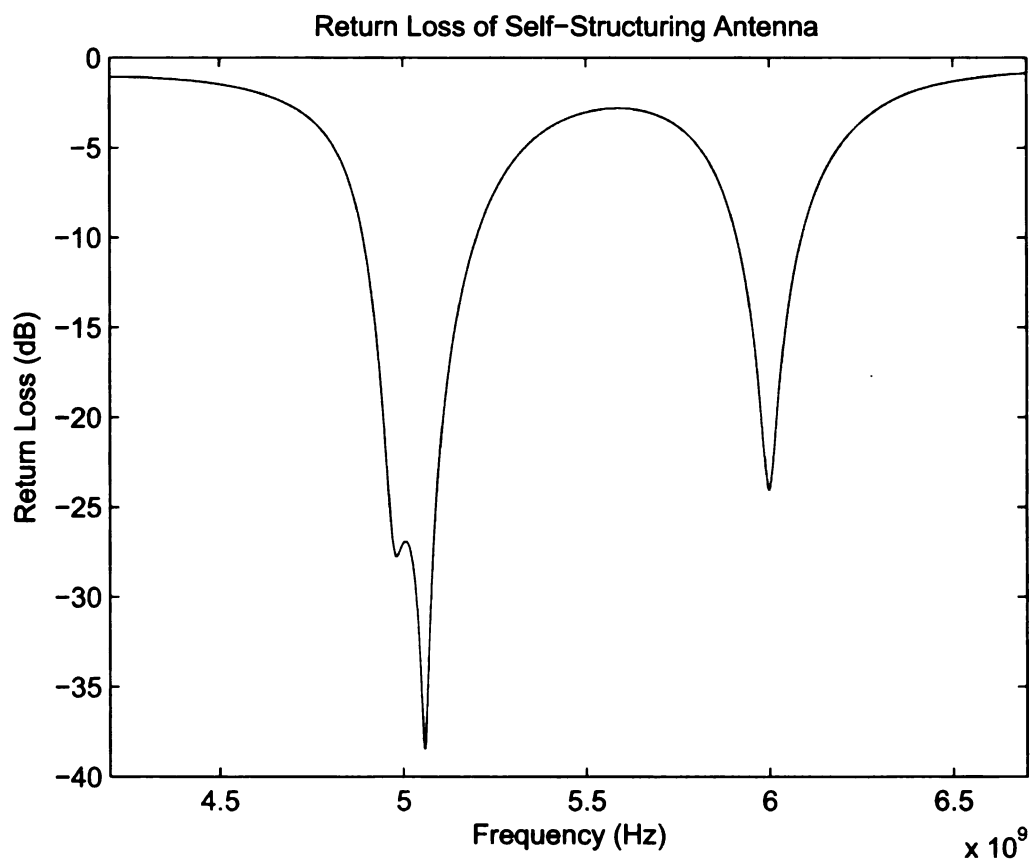


Figure 3.18. Return loss for the self-structuring patch antenna optimized at 5.0 GHz and 6.0 GHz.

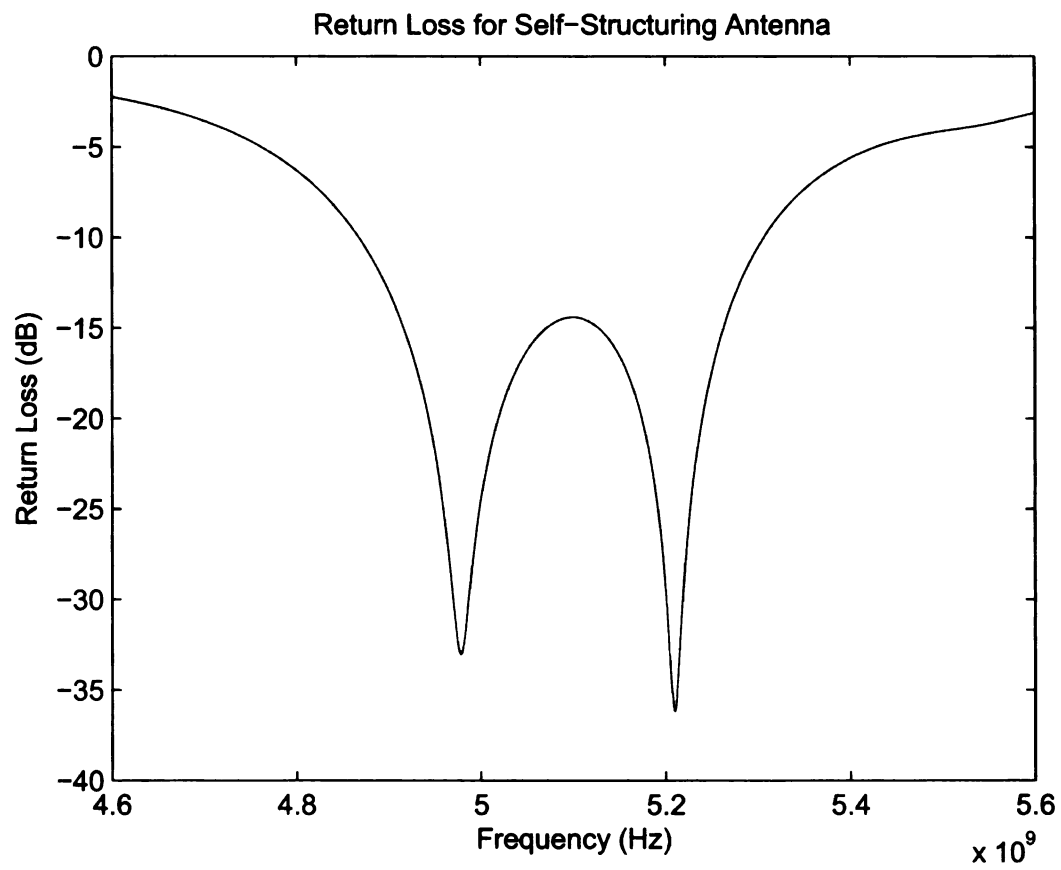


Figure 3.19. Return loss for the self-structuring patch antenna optimized at 5.0 GHz and 5.2 GHz.

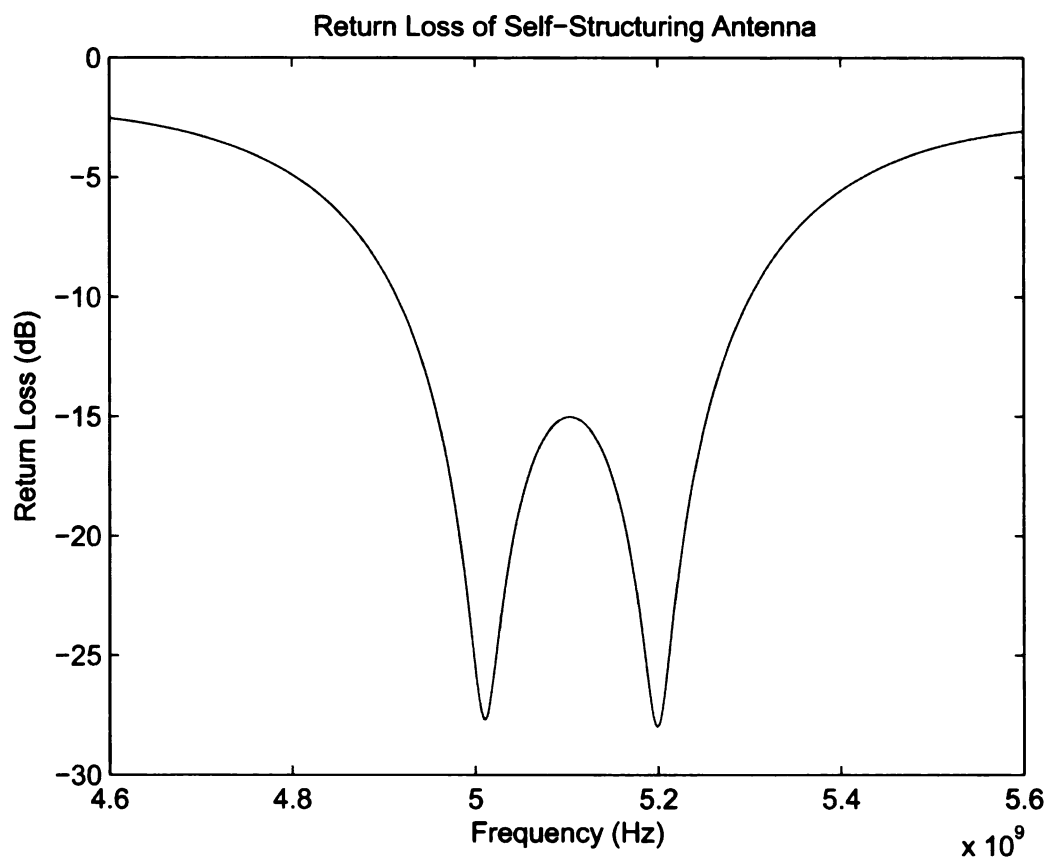


Figure 3.20. Return loss for the self-structuring patch antenna optimized at 5.0 GHz, 5.1 GHz, and 5.2 GHz.

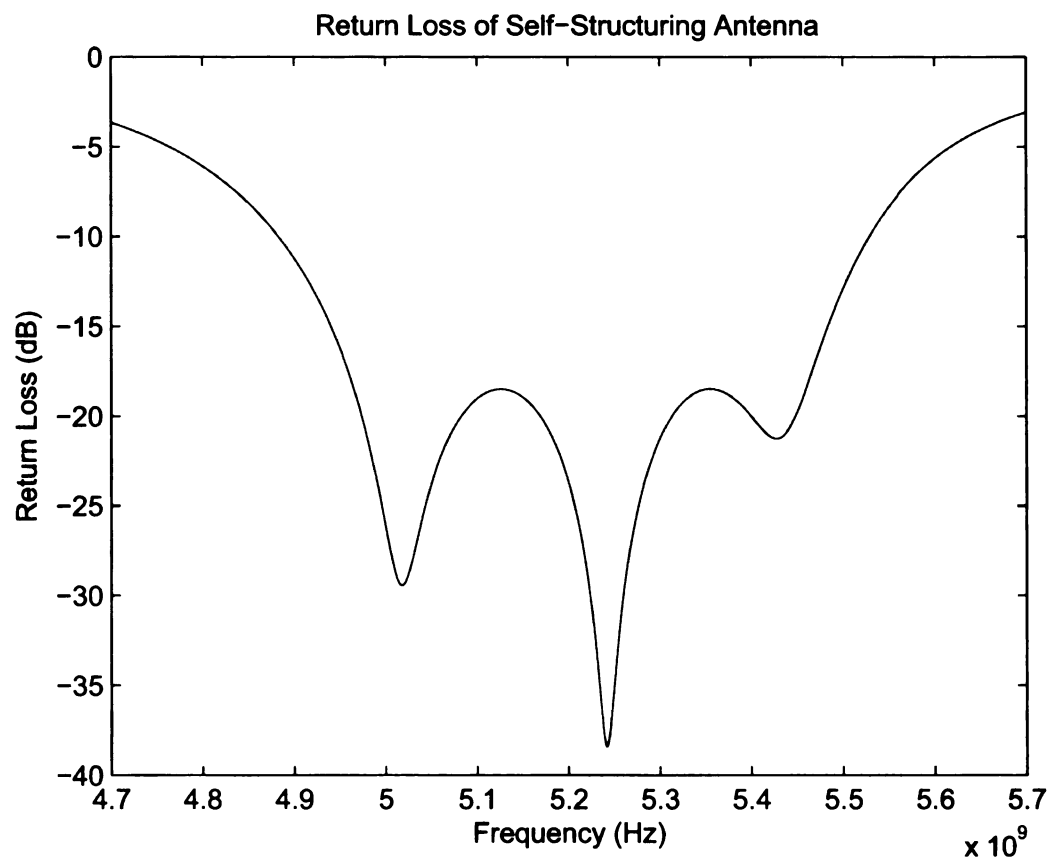


Figure 3.21. Return loss for the self-structuring patch antenna optimized at 5.0 GHz, 5.2 GHz, and 5.4 GHz.

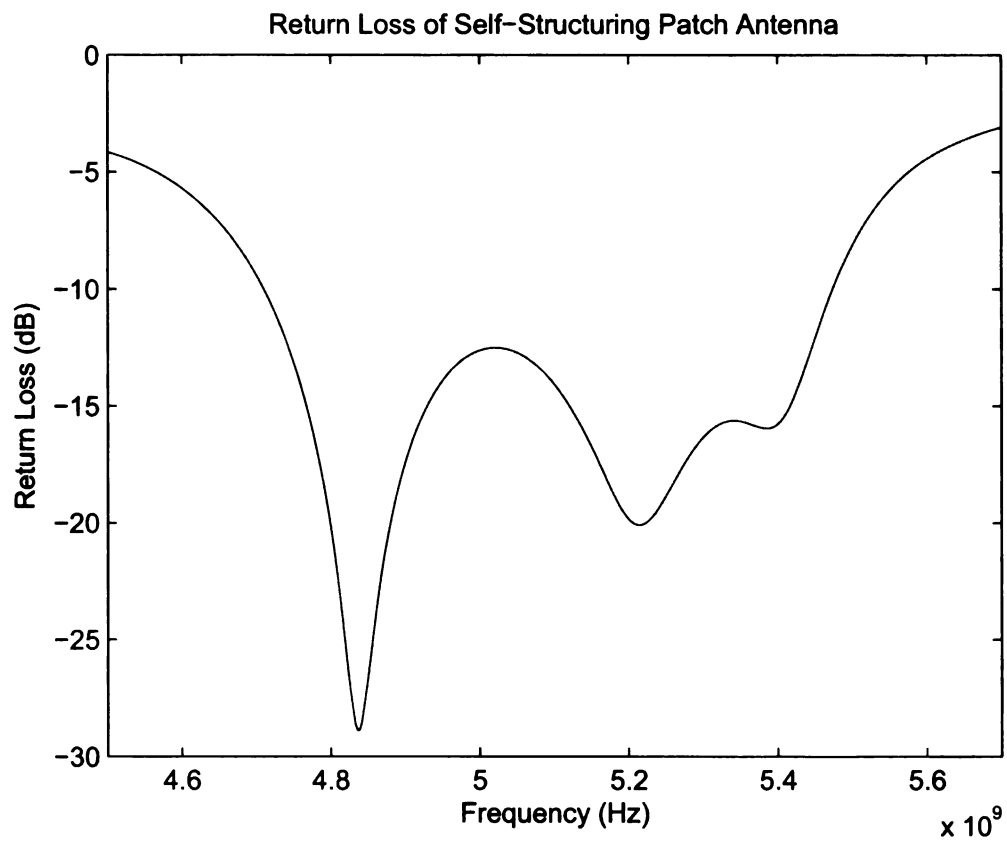


Figure 3.22. Return loss for the self-structuring patch antenna optimized at 4.8 GHz, 5.0 GHz, 5.2 GHz, and 5.4 GHz.

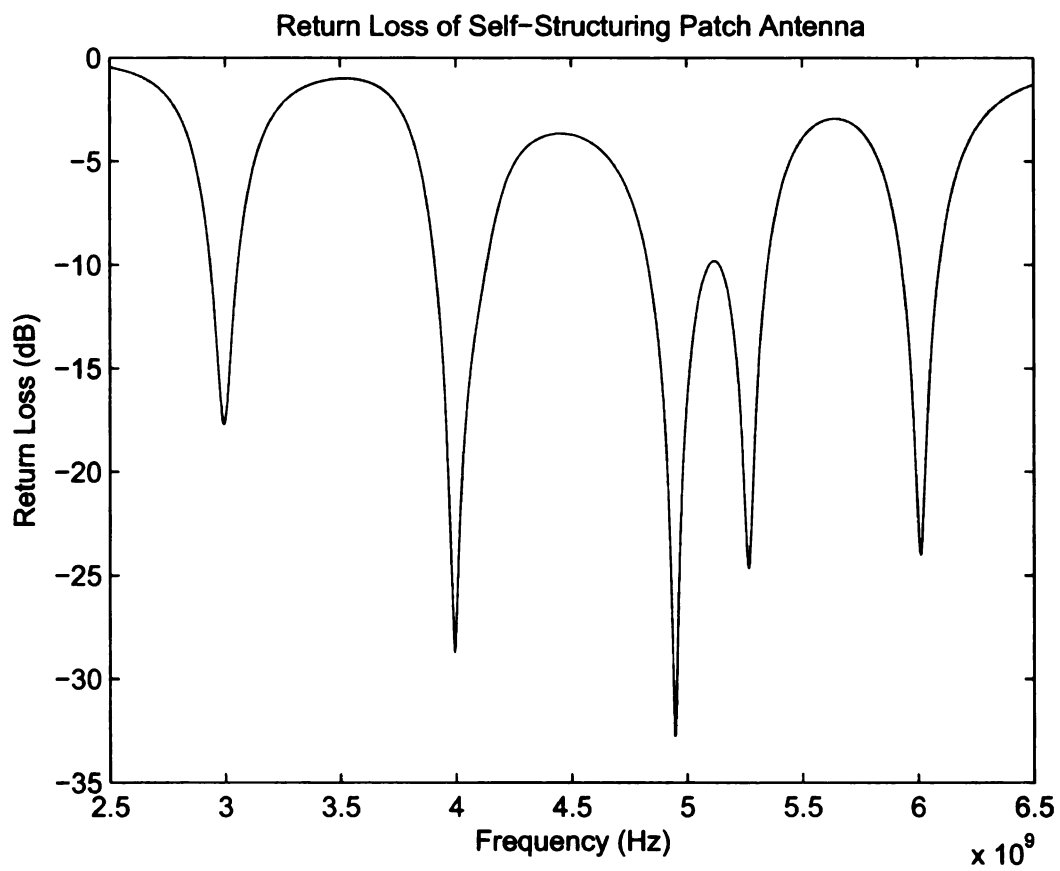


Figure 3.23. Return loss for the self-structuring patch antenna optimized at 3.0 GHz, 4.0 GHz, 5.0 GHz, and 6.0 GHz.

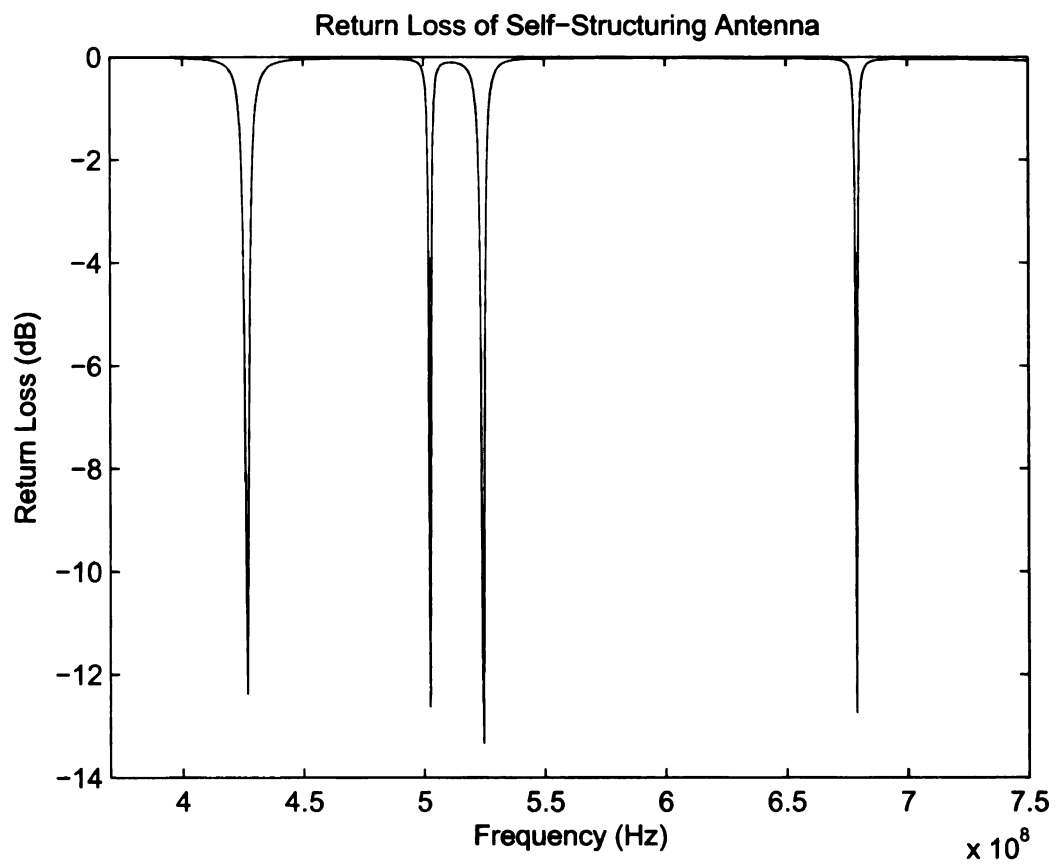


Figure 3.24. Return loss for the self-structuring patch antenna with no shorting pins with a 1.575 mm thick board.

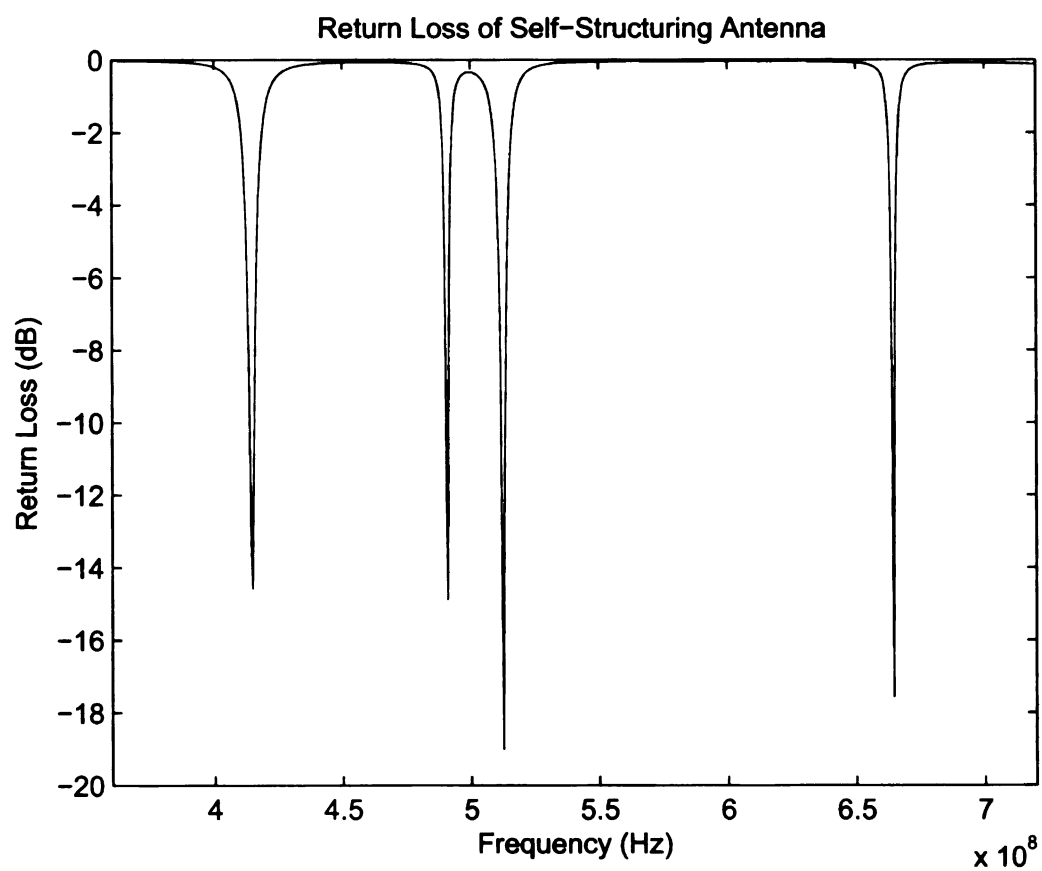


Figure 3.25. Return loss for the self-structuring patch antenna with no shorting pins with a 3.175 mm thick board.

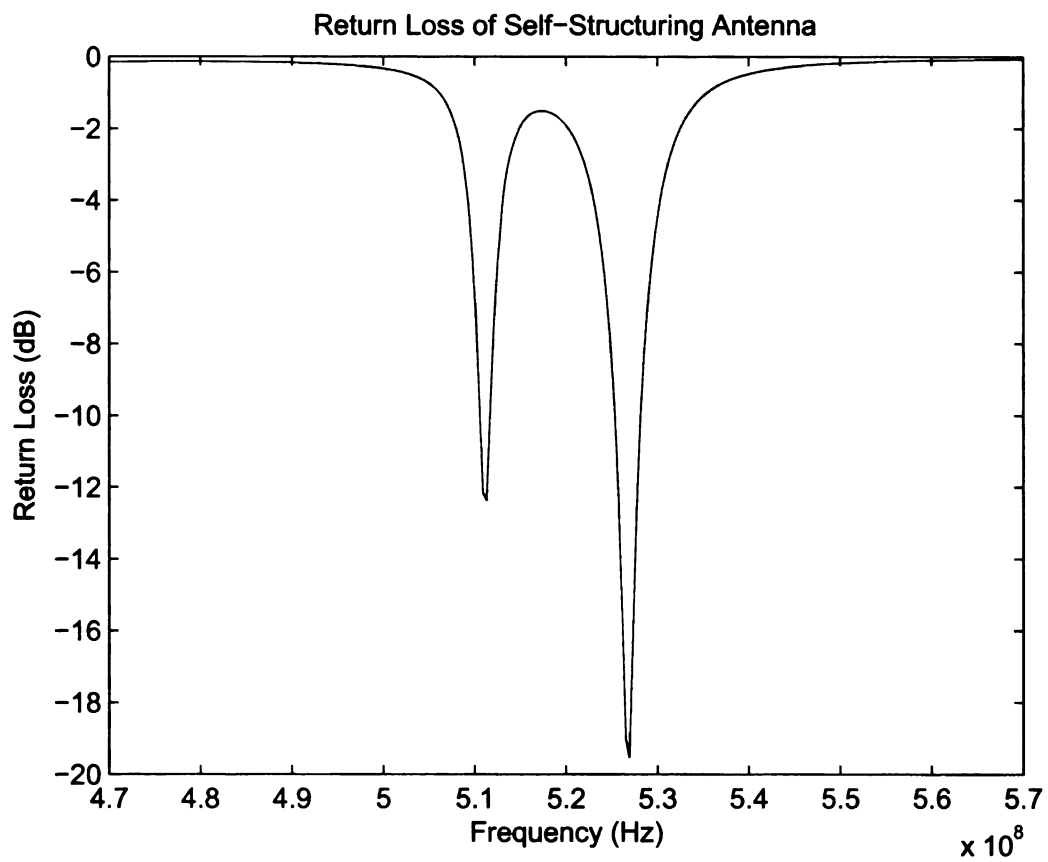


Figure 3.26. Return loss for the self-structuring patch antenna with no shorting pins with a 5.0 mm thick board.

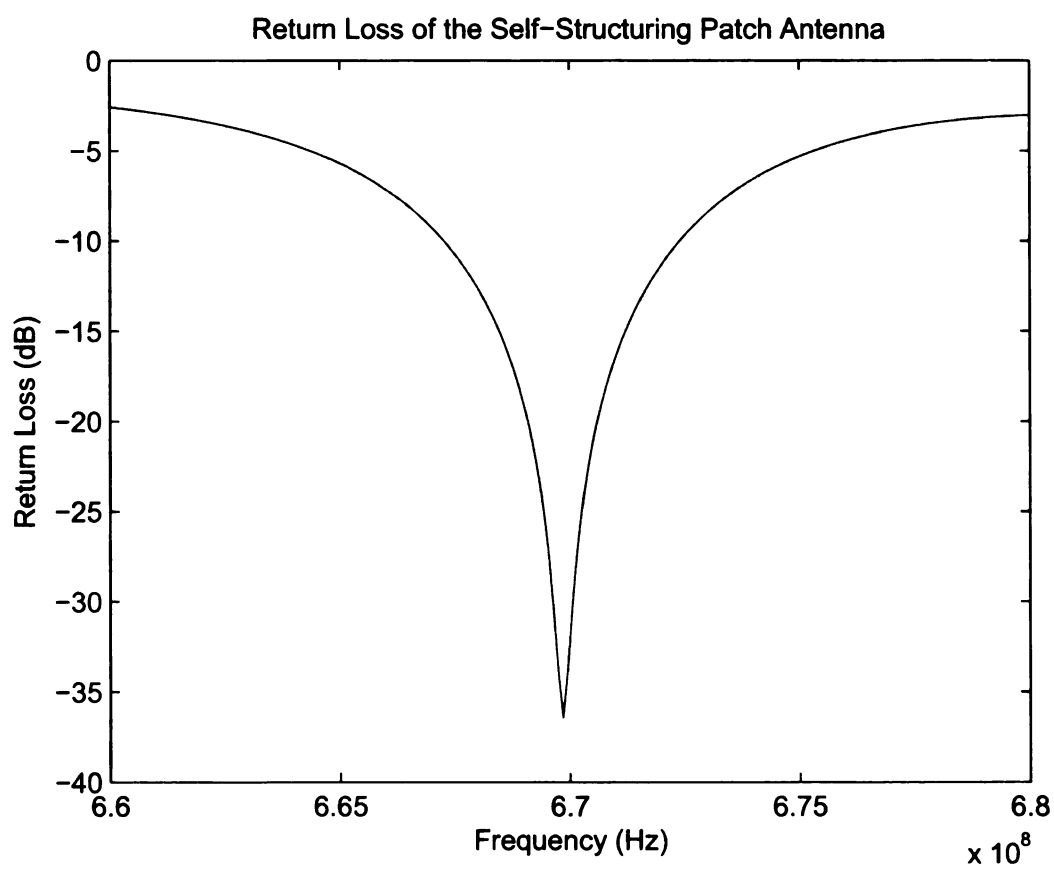


Figure 3.27. Return loss for the self-structuring patch antenna optimized at 670 MHz.

CHAPTER 4

CONSTRUCTION OF A SELF-STRUCTURING ANTENNA PROTOTYPE AND EXPERIMENTAL RESULTS

This chapter discusses the design, construction, and testing of a self-structuring antenna prototype. The layout of the antenna prototype was completed in Autodesk AutoCAD (<http://www.autodesk.com>). Thirty-two switches were used, just as in the simulations in Chapter 3. In Section 4.1, the design and construction of the self-structuring patch antenna prototype are discussed. The experimental setup for measuring the voltage standing wave ratio (VSWR) is detailed in Section 4.2. Section 4.3 discusses the results from the random searches that were run, where a random configuration of switches was closed for each state investigated. The genetic algorithm optimizations are discussed in Section 4.4. Finally, Section 4.5 discusses the electromagnetic compatibility (EMC) investigations that were done for the self-structuring patch antenna.

4.1 Design and construction

Design and layout of the self-structuring patch antenna began with the completion of the layout by James P. Greetis using Autodesk AutoCAD 2007. The antenna was laid out to be identical in geometry to the antenna that was simulated in Section 3.3 of Chapter 3. The TLY-5 board that was received from Taconic had dimensions of 15 inches by 18 inches, with a thickness of 5 mm. Since the board was to be machined in the Michigan State University ECE Shop, 17.5 inches by 11.5 inches was the maximum size that the milling machine in the ECE Shop could accommodate. The dimensions of the patch were chosen to be 15 inches by 9 inches. These dimensions were chosen so the edge of the patch would be 1.25 inches away from the edge of a 17.5 inch by 11.5 inch board on each side. Luckily, the technicians in the ECE Shop

were able to find a way to mill away the necessary copper without cutting the board down, so the edge of the patch is actually 2.5 inches from the top and bottom edges of the board and 1.5 inches from the right and left edges of the board on the prototype.

The top and bottom of the self-structuring antenna as laid out in AutoCAD are shown in Figure 4.1 and Figure 4.2, respectively. The spots marked with a “+” on the top of the board are locations where holes were drilled through the board. On the bottom of the board, copper rings were removed around each hole in order to electrically isolate small areas of copper, called copper pads. A wire was placed through the hole and soldered to the top of the patch and the copper pad on the bottom of the board. The wire was then soldered to one outer leg of a switch, a Coto Technology SIP Reed relay series 9011-05-10, and the other outer leg was soldered to the ground plane. These switches have an operating voltage of 5 V, but they will switch anywhere between 3.75 V and 6.5 V. They have a coil resistance of 500Ω and a nominal current of 10 mA. Each switching cycle takes 0.45 milliseconds to complete, which allows 2222 switching cycles per second. The switches have an expected lifetime of 250 million switching cycles. These particular switches were chosen because they are the same switches that were used on previous prototypes of self-structuring antennas [2],[3].

A diagram of one shorting pin and the feed pin is shown in Figure 4.3. When the switch is open, the surface of the patch and the ground plane are disconnected and the top of the board remains electrically isolated from the bottom. When the switch is closed, the wire becomes connected to the ground plane through the switch, effectively shorting the surface of the patch and the ground plane together. Wires were then soldered to the two inner legs of the switches and connected to the header of a six-inch 64-line ribbon cable that was epoxied to the bottom of the board. A photograph of one of the switches is shown in Figure 4.4. The ribbon cable has 32 control lines and 32 ground lines. This ribbon cable was then connected to the

control board, which provides an interface between the computer and the antenna. The control board is necessary because the computer does not supply the necessary current to power the switches, so an external power supply is needed. On the control board are connections for the cables from the computer, a connection for the ribbon cable coming from the antenna, four Toshiba TD62783AP high-voltage source driver integrated circuits to power the switches, and a connection for the 5 volt power supply to power the integrated circuits. A schematic of the control board is given in Figure 4.5. The control board used was set up on a ProtoBoard PB104. Photographs of the surface of the patch and the ground plane of the self-structuring antenna prototype are seen in Figure 4.6 and Figure 4.7, respectively. A photograph of the control board is shown in Figure 4.8.

Before any experiments were run on the self-structuring patch antenna, it was connected to a Hewlett-Packard 8753D Vector Network Analyzer to determine its fundamental resonant frequencies with all switches turned off. The antenna showed three resonances below -10 dB between 100 MHz and 1 GHz: a resonance of -17.7 dB at 384.6 MHz with a -10 dB bandwidth of 1.7%, a resonance of -37 dB at 467.3 MHz with a -10 dB bandwidth of 3.7%, and a resonance of -13.2 dB at 597.5 MHz with a -10 dB bandwidth of 2.8%. The return loss plot for the antenna with all switches disconnected is shown in Figure 4.9. If the self-structuring patch antenna has any resonances outside of this frequency range, they were not investigated because this band is the intended frequency band of use for the antenna.

4.2 Measurement of antenna voltage standing wave ratio

A simple block diagram of the experimental setup for measuring VSWR is shown in Figure 4.10. The source used is a Hewlett-Packard 8657A Signal Generator, the receiver is a Singer Stoddart NM-37/57 EMI/Field Intensity Meter, the dual directional coupler is a Hewlett-Packard 778D Dual Directional Coupler, and the computer used

to control the elements of the setup is a Fujitsu B-Series Lifebook with a 700 MHz Pentium 3 processor and 512 MB of RAM. Five square sections of radio frequency absorber, four sides and a top, were set up on a table in the lab to make a miniature anechoic chamber for testing. To set up the experiment, first the antenna feed is connected to the test port of the dual directional coupler. The input of the dual directional coupler is connected to the source, which is set to the desired frequency with an amplitude of 1 volt. The incident port is then terminated with a 50Ω load and the reflected port is connected to the front port of the receiver.

The computer connects to the receiver and the control board using two National Instruments DAQCards. One of these cards is a DAQCard-DIO-24, which provides 24 bits of digital input/output (I/O). This card is connected by a National Instruments cable to the 50 pin header (2 rows of 25 pins) on the control board. The other card is a DAQCard-6024E. This card also provides 12 bits of digital I/O in addition to a 16 channel in, 2 channel out analog to digital (A/D) converter that can sample up to 200,000 samples per second. The National Instruments ribbon cable that is connected to this card splits into two connections at the end of the ribbon. These two connections are shown in Figure 4.11. A coaxial BNC cable is affixed to one of these connections and is then attached to the Y-output on the back of the receiver. The other connection is attached to a 10-line ribbon cable that connects to the 10-pin header on the control board. The 5 volt power supply is then plugged in to its connector on the control board. To complete the setup, the 6-inch ribbon cable epoxied to the antenna is connected through a jumper to a longer ribbon cable. This jumper is just a 64-pin to 64-pin male-to-male adapter used for connecting the two ribbon cables together, as shown in Figure 4.12. This longer ribbon cable is then plugged into the 64-pin header on the control board. A photograph of the entire experimental setup is shown in Figure 4.13.

To test the switches for functionality, the National Instruments Measurement and

Automation Software (MAX) is used. MAX is opened, and one of the DAQCards is selected in the device tree. Right-clicking on the device gives the option of opening the test panel for the card. Once in the test panel, the Digital I/O option is selected. In this panel, each switch can be toggled on or off by selecting the appropriate radio button. The switch connection is verified by using a hand-held multimeter between the top and bottom surfaces of the patch.

A Visual Basic program, written by Raoul Ouedraogo for use with this self-structuring patch antenna and future research into self-structuring antennas, was used to compute the VSWR of the antenna. The system must first be calibrated by removing the cable connected to the antenna feed and placing a short on the end. The reflected voltage is then measured from the receiver by the analog to digital converter. This is the reference voltage that will be used for all subsequent measurements at a given frequency, and is called V_{sc} . To calculate the VSWR, the computer first measures the reflected voltage for a given state, which is called V_m . However, the voltage that the computer reports is not the actual voltage of interest. Let the voltage that the computer reports (as presented at the Y-output of the receiver) be called V_{rcvr} , and similarly the voltage that the computer reports from the receiver when a short circuit is attached $V_{rcvr,sc}$. A number of these voltages were compared to voltages measured with a hand-held multimeter and the calibration equation for V_m was found to be

$$V_m = 10^{3V_{rcvr}/2}. \quad (4.1)$$

Similarly, the calibration equation for V_{sc} is

$$V_{sc} = 10^{3V_{rcvr,sc}/2}. \quad (4.2)$$

These calibration equations were incorporated into the Visual Basic program that controls the switches in order to convert from the computer voltage to the voltage of

interest. Once the computer has obtained V_m and V_{sc} from (4.1) and (4.2) respectively, the reflection coefficient is calculated from

$$|\Gamma| = \frac{V_m}{V_{sc}}. \quad (4.3)$$

The VSWR is subsequently calculated from

$$VSWR = \frac{1 + |\Gamma|}{1 - |\Gamma|}. \quad (4.4)$$

This VSWR value is then written to a text file. Depending on the type of search being done, the program may then use this VSWR value to decide what state of the antenna to look at next.

4.3 Random searches

Since there are 2^{32} (4.3 billion) possible antenna states, it is impossible to exhaustively examine the behavior of the antenna at every state. Instead, a random selection of 75,000 states was examined, to get a statistical sense of the antenna performance. Note that 75,000 states represent 0.0017% of all possible states. To do these random search experiments, a large file of random numbers was first converted to binary. These binary numbers were then put into eight-bit strings for the computer to read. Since the prototype has 32 switches, four of these strings were used to set the 32 switches. When the computer encountered a 1, it would close the corresponding switch. When the computer encountered a 0, it would leave the corresponding switch open. Using a simple Visual Basic program, the computer was set up to run 75,000 of these random states and write the VSWR values to a text file. This process was then repeated at many different frequencies between 200 MHz and 900 MHz. The Visual Basic code used for this section of the thesis is given in Appendix A. These frequencies were arbitrarily chosen. Note that the same 75,000 states were run at

each frequency chosen.

The first frequency chosen was 200 MHz. At this frequency, there were many states with a VSWR greater than 50, but there were also many states with low VSWRs. The lowest VSWR found by the random search was 1.022. The histogram of all states with a VSWR less than 50 is shown in Figure 4.14. This distribution is strongly skewed toward the lower VSWR values. There were 7691 states with a VSWR less than 3, 3490 states with a VSWR less than 2, and 1043 states with a VSWR less than 1.5. That is 1.39% of states with a VSWR below 1.5, or just under 60 million states out of the possible 4.3 billion for this antenna. The histogram of states with a VSWR less than 2 is shown in Figure 4.15. In this range, the VSWRs are skewed towards the higher values closer to 2. There are less than 50 states with a VSWR less than 1.1.

The next frequency at which 75,000 random states were searched was 285 MHz. The lowest VSWR was 3.25. At this frequency, there were 6338 states with a VSWR below 50. The histogram of these states is shown in Figure 4.16. For each frequency, bin sizes were chosen so that there would be ten equally sized bins over the VSWR range for that frequency. There are only 29 states with a VSWR below 5 at 285 MHz. The rest of the states are fairly evenly distributed between a VSWR of 10 and a VSWR of 50.

The next random search frequency was 330 MHz. The lowest VSWR was 2.81. At this frequency, there were 41,596 states with a VSWR below 50, 16 states with a VSWR below 5, and only 1 state with a VSWR below 3. The histogram of states with VSWR below 50 is shown in Figure 4.17. From this plot, one can see that the distribution is strongly skewed towards VSWR values at the high end of the range.

The next frequency chosen was 380 MHz. The lowest VSWR of the 75,000 random states searched was 5.01. The histogram of all states is shown in Figure 4.18. One can see from this plot that there are very few states that exist with a VSWR under

10. In fact, the majority of states at this frequency fall between a VSWR of 10 and a VSWR of 20.

The next frequency at which 75,000 random states were searched was 400 MHz. The lowest VSWR found at this frequency was 1.036. The histogram of all states is shown in Figure 4.19. There is a sharp peak in the distribution around a VSWR of 10, but there are still quite a few states with a VSWR below 5. There were 1202 states with a VSWR below 3, 391 states with a VSWR below 2, and 165 states with a VSWR below 1.5. These states with a VSWR below 1.5 represent 0.2% of the 75,000 random states. We can then expect that out of the 4.3 billion possible states of the antenna, just under 9.5 million states will have a VSWR below 1.5. The histogram of states with a VSWR below 2 is shown in Figure 4.20. While these states tend toward the higher VSWRs in this range, there are still over 20 states with a VSWR less than 1.1, which is 0.03% of all states, or 1.29 million out of 4.3 billion.

The next frequency tested was 417 MHz. Out of the 75,000 random states, the lowest VSWR found was 1.019. There were 496 states with a VSWR over 50. The histogram of the states with a VSWR below 50 is shown in Figure 4.21. At this particular frequency, over half of the states fall between a VSWR of 1 and a VSWR of 5. There were 22,521 states that had a VSWR below 3, 11,649 states that had a VSWR below 2, and 4511 states that had a VSWR below 1.5. One could extrapolate that because 4511 states out of 75,000 had a VSWR below 1.5, it would be expected that 250 million of the 4.3 billion possible states of the antenna would have a VSWR below 1.5. That is just over 6% of states. The histogram of states with a VSWR below 2 is shown in Figure 4.22. This plot shows that below 2, most of the states fall between a VSWR of 1.3 and a VSWR of 2. However, there are still about 250 states with a VSWR of 1.1 or below. This is equivalent to one-third of one percent, or 14 million states with a VSWR below 1.1 out of the total 4.3 billion states of the antenna.

The next random search frequency chosen was 450 MHz. The lowest VSWR found was 1.029. Of the 75,000 random looks, 12,832 states had a VSWR value over 50. The histogram of states with a VSWR below 50 is shown in Figure 4.23. Again, there are a large number of states between a VSWR of 1 and a VSWR of 5, and the majority of the states fall below a VSWR of 20. There were 5975 states with a VSWR less than 3, 1927 states with a VSWR less than 2, and 394 states with a VSWR less than 1.5. The number of states with a VSWR less than 1.5 is 0.5% of the 75,000 random states. This would lead to around 22.5 million states out of the possible 4.3 billion states of the antenna having a VSWR below 1.5. This is far less than the number of states with a VSWR below 1.5 for 417 MHz, but still a very large number of states. The histogram of states with a VSWR below 2 is shown in Figure 4.24. This distribution is skewed toward the high end of the range, with the majority of states falling between a VSWR of 1.6 and a VSWR of 2. Very few states exist with a VSWR below 1.1.

The next frequency at which 75,000 random states were examined was 473 MHz. The lowest VSWR was 1.031. There were still a high number of states with poor VSWRs, with 14,781 states having VSWRs above 50. The histogram of the states with a VSWR below 50 is shown in Figure 4.25. Unlike the previous two frequencies, this distribution peaks between a VSWR of 25 and a VSWR of 30. Other than between 40 and 45, the states are nearly evenly distributed between all of the VSWRs from 1 to 50. There were 1084 states with a VSWR less than 3, 448 states with a VSWR less than 2, and 162 states with a VSWR less than 1.5. States with a VSWR less than 1.5 account for 0.2% of all states, or approximately 9 million of the total possible states. A graph showing the histogram of states with a VSWR less than 2 is shown in Figure 4.26. Once again, this distribution is skewed towards the higher VSWRs in this range. The majority of states have VSWRs greater than 1.4, and only 18 states (0.02%) have a VSWR below 1.1.

The next experimental frequency was 513 MHz. At this frequency, the lowest VSWR was 1.02. Only 42 states had a VSWR above 50. The states with a VSWR below 50 are shown in Figure 4.27. This histogram shows that well over half of all states out of the 75,000 random looks had a VSWR below 5. This is confirmed by the fact that 33,917 states had a VSWR below 3, 18,246 states had a VSWR below 2, and 7423 states had a VSWR below 1.5. At this particular frequency, nearly 10% of the states had a VSWR below 1.5, which would lead to 425 million states out of the possible 4.3 billion. The histogram of states with a VSWR below 2 are shown in Figure 4.28. This graph shows a nearly even distribution of states between VSWRs of 1.2 and 2. There are still close to 500 states that have a VSWR less than 1.1, or two-thirds of one percent. While this seems like a very small percentage, it would still be more than 28 million states out of the 4.3 billion possible for this antenna.

The next frequency chosen was 555 MHz. The lowest VSWR at this frequency was 1.11. Only 139 states had a VSWR greater than 50. The histogram of the states with VSWR below 50 is shown in Figure 4.29. This graph shows that the majority of states for this frequency lie between a VSWR of 15 and a VSWR of 30. There were 425 states with a VSWR less than 3, 139 states with a VSWR less than 2, and only 33 states with VSWRs less than 1.5. This is only 0.04% of the 75,000 states, which would mean slightly less than 2 million states out of all possible states would have a VSWR less than 1.5. A graph of the states with a VSWR less than 2 is shown in Figure 4.30. Again we see that the histogram is skewed toward the higher VSWR values in this range, with only four states below 1.1. Extrapolating out to the 4.3 billion possible states, this would only give 229 thousand states with a VSWR below 1.1, or 0.005%.

The next experimental frequency at which 75,000 random states were examined was 597 MHz. This frequency had a low VSWR of 1.4. The histogram of all states searched is shown in Figure 4.31. From the graph we can see that the majority of

states at this frequency lie between a VSWR of 10 and a VSWR of 20. Very few states have a VSWR below 5. In fact, there were 101 states with a VSWR less than 3, seven states with a VSWR below 2, and only two states with a VSWR below 1.5. Since there are so few states with low VSWRs, the histogram of states with VSWR below 2 will not be shown here.

The next frequency tested was 635 MHz. The lowest VSWR found by the random search at this frequency was 1.004. There were 1021 states with a VSWR greater than 50. The histogram of states with VSWR less than 50 is shown in Figure 4.32. From this graph, it is clear that over half the states at this frequency have a VSWR between 1 and 5. In fact, there were 19,796 states with a VSWR below 3, 10,842 states with a VSWR below 2, and 5449 states with a VSWR below 1.5. This is 7.3% of states with a VSWR below 1.5, or 312 million states out of the possible 4.3 billion. The histogram of states with VSWR below 2 is shown in Figure 4.33. There are close to 400 states with a VSWR below 1.1, or one half of one percent.

The next random search frequency chosen was 670 MHz. The lowest VSWR found at this frequency was 1.02. Only 131 states had a VSWR greater than 50. The histogram of states with VSWR below 50 is shown in Figure 4.34. As with some of the frequencies previously discussed, this graph shows that the majority of these states have VSWRs that lie between 1 and 5. There were 21,902 states with a VSWR below 3, 10,257 states with a VSWR below 2, and 3573 states with a VSWR below 1.5. This gives 4.8% of states with a VSWR below 1.5, or 204 million states out of the possible 4.3 billion. The states with a VSWR below 2 are shown in Figure 4.35. Again, the majority of these states fall between a VSWR of 1.5 and a VSWR of 2, but there are still over 200 states with a VSWR below 1.1, or approximately 0.3%.

The next frequency to be searched was 695 MHz. At this frequency, the low VSWR was 1.047. Figure 4.36 shows the histogram of all states. This distribution shows that the majority of states fall between a VSWR of 5 and a VSWR of 15.

There are few states with a VSWR below 5. In fact, there were 904 states with a VSWR below 3, 184 states with a VSWR below 2, and only 56 states with a VSWR below 1.5. These states with a VSWR less than 1.5 represent only three quarters of one percent of the 75,000 random looks. This extrapolates to 3.2 million states out of all of the possible states of the antenna. The histogram of states with VSWR below 2 is shown in Figure 4.37. While the distribution is skewed towards VSWRs closer to 2, there are still close to 15 states with a VSWR below 1.1. This is only 0.02% of states.

The next frequency chosen was 715 MHz. This frequency did not fare as well as some previous frequencies, with a low VSWR of only 1.8. The histogram of all states is shown in Figure 4.38. Once again, the majority of states at this frequency fall between VSWRs of 5 and 15. There are very few states with a VSWR below 5. There were 237 states with a VSWR below 3, but only 5 states with a VSWR below 2 and no states with a VSWR below 1.5. Since there were so few states with low VSWRs, the histogram of states with a VSWR below 2 is not shown here.

The next frequency tested was 770 MHz. The lowest VSWR at this frequency was 2.046. The histogram of all states with a VSWR below 50 is shown in Figure 4.39. The majority of states at this frequency have VSWRs below 10. There were 10,453 states with a VSWR below 5, but only 393 states with a VSWR below 3.

The next frequency at which 75,000 random states were searched was 840 MHz. The lowest VSWR found in this search was 3.529. The histogram of all states with a VSWR below 50 is shown in Figure 4.40. At this frequency, the majority of the states fall between a VSWR of 10 and a VSWR of 20. There are very few states with a VSWR below 10.

The final frequency tested was 900 MHz. The lowest VSWR found at this frequency was 4.968. As the frequency has been getting farther from the fundamental resonant frequencies of the antenna, the random searches have been having more

trouble finding low VSWR values. In fact, that was the only state with a VSWR below 5. The histogram of all states with a VSWR below 50 is shown in Figure 4.41. Once again, most of the states at this frequency fall between a VSWR of 10 and a VSWR of 20.

After all the random searches were complete, the VSWRs at each frequency were compared. The plot of VSWR vs. frequency is shown in Figure 4.42. We can see from this plot that at many of the frequencies searched, VSWRs very close to 1 were found. However, we can also see that there are large numbers of states with VSWRs above 10, some going as high as 100,000. The proportion of states with a VSWR below 3 in this sample at each frequency is shown in Figure 4.43. There seems to be no real pattern to these proportions. The proportion of states with a VSWR below 2 in this sample at each frequency is shown in Figure 4.44. Again, there is no discernable pattern, but the graph follows the same trend and the previous figure. The proportion of states with a VSWR below 1.5 in this sample is shown in Figure 4.45. With the exception of a few frequencies, generally this proportion is quite low, well under one percent. From these sample statistics, the population proportions and 95% confidence intervals can be computed. A 95% confidence interval is computed from $p \pm z\sigma_p$, where p is the sample proportion, z is 1.96 for a 95% confidence interval, and σ_p is computed from

$$\sigma_p = \sqrt{\frac{p(1-p)}{N}} \quad (4.5)$$

where N is the sample size. The proportion of states with VSWR below 3 is shown in Figure 4.46 with 95% confidence intervals. The confidence intervals are much larger for frequencies where the sample proportion was very small. Figure 4.47 shows the proportion of states with VSWR below 2 with 95% confidence intervals. The proportion of states with VSWR below 1.5 with 95% confidence intervals is shown in Figure 4.48. There are some frequencies where the random search of 75,000 states failed to find

a state with an acceptably low VSWR. For these frequencies, the genetic algorithm used in the next section will be much more useful than at the frequencies where large percentages of good states exist.

4.4 Genetic algorithm optimizations

Once the searches of 75,000 random states of the self-structuring patch antenna were complete, the next step was to use a genetic algorithm to find good states of the antenna more efficiently. The genetic algorithm that was used for the original self-structuring antenna research at MSU was modified by Raoul Ouedraogo for the self-structuring patch antenna system and also for any future self-structuring research at MSU. The experimental setup for the genetic algorithm optimization is identical to that of the random searches, with the exception that the output on the receiver was changed to the video log output. The reason for this change was because during the course of the genetic algorithm development, it was discovered that the Y-output of the receiver had begun to oscillate, giving unrepeatabable results. This was not an issue at the time of the random search tests. The voltage that the computer reports from the video log output is called V_{log} , and the reflected voltage for a given state is called V_m . For the video log output, the calibration equation was found through experimentation to be

$$V_m = 10^{(V_{log}-0.244)/0.165}. \quad (4.6)$$

The VSWR is then computed from (4.4), where V_{sc} is given by

$$V_{sc} = 10^{(V_{log,sc}-0.244)/0.165} \quad (4.7)$$

and $V_{log,sc}$ is the voltage that the computer reports when a short circuit is attached.

The Visual Basic code for the genetic algorithm is given in Appendix B. In this particular genetic algorithm, the parameters that can be varied include the population

size, number of generations, and mutation probability. The crossover probability is set to 0.7 for all tests. After trying several other fitness functions, the fitness function chosen was to maximize $V_{log,sc} - VoltAvg$, where $V_{log,sc}$ is the same as defined above and $VoltAvg$ is the same parameter as V_{log} . $VoltAvg$ is the average of 50 voltage measurements that the computer takes in quick succession. $V_{log,sc}$ is different for each optimization frequency and is measured before the test is started. The initial population is randomly chosen and each state's fitness is evaluated. This fitness then is used to decide which members of the population will mate, or cross over. Once the crossovers are complete, the next generation is made up of some combination of states of the current population and their offspring. Since each generation will have the same number of states as the initial population, the remainder of the population that is not filled by offspring or existing states is filled by randomly chosen new states.

The genetic algorithm optimizations were run at the same frequencies that were chosen for the random search tests. This was done so that a direct comparison could be made between the random searches and the genetic algorithm. The purpose of using the genetic algorithm to search through the states is to find states that are as good or better than the random searches found in less looks. Once a good state was found, this state was set and the self-structuring patch antenna was hooked up to the network analyzer to examine its return loss and bandwidth. Since the antenna had to be physically disconnected from the equipment and carried to the network analyzer, small differences will be seen between the VSWR values found in the small anechoic chamber used in the experimental setup and the return loss plots seen on the network analyzer.

The first frequency at which the genetic algorithm optimization was run was 200 MHz. The lowest VSWR found by the random search at this frequency was 1.022. When the genetic algorithm was run, the lowest VSWR that it found was 1.0088. This VSWR was found after a population of 200 was run for 30 generations. The

return loss plot for this state is shown in Figure 4.49. The low point of the return loss curve is -33 dB at 200.3 MHz. This state has an input impedance of $48.5+j1.6\Omega$ and a bandwidth of 3.61%.

The next frequency to be tested was 285 MHz. At this frequency, the lowest VSWR that the random search found was 3.25. When the genetic algorithm was run, the lowest VSWR found was 2.588. A population size of 200 was used and the algorithm was run for 30 generations. The return loss plot for this state is shown in Figure 4.50. No bandwidth was calculated for this state because the low point of the return loss is only -5.3 dB. This state has an input impedance of $18.2+j21.6\Omega$.

The next frequency searched was 330 MHz. The lowest VSWR found by the random search was 2.81. The genetic algorithm found a VSWR of 2.56 after 30 generations with a population size of 200. The return loss plot for this state is shown in Figure 4.51. Once again, no bandwidth can be calculated for this state because the lowest point of the return loss curve is -7.8 dB. This state has an input impedance of $24.1+j21.1\Omega$. One possible explanation for why the VSWR values have been high for the last two frequencies is that these frequencies are below the fundamental resonant frequency of the self-structuring patch antenna.

The next frequency at which the genetic algorithm optimization was run was 380 MHz. The random search made it clear that there are very few good states at this frequency when the lowest VSWR that it found was 5.01. This was confirmed by the genetic algorithm. A population of 200 was run for 60 generations and the lowest VSWR that was found was 7.06. The return loss plot for this state is shown in Figure 4.52. This is an interesting case because the frequency of optimization is not the point with the best return loss. The lowest point on the return loss curve is at -19.5 dB and occurs at 389.1 MHz. The state has a bandwidth of 1.9%. However, if the intent was to use the antenna at 380 MHz, this is not helpful. The input impedance of this state is $60.1+j88.7\Omega$ at 380 MHz, with a return loss of only -4 dB. Another

interesting thing to note is that this frequency is very close to one of the natural resonant frequencies of the self-structuring patch antenna.

The next frequency optimized was 400 MHz. At this frequency, the lowest VSWR found in the random search was 1.036. The population size for the genetic algorithm was set to 200, and it was run for 30 generations. A state was found with a VSWR of 1.027. The return loss plot is shown in Figure 4.53. The low point of the curve is at 400.4 MHz with a return loss of -21.5 dB. The bandwidth for this state is 1.56%, and this state has an input impedance of $49.2-j8.6\Omega$.

The genetic algorithm optimization was then run at 417 MHz. The lowest VSWR from the random search was 1.019. For the genetic algorithm optimization, the population size was set to 250 and 30 generations were run. This population size was chosen because a search with a population size of 200 failed to find a VSWR lower than 1.019 after 40 generations. Using the larger population, a state with a VSWR of 1.013 was found. This state has an input impedance of $49.8-j3\Omega$. The return loss plot is shown in Figure 4.54. The low point is at 417.8 MHz, with a return loss of -29.9 dB. This state has a bandwidth of 1.96%.

The next frequency of optimization was 450 MHz. The lowest VSWR that the random search found was 1.029, and Figure 4.24 showed very few states with VSWRs below 1.1. The population for the genetic algorithm was set to 200, and it was run for 40 generations. After these 40 generations, the lowest VSWR found was 1.0076. The return loss plot for this frequency is shown in Figure 4.55. The bandwidth for this state is 2.03%. The low point of the return loss curve is at 450.8 MHz, with a return loss of -26.3 dB. This state has an input impedance of $49.1-j5.2\Omega$.

The genetic algorithm was then run at 473 MHz. The random search found a VSWR low of 1.031. The population at this frequency was set to 200, and 30 generations were run. The genetic algorithm was able to find a state with a VSWR of 1.0186. Figure 4.56 shows the return loss plot for this state. The low point is at

473.1 MHz, with a return loss of -43.3 dB. The bandwidth for this state is 1.11% with an input impedance of $50.6-j3.6\Omega$.

The next frequency at which the genetic algorithm was run is 513 MHz. When the random search was run, the lowest VSWR that was found was 1.02. For this frequency, the population size was again set to 200 and the algorithm was run for 30 generations. The lowest VSWR found was 1.008. Figure 4.57 shows the return loss plot for this state. The low point occurs at 513.9 MHz, with a return loss of -38.6 dB. The input impedance for this state is $49.0-j4.9$, with a bandwidth of 2.04%.

The next optimization frequency was 555 MHz. The lowest VSWR that was found by the random search was 1.11. A population of 200 was run for 30 generations, and found a low VSWR of 1.0094. Figure 4.58 shows the return loss plot for this state. The low point is at 554.5 MHz with a return loss of -27.6 dB. The bandwidth of this state is 2%, and it has an input impedance of $49.0-j4.2\Omega$.

The genetic algorithm was then run at 597 MHz. This was one of the frequencies at which the random search failed to find a state with a VSWR below 1.1, and in fact at this particular frequency there were only two states with a VSWR below 1.5. The lowest VSWR found in the random search was 1.4. The population for the genetic algorithm was set to 200. After 60 generations, the lowest VSWR was 1.624. While this is not lower than the state found by the random search, this was the lowest VSWR value found in several genetic algorithm searches at this frequency. The return loss plot for this frequency is shown in Figure 4.59. The low point is at 601.44 MHz, with a return loss of -36.3 dB. The bandwidth of this state is 2.18%, with an input impedance of $50.1+j1.5$. This is one example where the lowest point in the return loss curve does not necessarily occur at the frequency of optimization. The VSWR at the optimization frequency is not particularly low, but one can see from the return loss plot that it would be lower at 601.44 MHz. Optimizing at a certain frequency does not guarantee that frequency having the lowest possible VSWR. It is also interesting

to note that this frequency is one of the resonant frequencies of the antenna, and the genetic algorithm failed to find a state that had a better return loss than the -13.2 dB of the fundamental resonance. It should be noted that the genetic algorithm did not look at the state with all switches off at this frequency.

Due to equipment failure, no genetic algorithm data is available for 630 MHz.

The next frequency the genetic algorithm was run at was 670 MHz. The lowest VSWR that the random search found was 1.02. The genetic algorithm was run with a population of 200 for 30 generations, after which a VSWR of 1.027 was found. While the VSWR found by the genetic algorithm is not lower than the lowest VSWR found by the random search, it is still very close, and only 6000 states were searched. The possibility remains that if more states were searched, a better VSWR value would have been found. The return loss plot for this frequency is shown in Figure 4.60. The low point of the return loss curve is at 672.7 MHz, with a return loss of -24.1 dB. This state has a bandwidth of 2.97% and an input impedance of $51.6 + j6.1\Omega$.

The genetic algorithm was then run at 695 MHz. The lowest VSWR found by the random search was 1.047. A population of 200 was run for 40 generations. The lowest VSWR found was 1.0065. The return loss plot is shown in Figure 4.61. The low point is at 694.5 MHz, with a return loss of -38 dB. This state has a bandwidth of 2.4% and an input impedance of $51.1 + j0.5\Omega$.

The next optimization frequency that was chosen was 715 MHz. When the random search was run at this frequency, the lowest VSWR that was found was 1.8. The population for the genetic algorithm was set to 200 and run for 40 generations. The lowest VSWR that was found was 1.59. While this is a better VSWR value than the random search found, it is still not particularly low. Figure 4.62 shows the return loss plot, where the low point is at 717.8 MHz with a return loss of -19.4 dB. The bandwidth of this state is 1.28%, with an input impedance of $50 + j10.6\Omega$. This somewhat low percentage bandwidth is most likely due to the fact that the return

loss of this state is not as low as some of the others searched.

Due to equipment failure, no genetic algorithm data is available for 770 MHz.

The next frequency of optimization was 840 MHz. The lowest VSWR found by the random search at this frequency was 3.529. The genetic algorithm found a state with a VSWR of 5.16 after 30 generations of 200 states. This state has an input impedance of $60+j100$. Since there is no real resonance at this frequency, the return loss plot is not shown here.

The final frequency at which the genetic algorithm was run was 900 MHz. The lowest VSWR found during the random search was 4.968. After the genetic algorithm was run for 30 generations with 200 states, a VSWR of 6.419 was found. Like the last few frequencies, it looks like there are very few good states at this high frequency. This makes it very difficult for even the genetic algorithm to find good states. The input impedance of this state is $99.3+j93.6\Omega$, and once again the return loss plot is not shown because there is no resonance at this frequency.

The chromosomes for the best states found in the genetic algorithm searches at each frequency are given in Table 4.1. In order to correspond these chromosomes to actual switches on the self-structuring patch antenna prototype, a bit-to-switch number reference chart is given in Table 4.2. Figure 4.63 then shows the switch numbers on the prototype.

A table with the lowest VSWR found by the random search at the target frequency, the lowest VSWR found by the genetic algorithm at the target frequency, the measured resonant frequency, the return loss at the measured resonant frequency, the percentage bandwidth of the state found by the genetic algorithm at the measured resonant frequency, and the input impedance of the state found by the genetic algorithm at the measured resonant frequency is given in Table 4.3. The percentage bandwidths of these states remain fairly constant, between 1% and 4%. The genetic algorithm generally found better VSWR values than the random search did, in far

less looks. A graph directly comparing the lowest VSWR values found by the random search and the genetic algorithm is given in Figure 4.64. The frequencies at which the genetic algorithm did not find a lower VSWR value are either far above the fundamental resonant frequencies of the antenna or very near to one of the fundamental resonant frequencies. For all of the frequencies investigated, it is certainly possible that lower VSWR values could be found with further optimization of the genetic algorithm. This could include changing the population size, crossover probability, number of generations, or any of the other genetic algorithm parameters. Interestingly, some of the frequencies at which the genetic algorithm failed to find a very good state are frequencies which are very close to the fundamental resonant frequencies of the antenna. However, it should be noted that the genetic algorithm did not look at the state with all switches off, but the best states at these frequencies do have only at most 5 switches turned on.

4.5 Electromagnetic compatibility investigations

Another area of investigation for the self-structuring patch antenna was EMC issues. The experimental setup for both the random searches and the genetic algorithm optimizations includes a 64 line ribbon cable with 32 control lines and 32 ground lines. Once this ribbon cable reaches the control board, all 32 ground lines terminate at a common point and become one ground path. Because of this, there is the potential for differential mode current to develop, raising an EMC issue. When the switches on the self-structuring antenna are switched at a very fast rate, the computer sends a clock signal down the ribbon cable that will be at the switching frequency. For the experiments described here, a frequency of 150 Hz was chosen (150 states/sec). The spectrum of this signal contains both the fundamental switching frequency as well as its harmonics. In a real-world system, the switching frequency would most likely be far greater than 150 Hz, which would lead to more EMC issues.

A block diagram of the experimental setup is shown in Figure 4.65. A current probe is placed around the common ground wire in order to measure the harmonics of the control signal. The probe will actually measure the total current going to ground, which is made up of both common mode and differential mode current. The computer used for these tests is the same Fujitsu Lifebook that was used for the random search experiments. The spectrum analyzer used is an Agilent 4936B, and the current probe is a Hewlett-Packard 8710-1744 current probe. To set up the experiments, the National Instruments 50-pin cable and the 10-pin ribbon cable are connected to the control board just as they were for the random search tests. This time, the BNC and feed cables are left disconnected since no reflected voltage measurements are made. The ribbon cable from the antenna is connected to the control board as well. The input of the spectrum analyzer is then connected to the current probe, which is placed around the common ground wire.

To run the EMC experiments, the switching speed was set to 150 switches per second. When the switches are switching, 16 waveforms are averaged on the spectrum analyzer. The spectrum is shown in Figure 4.66. The fundamental has an amplitude of 62.1 dB μ V at 148.43 Hz. There are 16 higher frequency harmonics between the fundamental and 5 kHz. For this spectrum, only odd harmonics are present.

The background noise was then measured, as shown in Figure 4.67. Here the fundamental is at 60 Hz. While these peaks are small, they are the result of AC current leaking into the system. The fundamental when the switches are switching has an amplitude approximately 50 dB higher than this background.

To reduce the currents on the control lines, blocking inductors are used. Since these harmonic frequencies are low, using ferrite materials has little to no effect. A 390 μ H inductor and a 65 μ H inductor are put in series with the ground wire on the control board. The spectrum is then measured, as shown in Figure 4.68. The fundamental has been reduced to 55.5 dB μ V, which is a 6.6 dB reduction in amplitude. A few

odd harmonics are now present as well, so there are 22 higher frequency harmonics between the fundamental and 5 kHz. While this is not a large reduction, the fact that these radiated emissions are at such low frequencies means that they will never be an EMC issue for agencies such as the Federal Communications Commission.

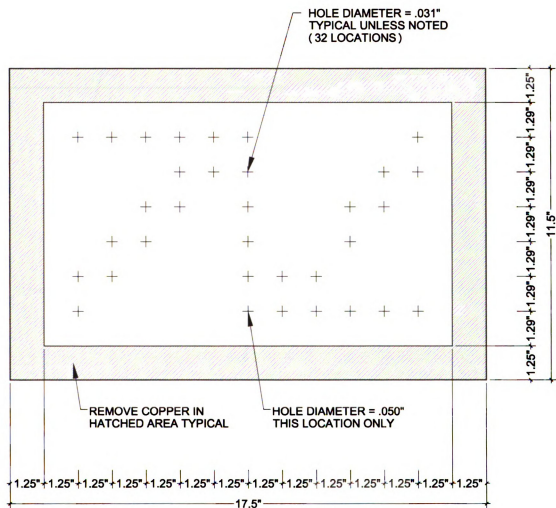


Figure 4.1. Top of self-structuring antenna circuit board as laid out in AutoCAD. All dimensions given in inches.

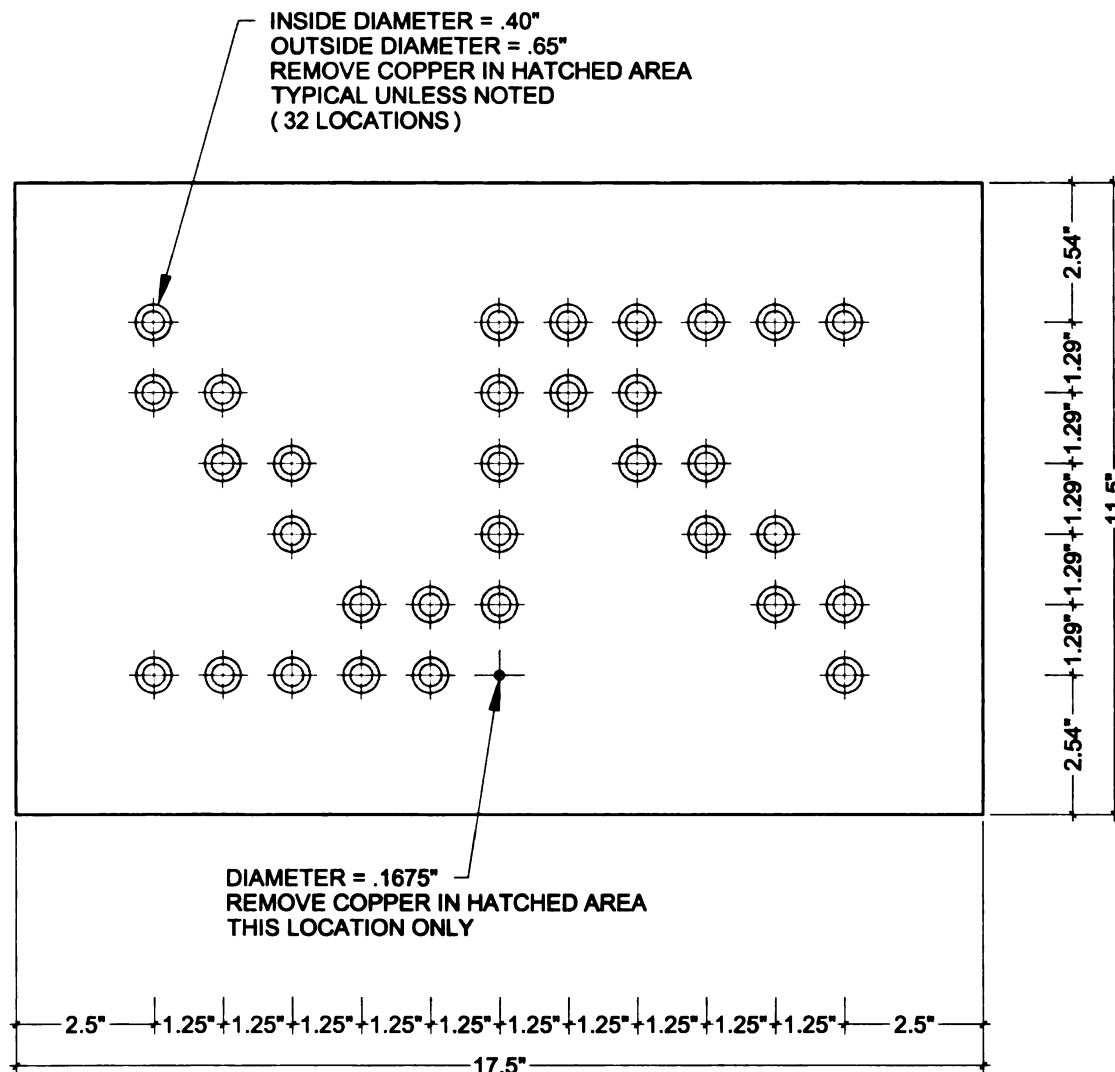


Figure 4.2. Bottom of self-structuring antenna circuit board as laid out in AutoCAD.
 All dimensions given in inches.

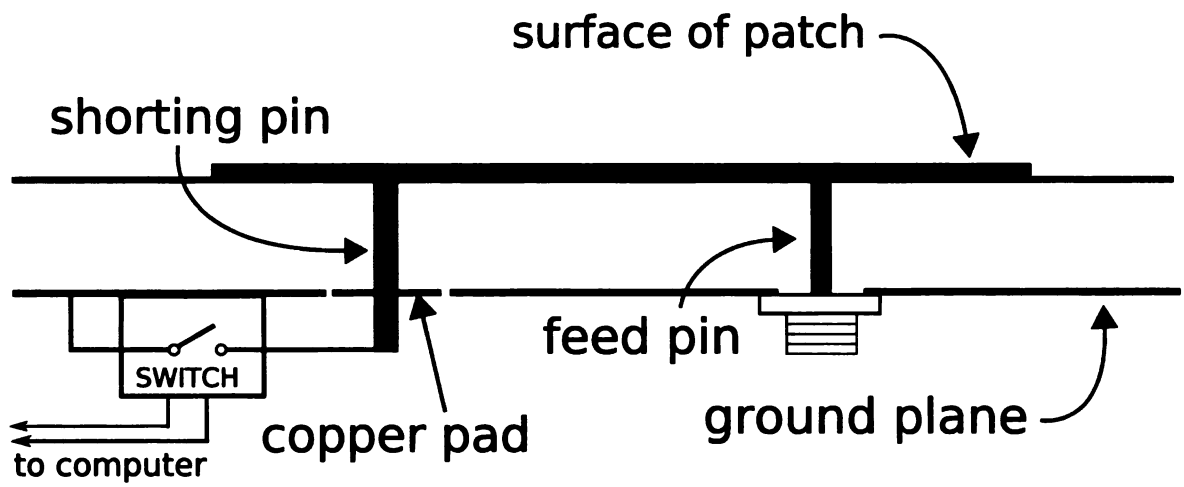


Figure 4.3. Diagram of shorting pin connections.

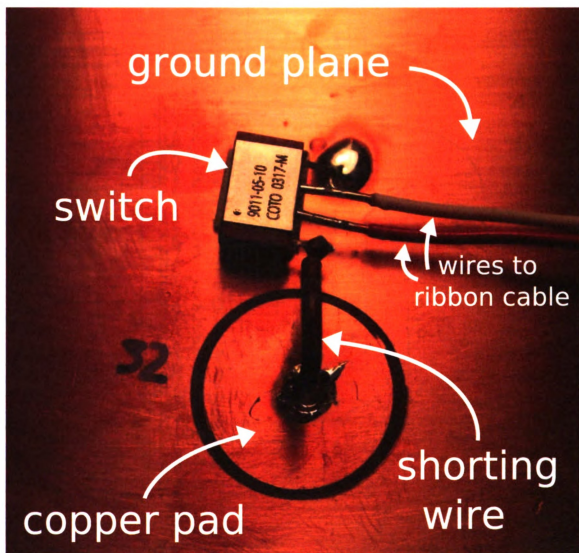


Figure 4.4. Photograph of one of the switches on the self-structuring patch antenna.

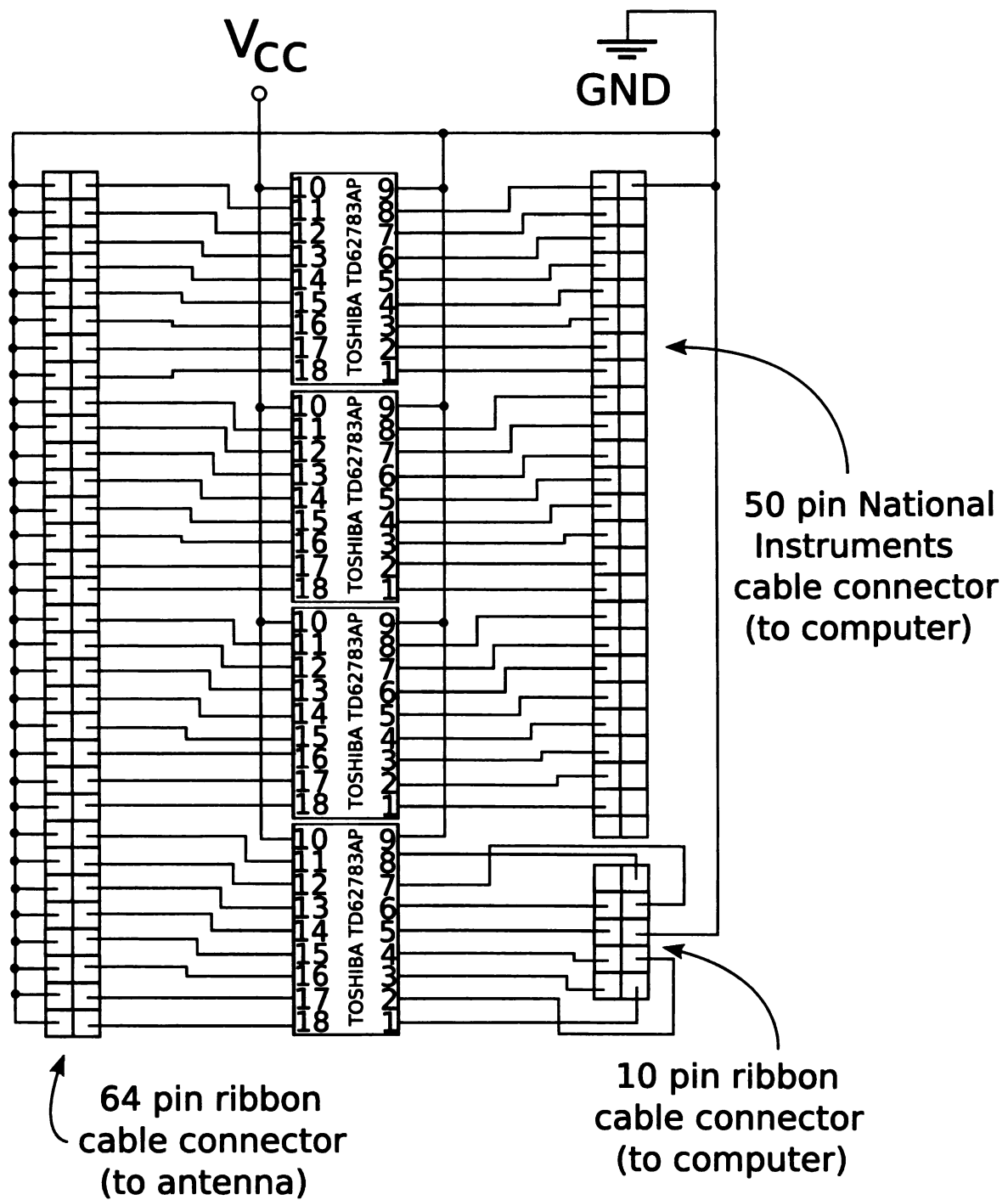


Figure 4.5. Schematic of the control board.

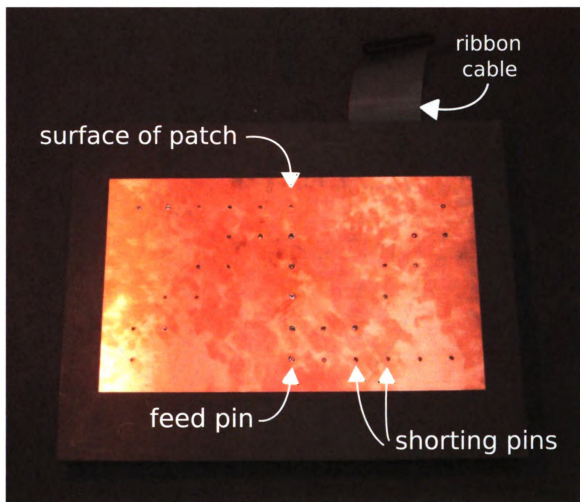


Figure 4.6. Photograph of the surface of the self-structuring patch antenna.

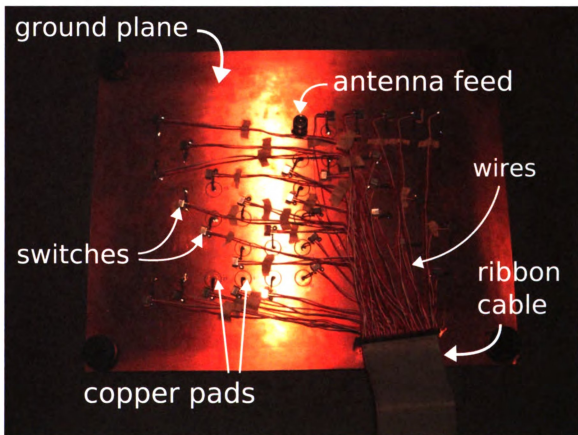


Figure 4.7. Photograph of the ground plane of the self-structuring antenna with switches and control lines.

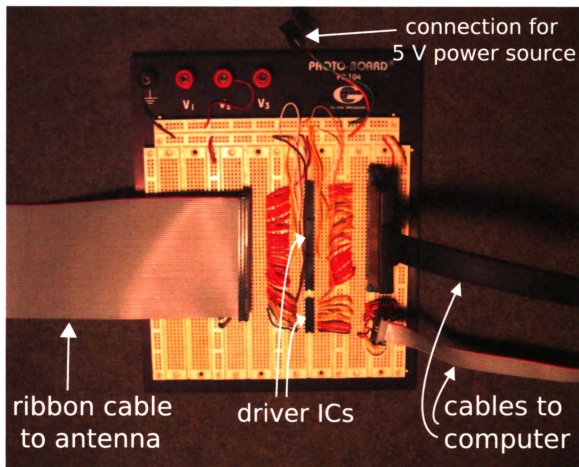


Figure 4.8. Photograph of the control board.

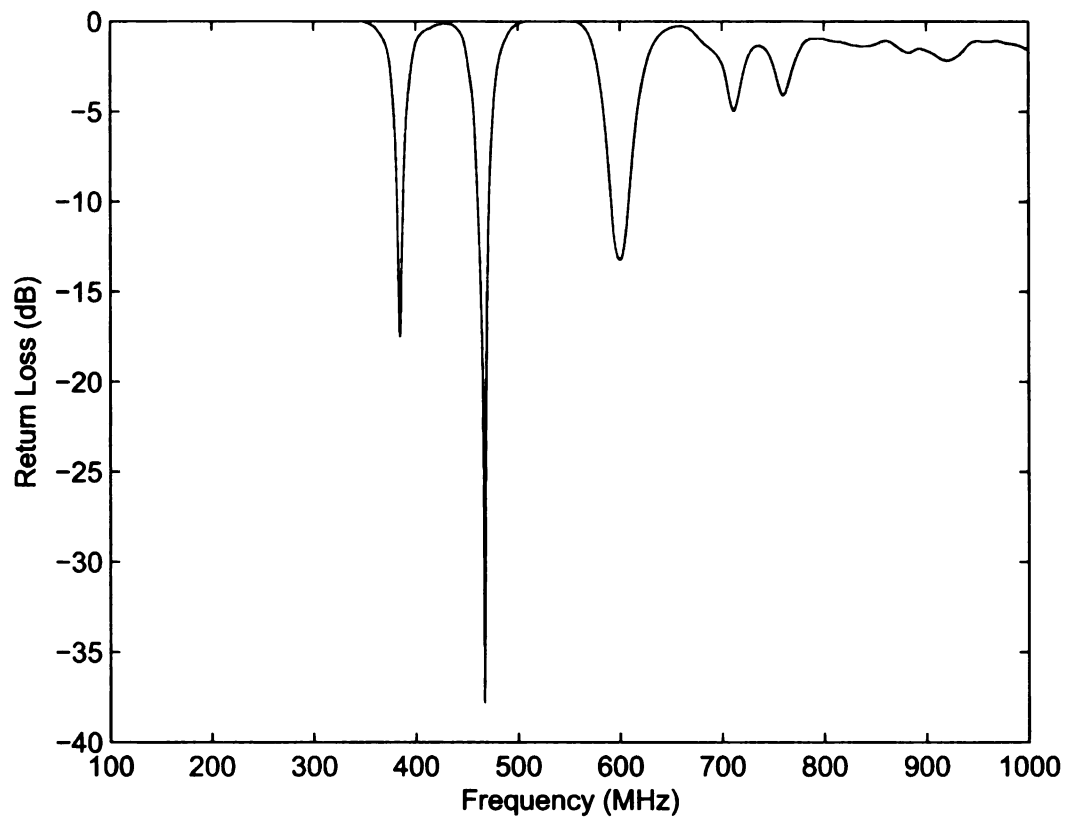


Figure 4.9. Return loss plot for the self-structuring patch antenna with all switches disconnected.

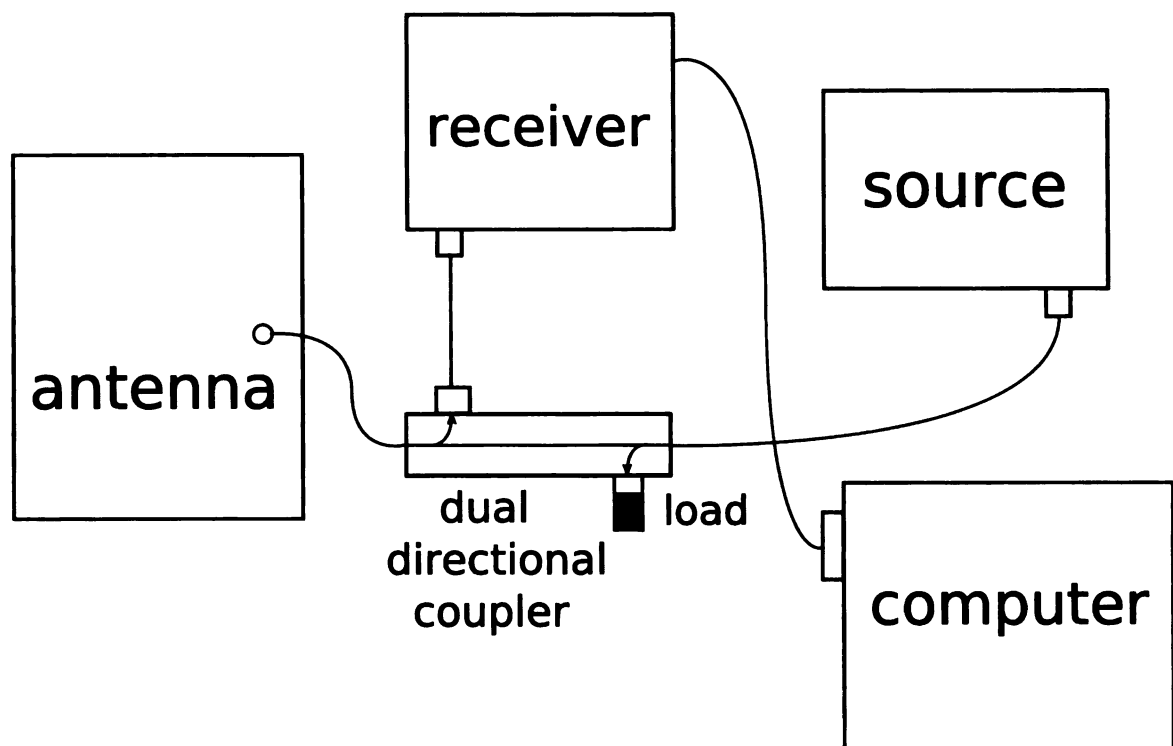


Figure 4.10. Block diagram of the experimental setup.

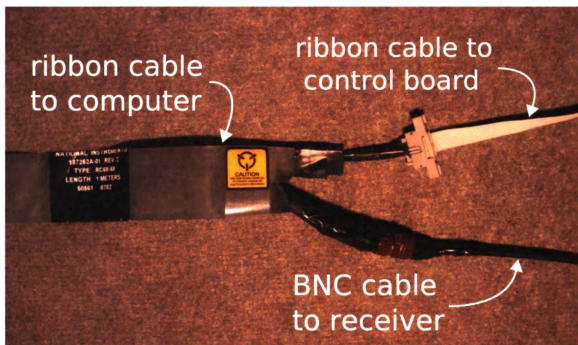


Figure 4.11. Photograph of the National Instruments ribbon cable splitting into a BNC cable and a 10-line ribbon cable.

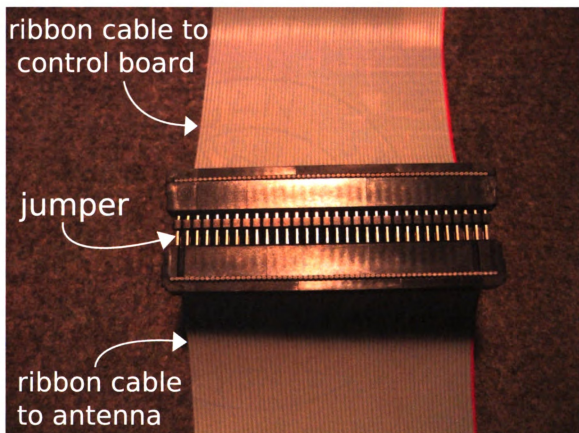


Figure 4.12. Photograph of the connection between the two ribbon cables.

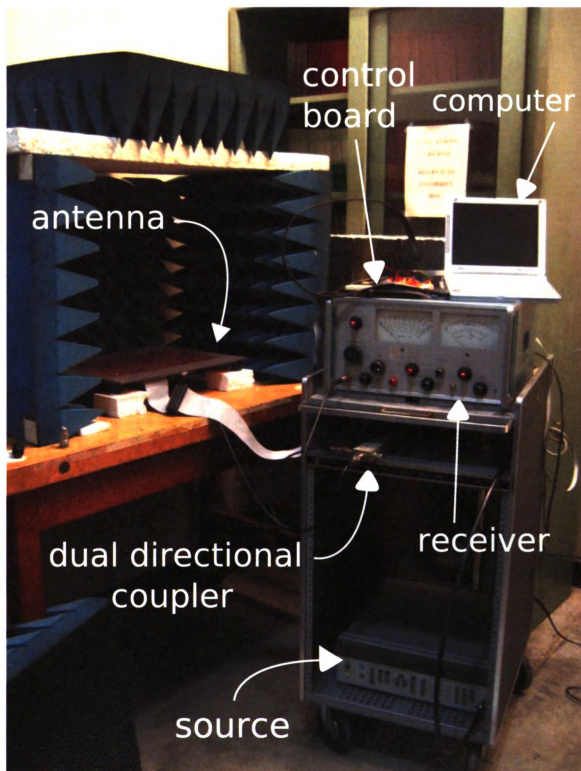


Figure 4.13. Photograph of the experimental setup.

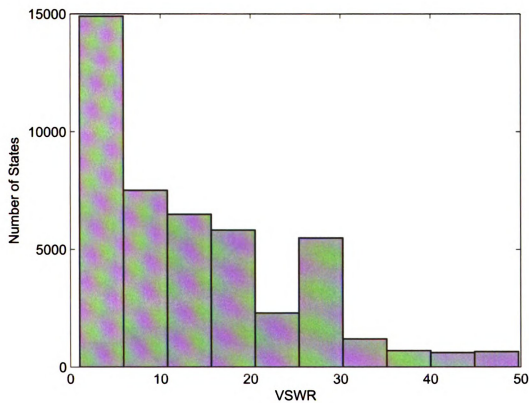


Figure 4.14. Number of states per VSWR, showing all states with VSWR under 50 at 200 MHz.

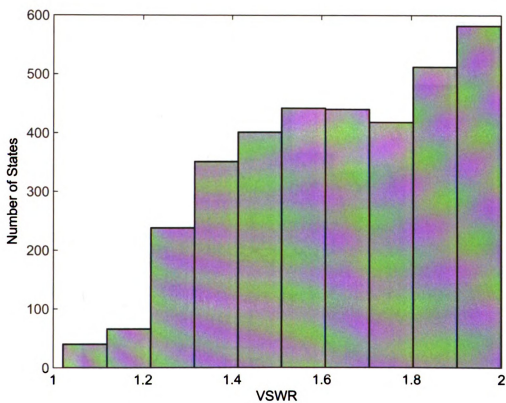


Figure 4.15. Number of states per VSWR, showing all states with VSWR under 2 at 200 MHz.

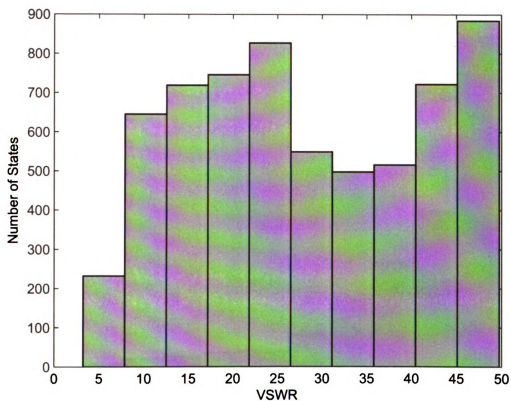


Figure 4.16. Number of states per VSWR, showing all states with VSWR under 50 at 285 MHz.

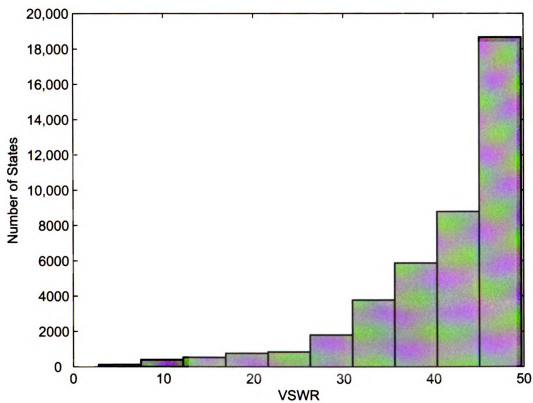


Figure 4.17. Number of states per VSWR, showing all states with VSWR under 50 at 330 MHz.

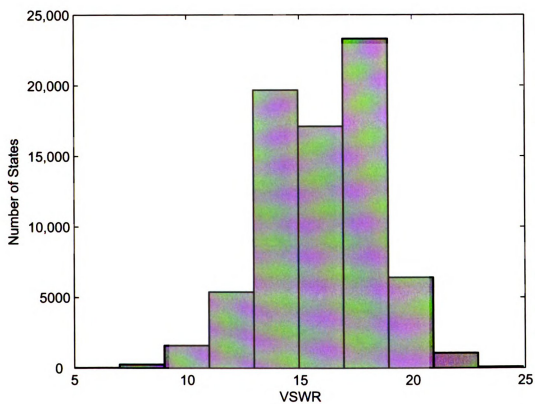


Figure 4.18. Number of states per VSWR, showing all states at 380 MHz.

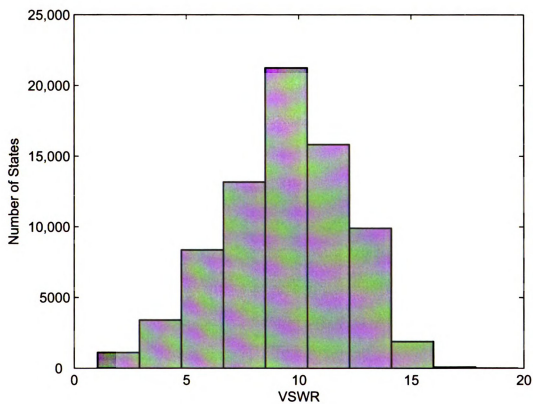


Figure 4.19. Number of states per VSWR, showing all states at 400 MHz.

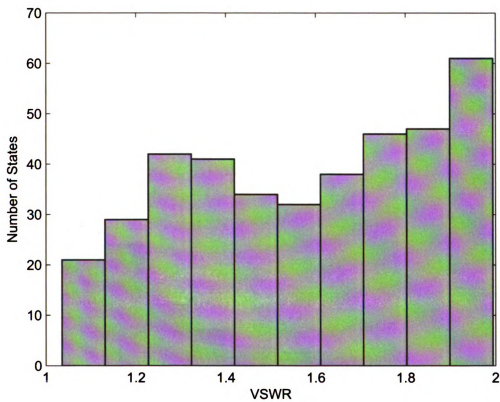


Figure 4.20. Number of states per VSWR, showing all states with VSWR under 2 at 400 MHz.

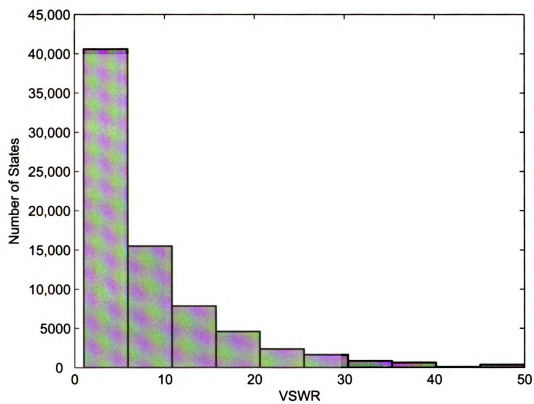


Figure 4.21. Number of states per VSWR, showing all states with VSWR under 50 at 417 MHz.

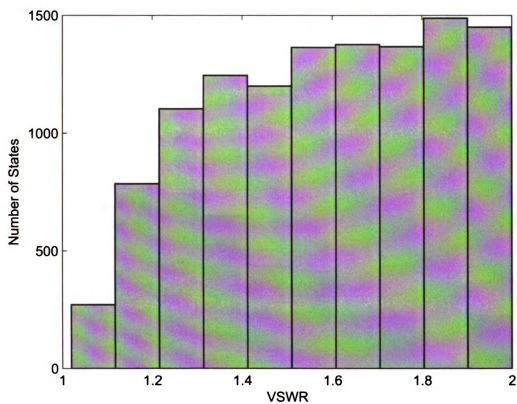


Figure 4.22. Number of states per VSWR, showing all states with VSWR under 2 at 417 MHz.

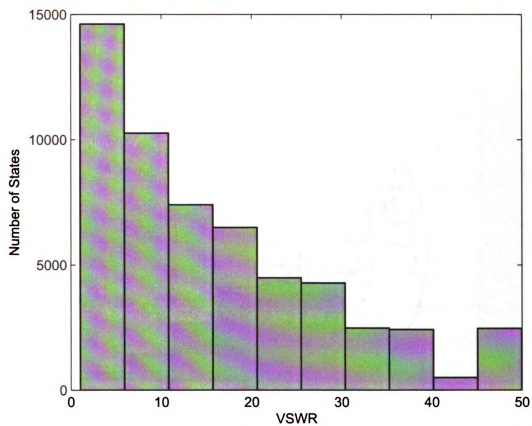


Figure 4.23. Number of states per VSWR, showing all states with VSWR under 50 at 450 MHz.

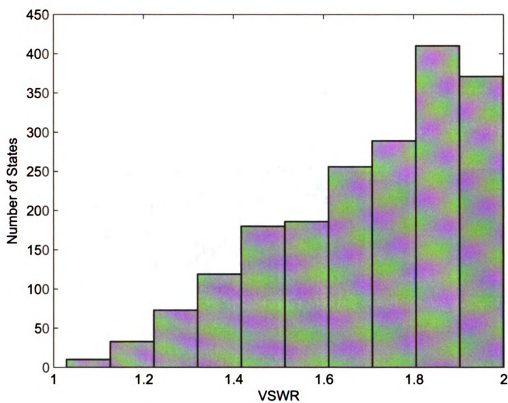


Figure 4.24. Number of states per VSWR, showing all states with VSWR under 2 at 450 MHz.

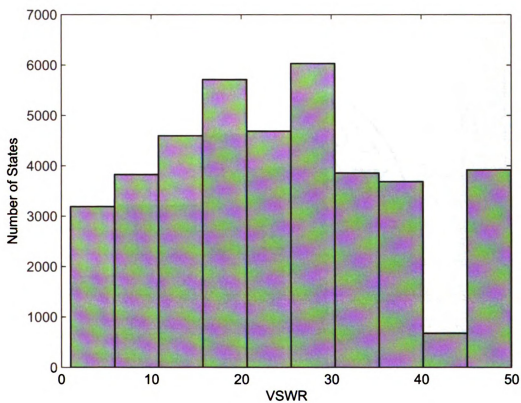


Figure 4.25. Number of states per VSWR, showing all states with VSWR under 50 at 473 MHz.

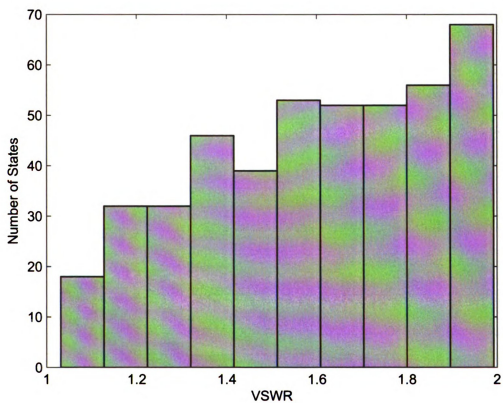


Figure 4.26. Number of states per VSWR, showing all states with VSWR under 2 at 473 MHz.

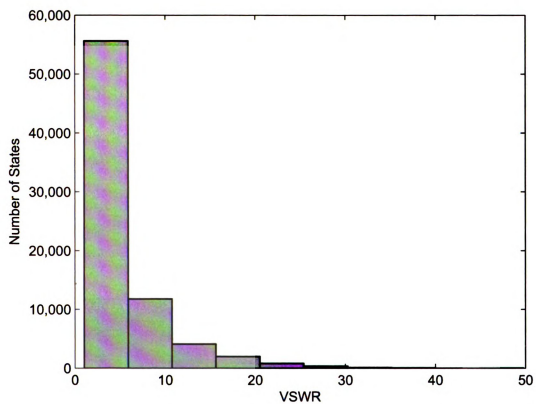


Figure 4.27. Number of states per VSWR, showing all states with VSWR under 50 at 513 MHz.

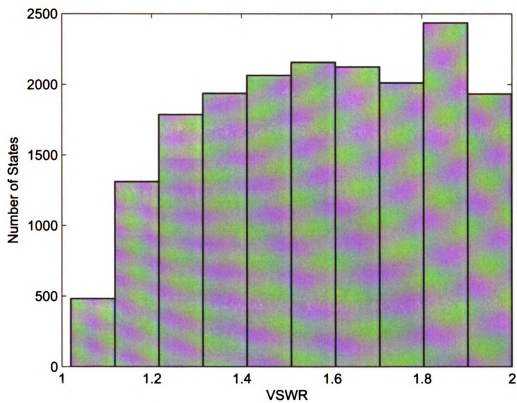


Figure 4.28. Number of states per VSWR, showing all states with VSWR under 2 at 513 MHz.

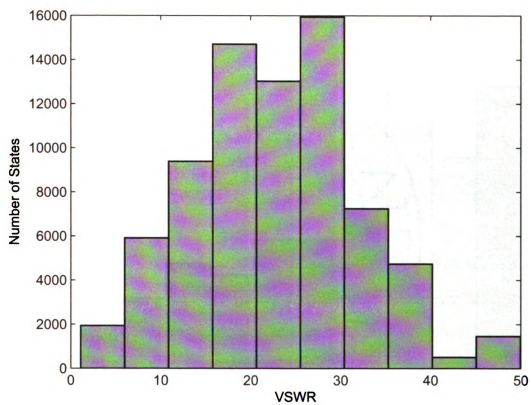


Figure 4.29. Number of states per VSWR, showing all states with VSWR under 50 at 555 MHz.

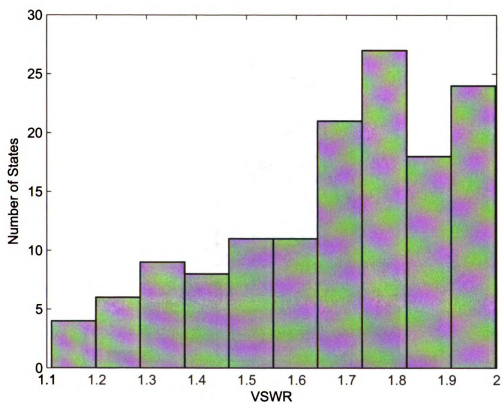


Figure 4.30. Number of states per VSWR, showing all states with VSWR under 2 at 555 MHz.

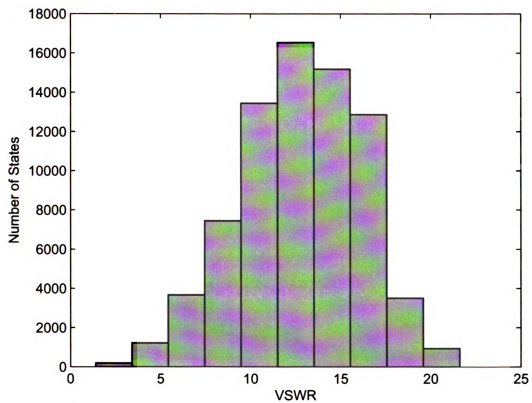


Figure 4.31. Number of states per VSWR, showing all states at 597 MHz.

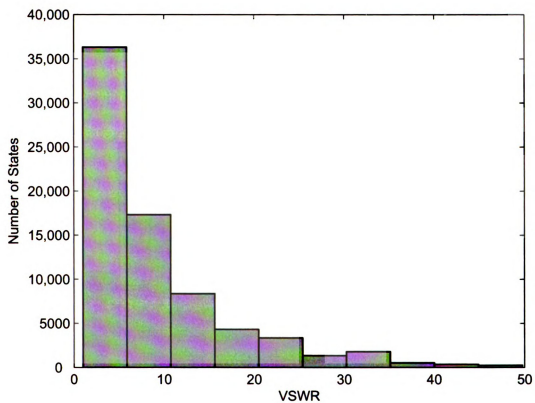


Figure 4.32. Number of states per VSWR, showing all states with VSWR under 50 at 635 MHz.

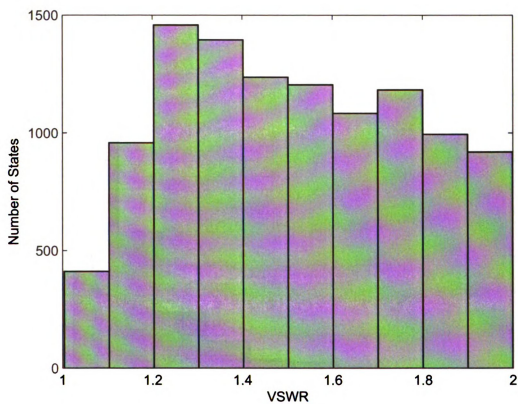


Figure 4.33. Number of states per VSWR, showing all states with VSWR under 2 at 635 MHz.

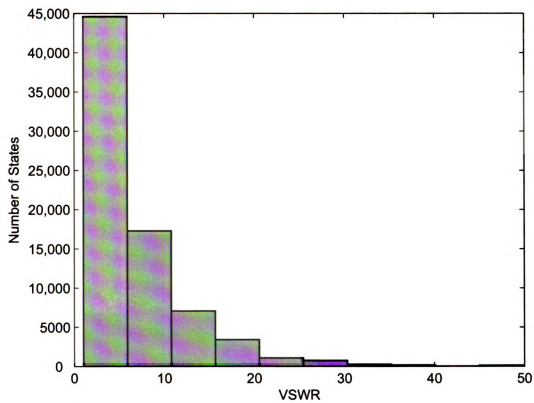


Figure 4.34. Number of states per VSWR, showing all states with VSWR under 50 at 670 MHz.

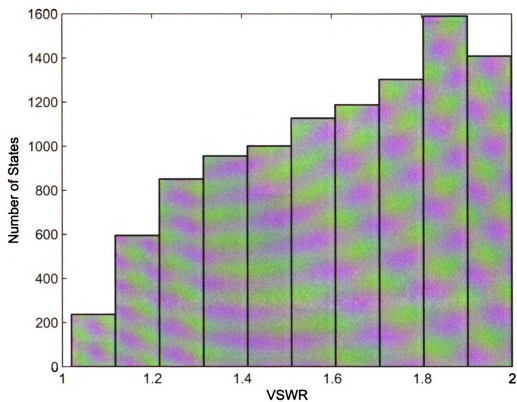


Figure 4.35. Number of states per VSWR, showing all states with VSWR under 2 at 670 MHz.

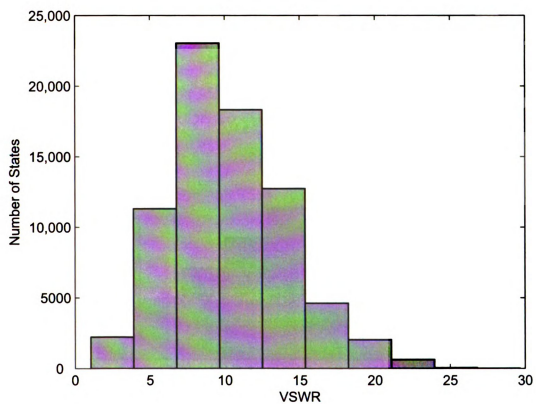


Figure 4.36. Number of states per VSWR, showing all states at 695 MHz.

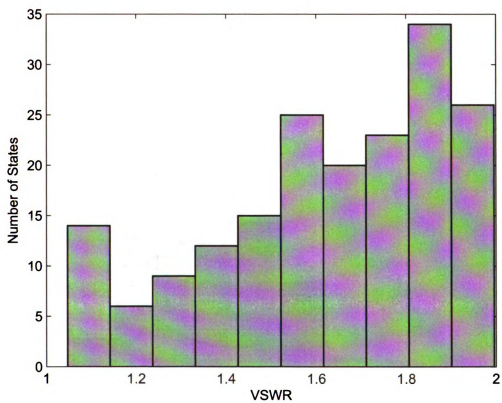


Figure 4.37. Number of states per VSWR, showing all states with VSWR under 2 at 695 MHz.

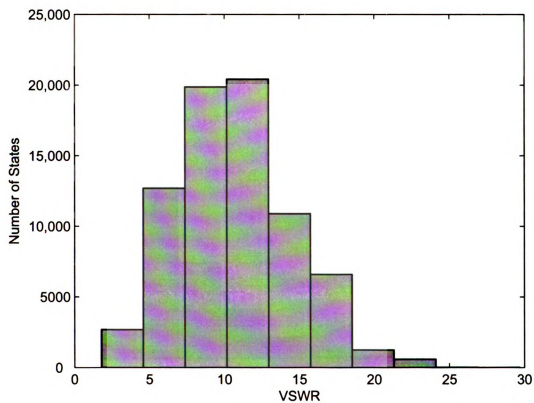


Figure 4.38. Number of states per VSWR, showing all states at 715 MHz.

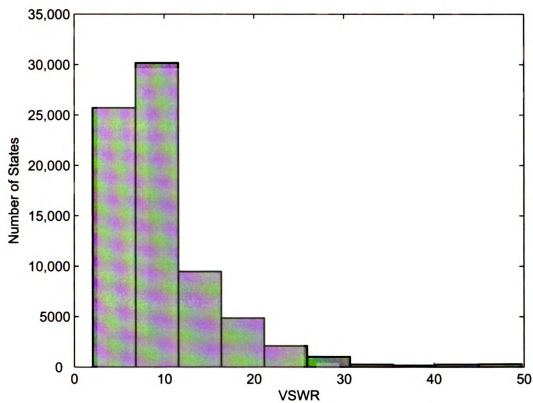


Figure 4.39. Number of states per VSWR, showing all states with VSWR less than 50 at 770 MHz.

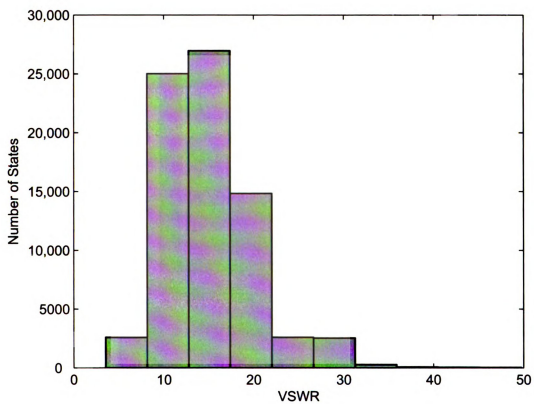


Figure 4.40. Number of states per VSWR, showing all states with VSWR less than 50 at 840 MHz.

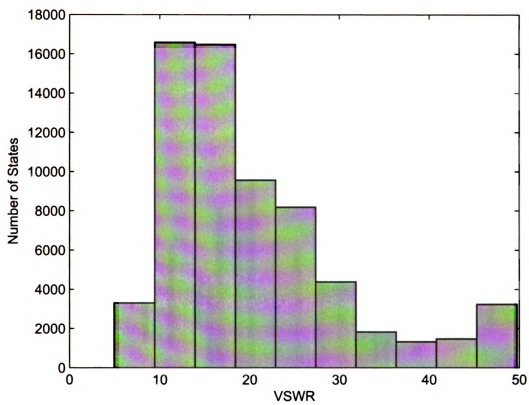


Figure 4.41. Number of states per VSWR, showing all states with VSWR less than 50 at 900 MHz.

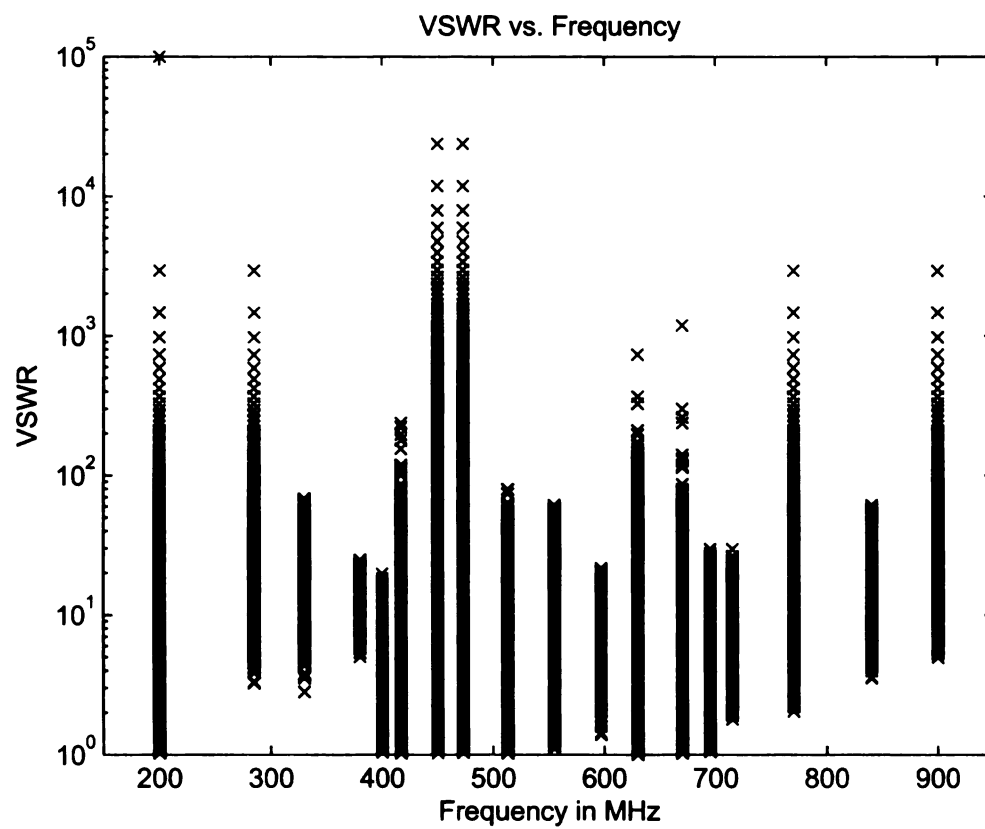


Figure 4.42. VSWR vs. frequency for all randomly searched states.

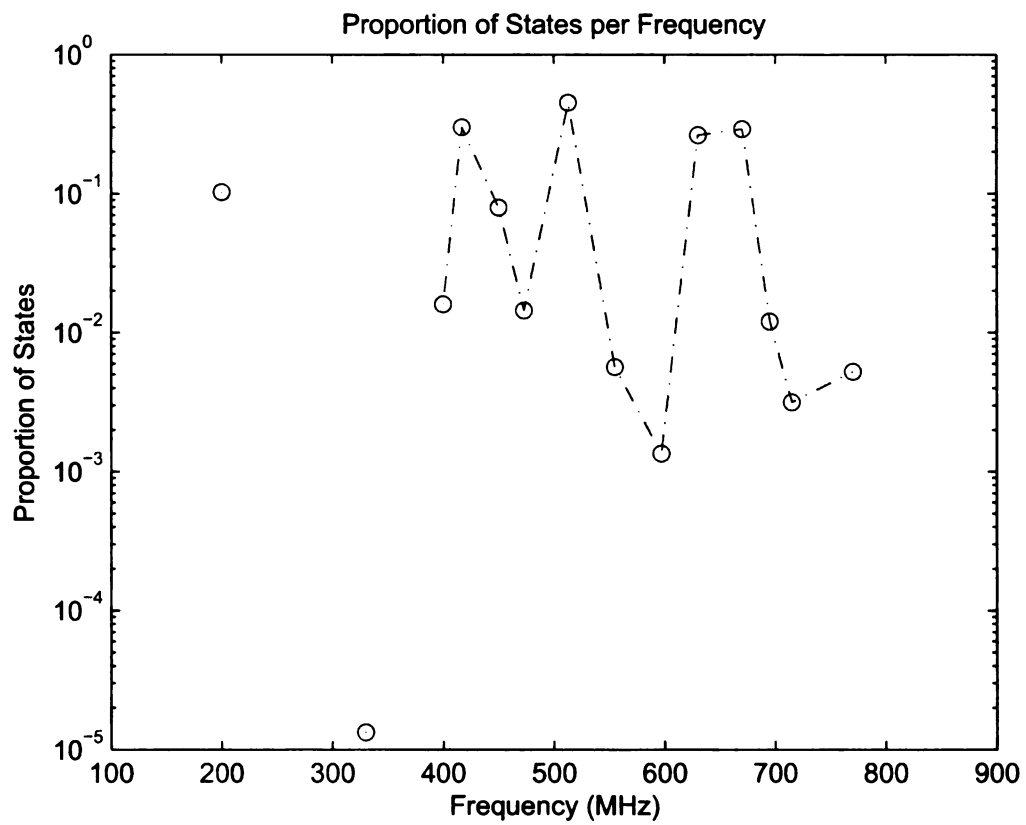


Figure 4.43. Sample proportion of states with a VSWR below 3 for each randomly searched frequency.

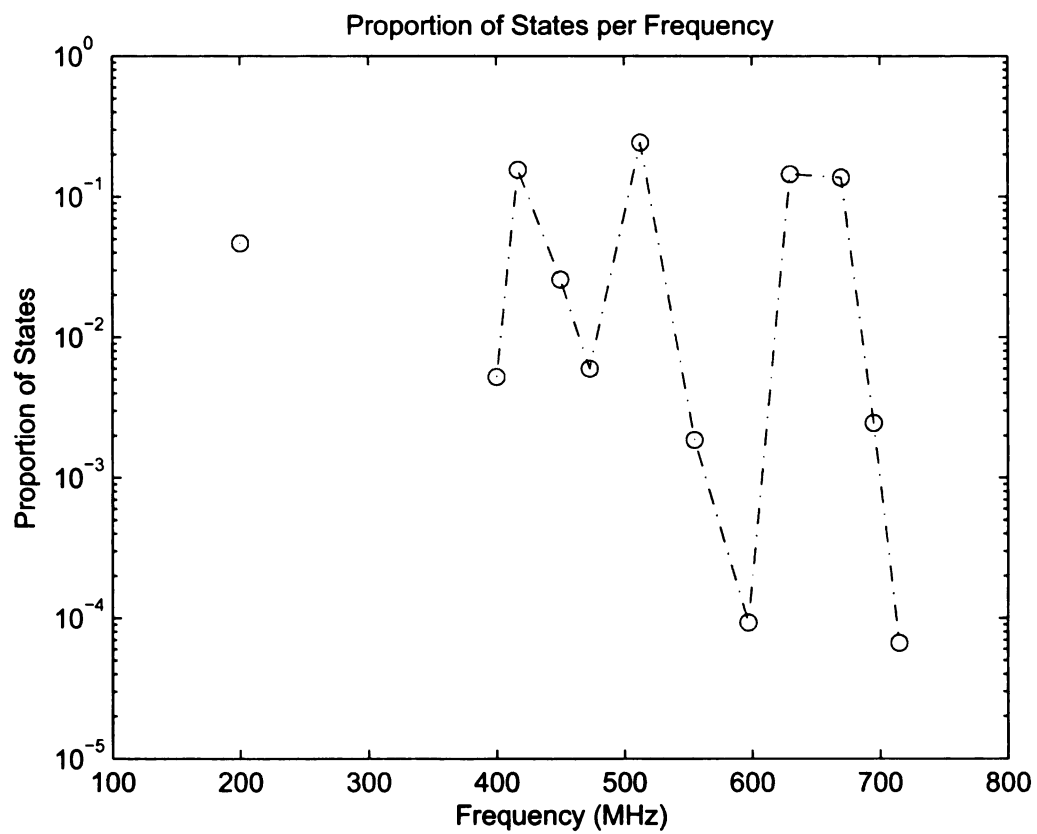


Figure 4.44. Sample proportion of states with a VSWR below 2 for each randomly searched frequency.

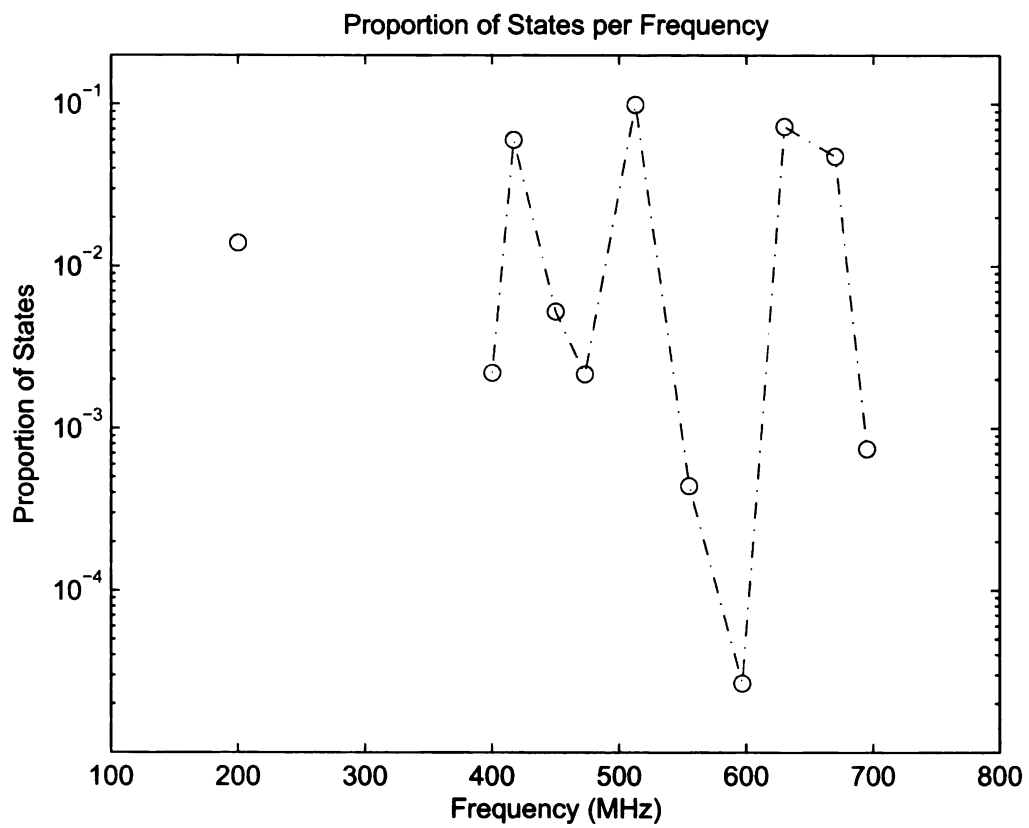


Figure 4.45. Sample proportion of states with a VSWR below 1.5 for each randomly searched frequency.

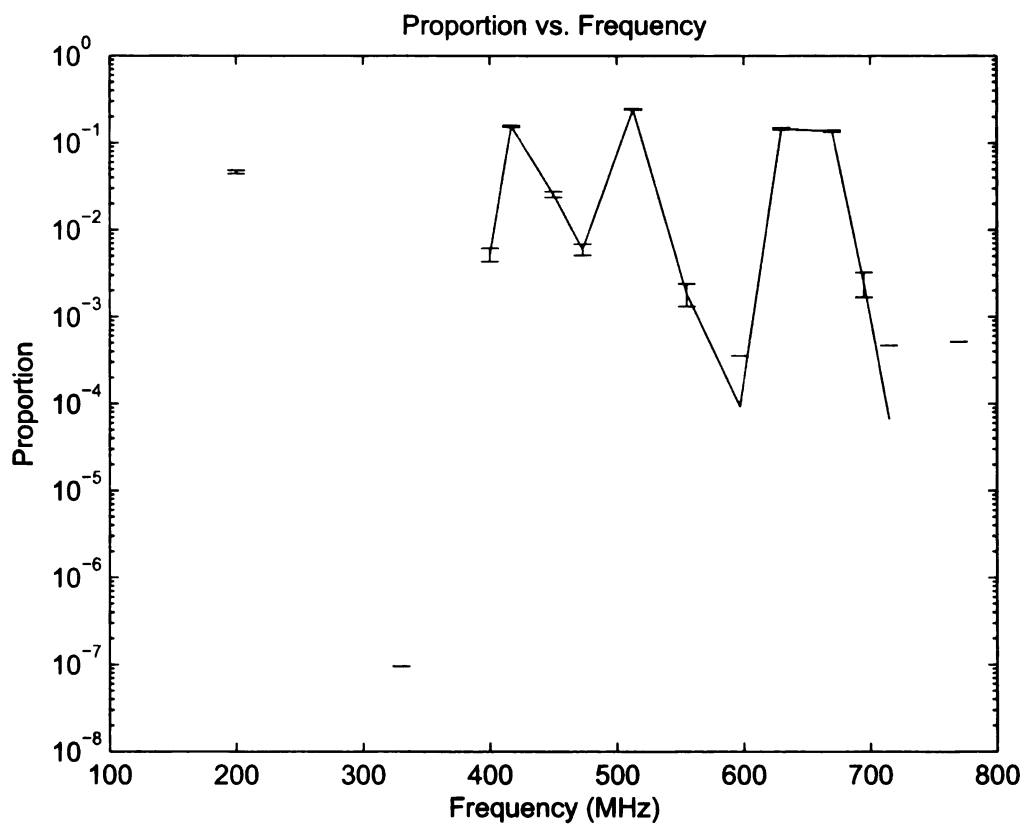


Figure 4.46. Proportion of states with a VSWR below 3 for each randomly searched frequency. Error bars are 95% confidence intervals.

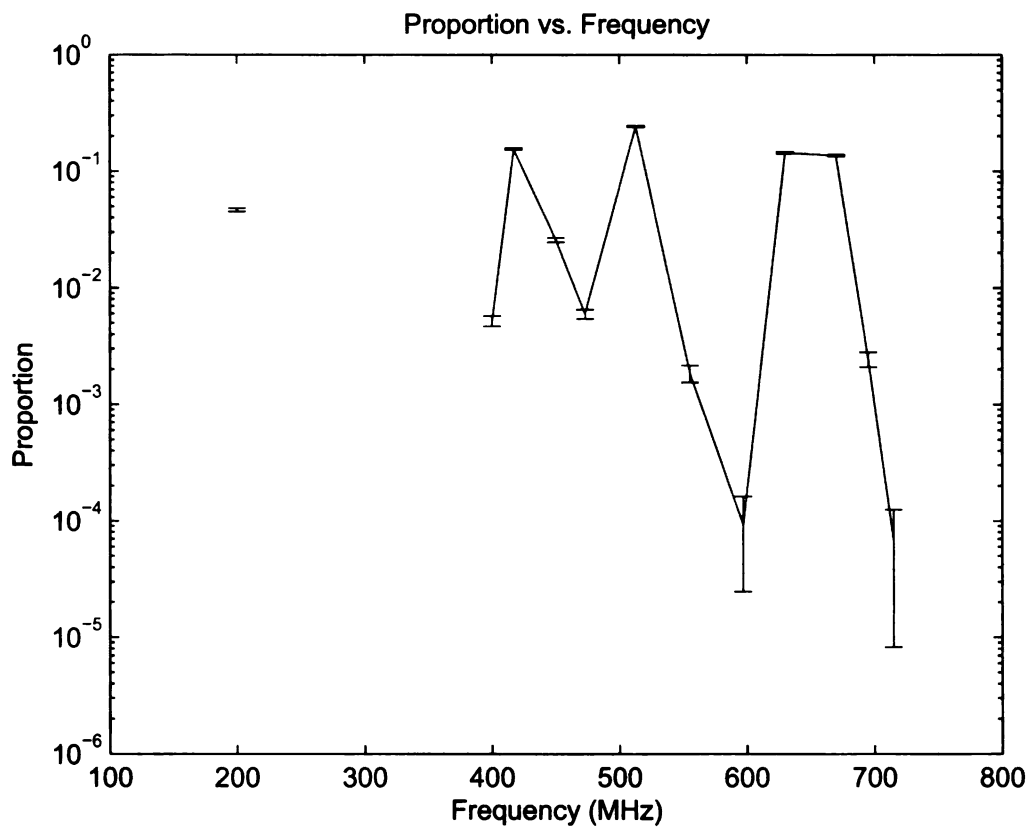


Figure 4.47. Proportion of states with a VSWR below 2 for each randomly searched frequency. Error bars are 95% confidence intervals.

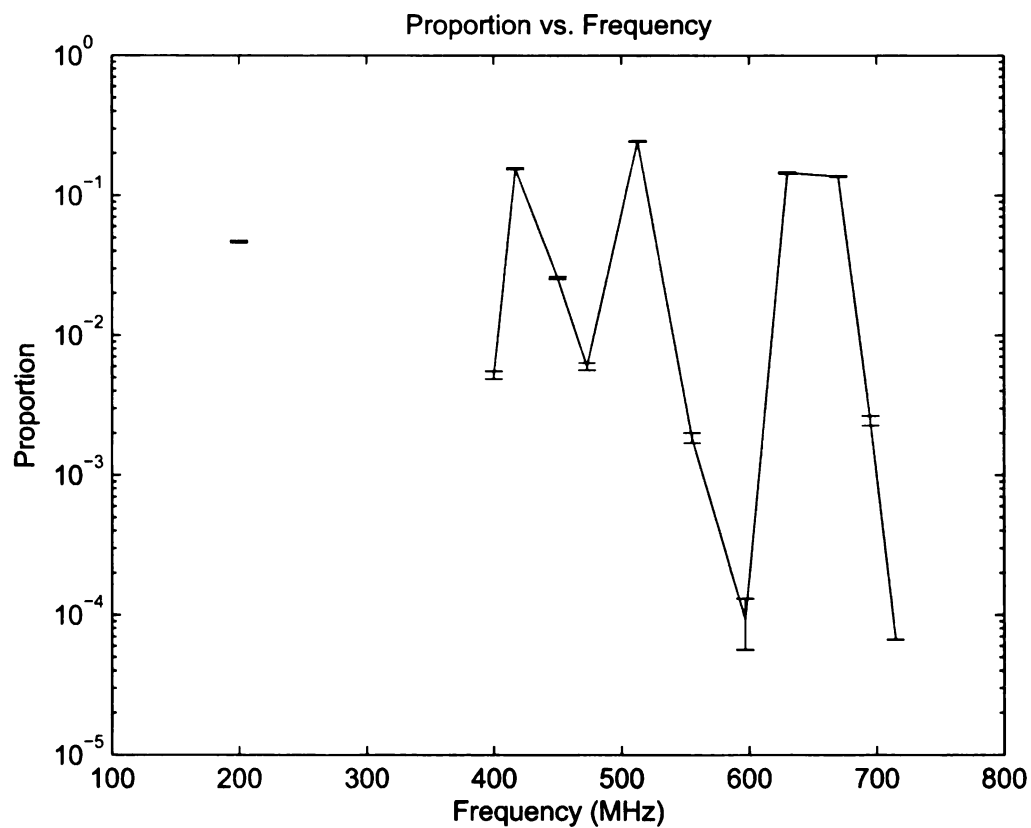


Figure 4.48. Proportion of states with a VSWR below 1.5 for each randomly searched frequency. Error bars are 95% confidence intervals.

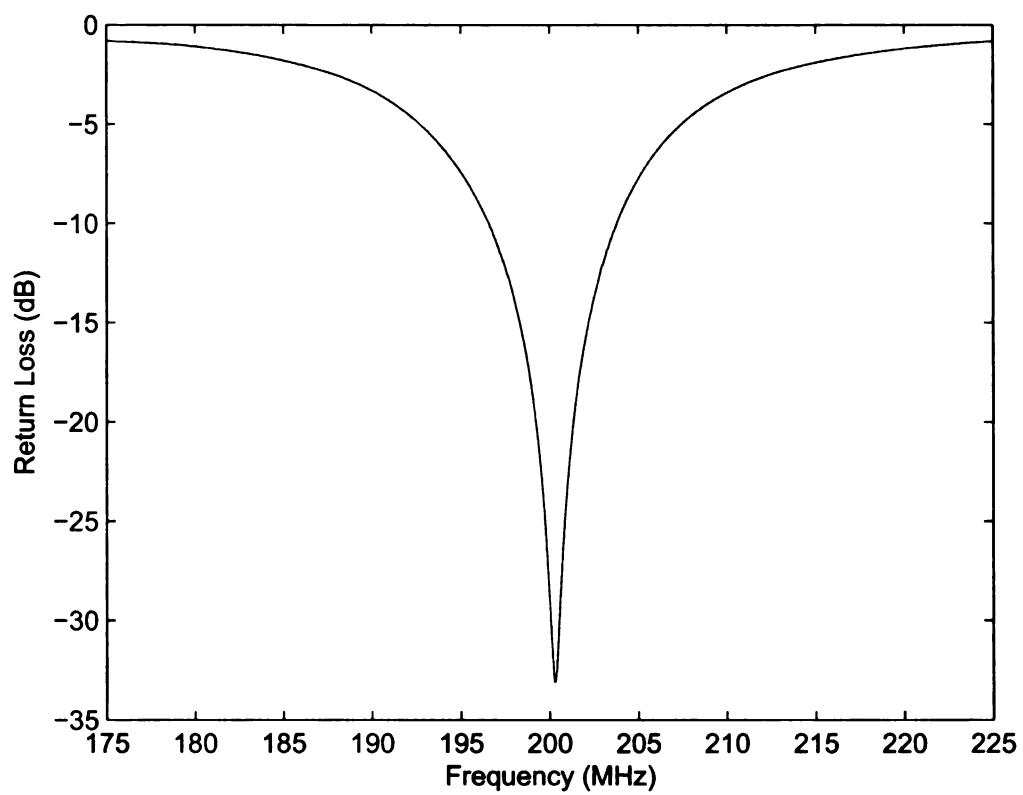


Figure 4.49. Return loss for a state with VSWR of 1.0088 at 200 MHz.

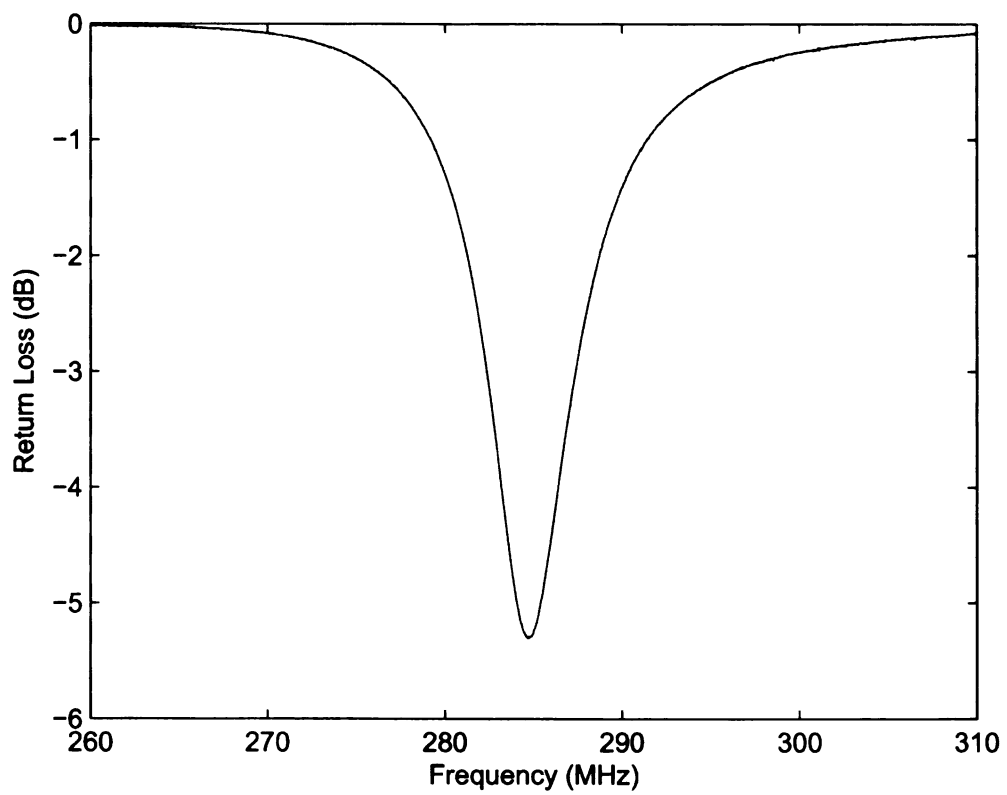


Figure 4.50. Return loss for a state with VSWR of 2.588 at 285 MHz.

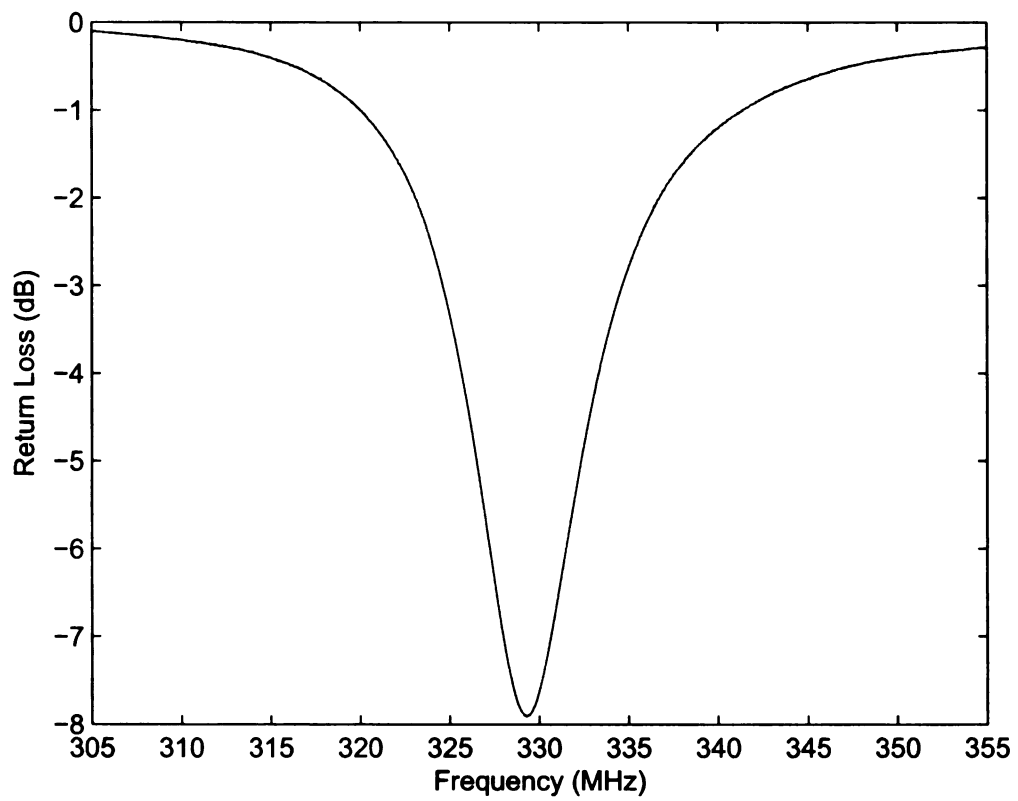


Figure 4.51. Return loss for a state with VSWR of 2.56 at 330 MHz.

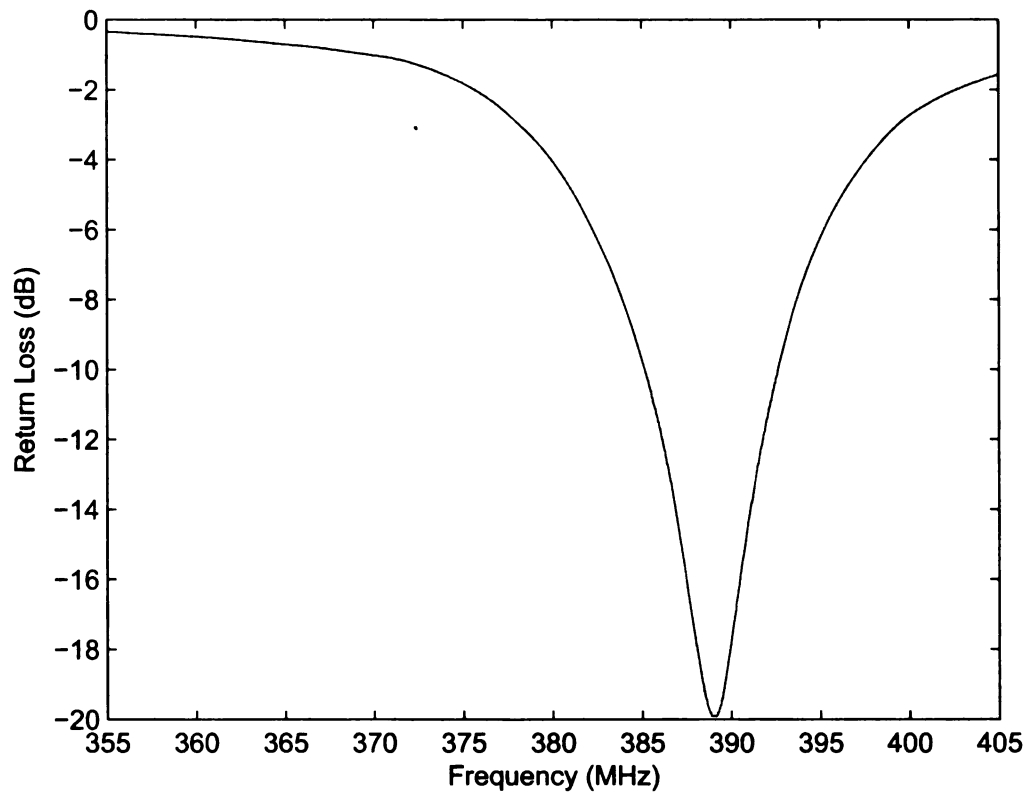


Figure 4.52. Return loss for a state with VSWR of 7.06 at 380 MHz.

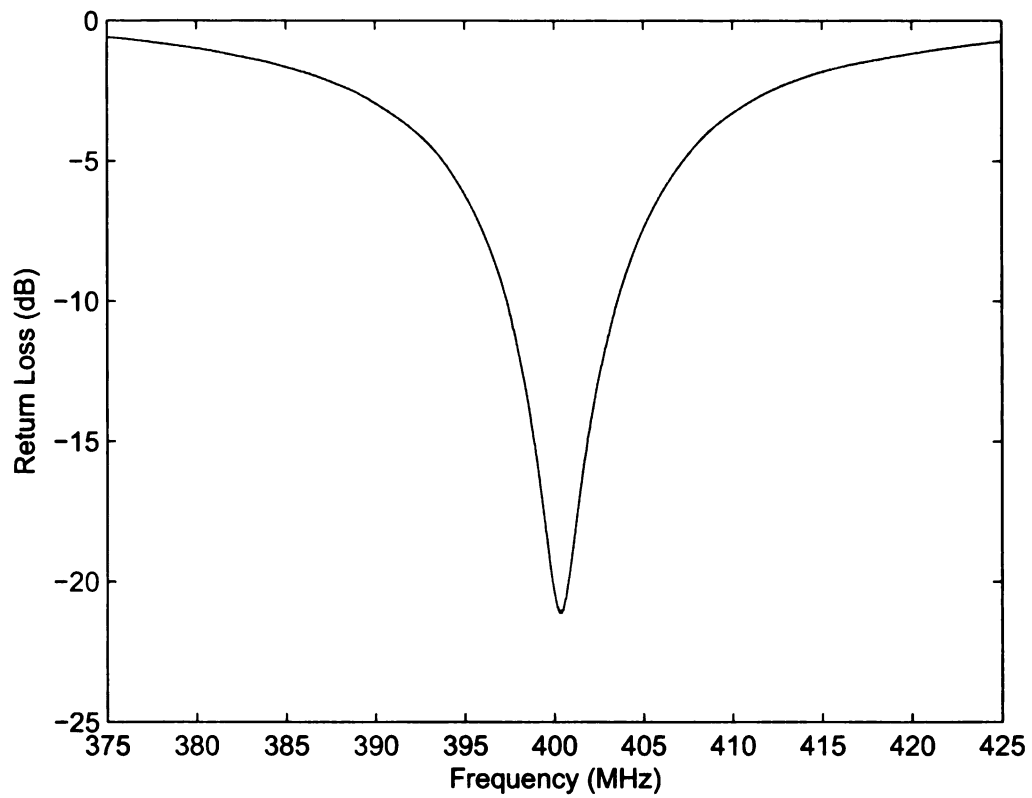


Figure 4.53. Return loss for a state with VSWR of 1.027 at 400 MHz.

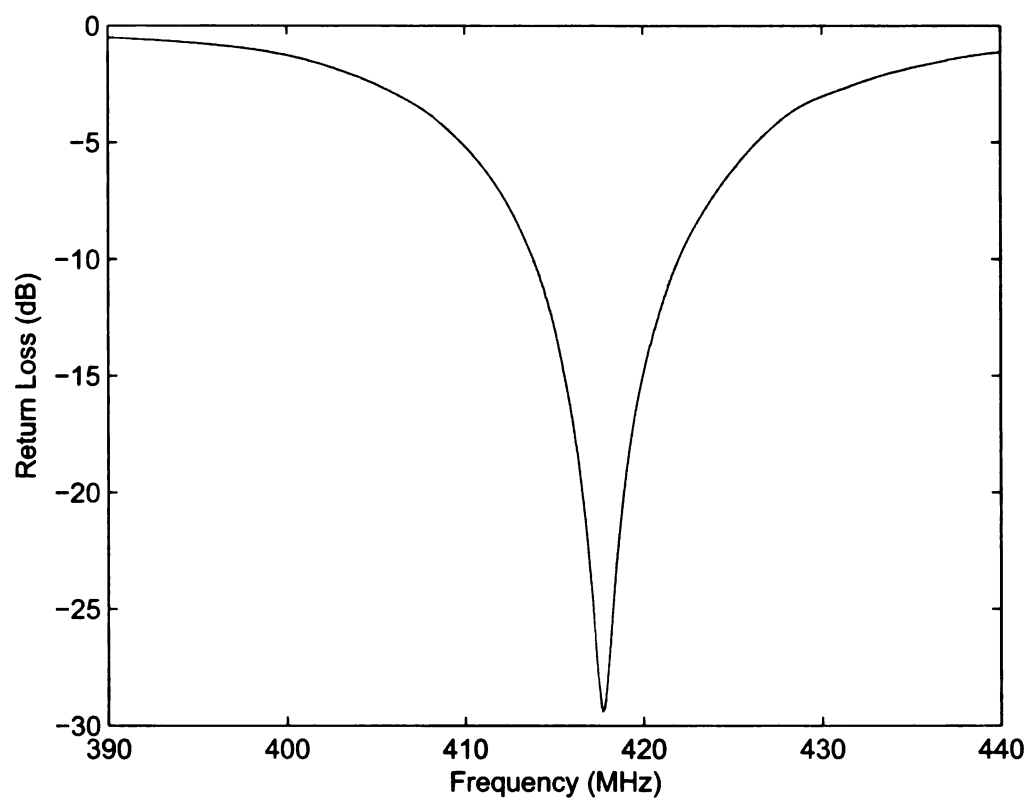


Figure 4.54. Return loss for a state with VSWR of 1.013 at 417 MHz.

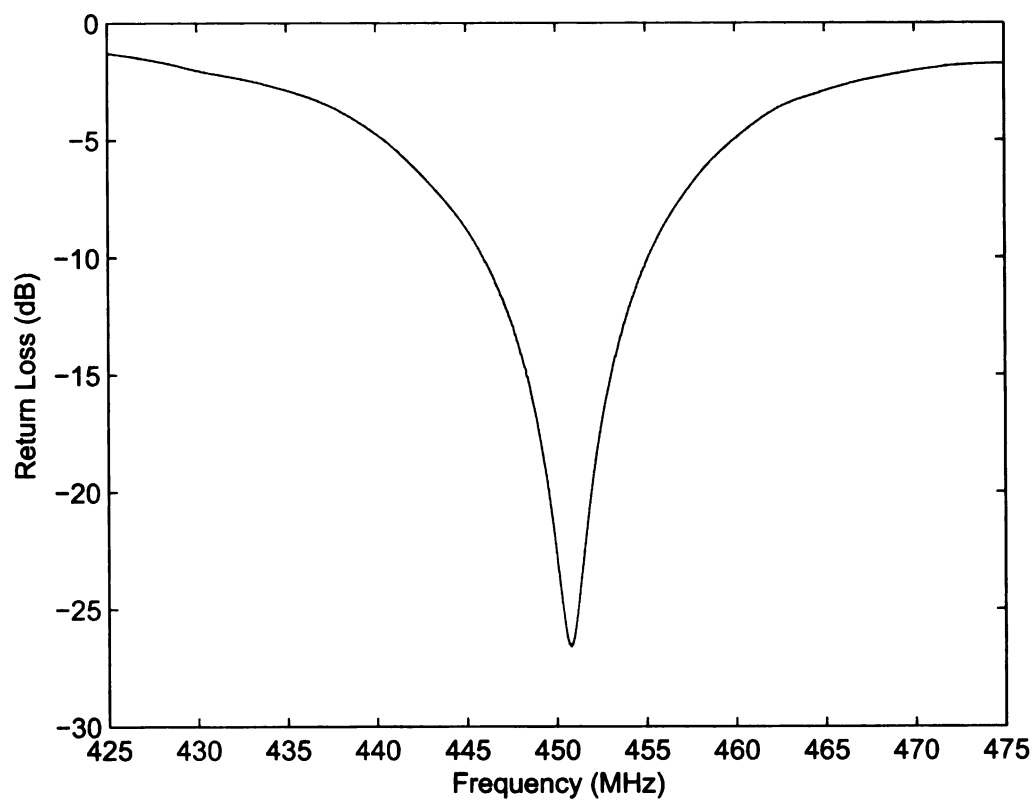


Figure 4.55. Return loss for a state with VSWR of 1.0076 at 450 MHz.

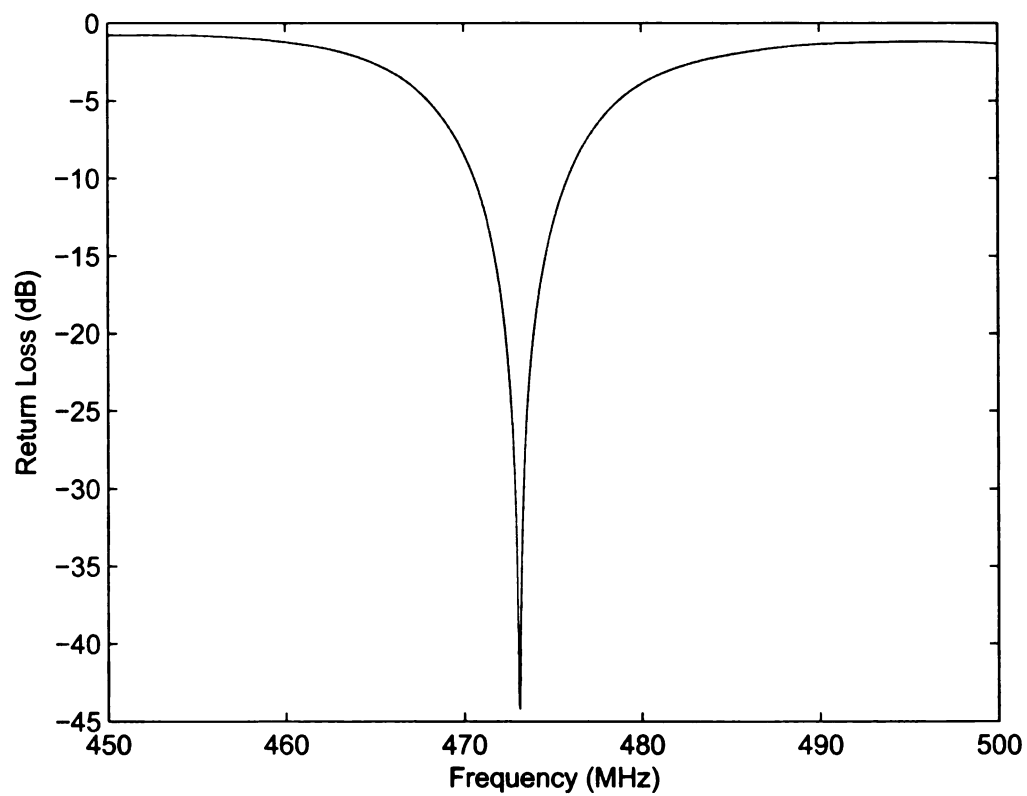


Figure 4.56. Return loss for a state with VSWR of 1.0186 at 473 MHz.

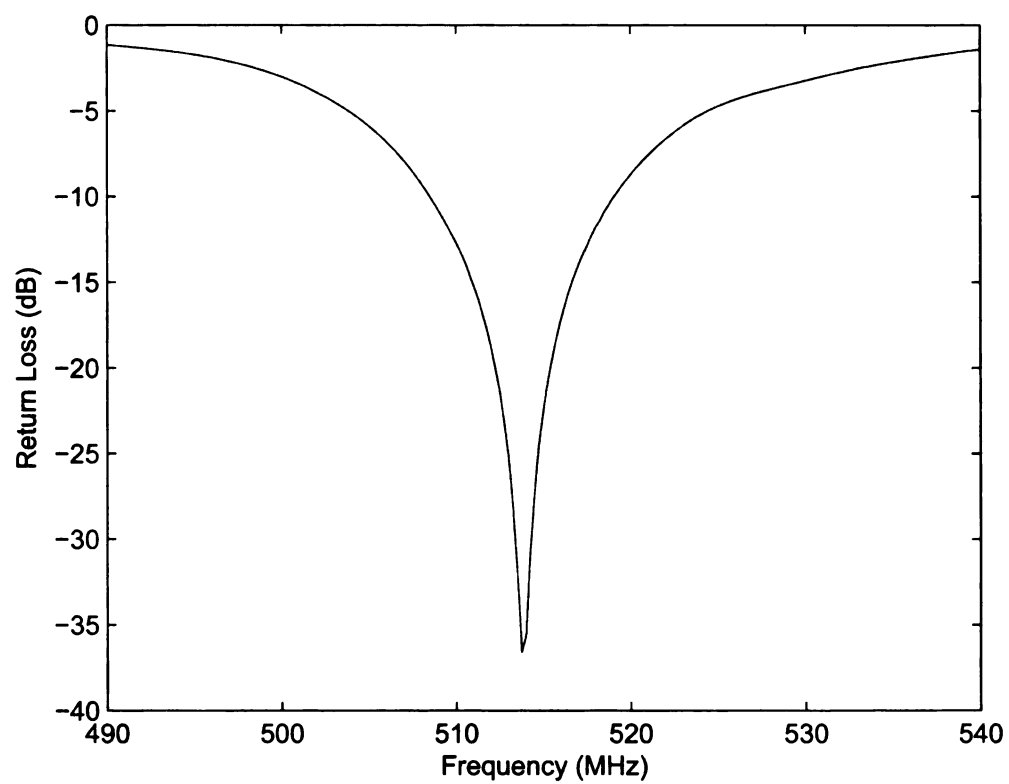


Figure 4.57. Return loss for a state with VSWR of 1.008 at 513 MHz.

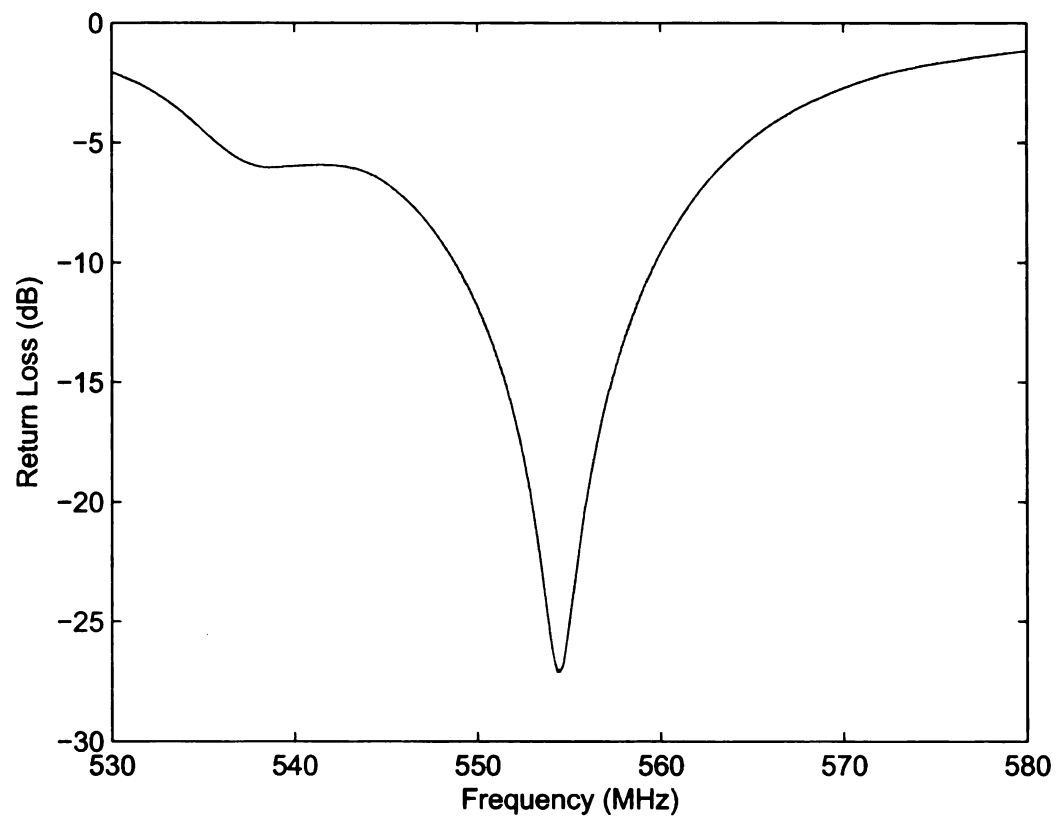


Figure 4.58. Return loss for a state with VSWR of 1.0094 at 555 MHz.

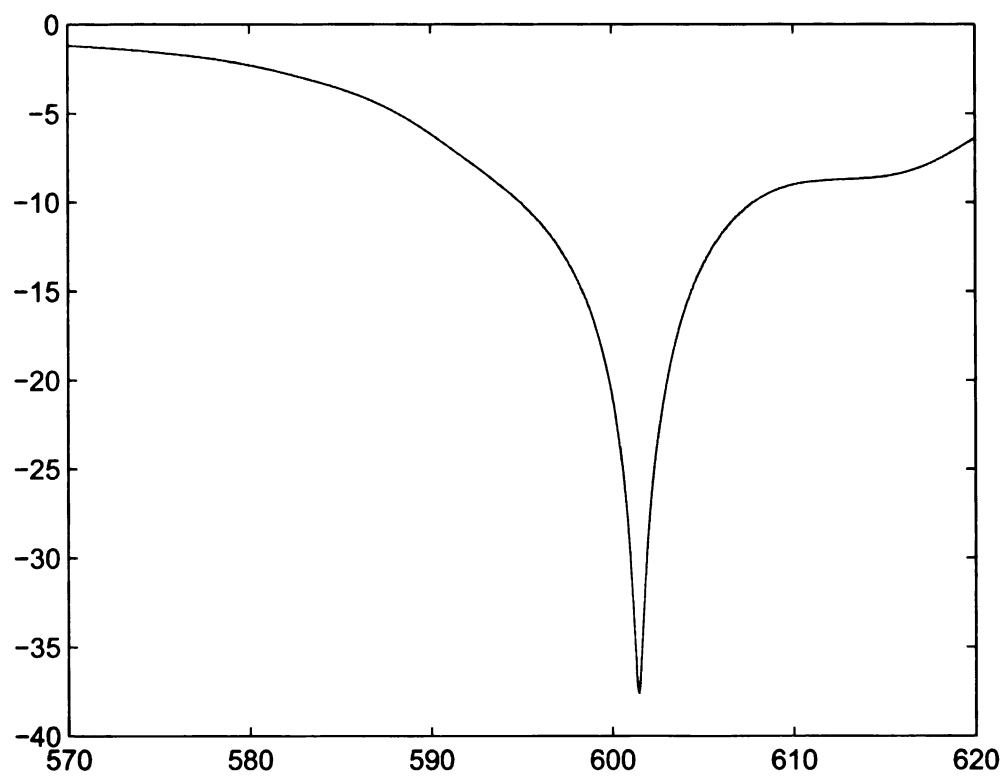


Figure 4.59. Return loss for a state with VSWR of 1.443 at 597 MHz.

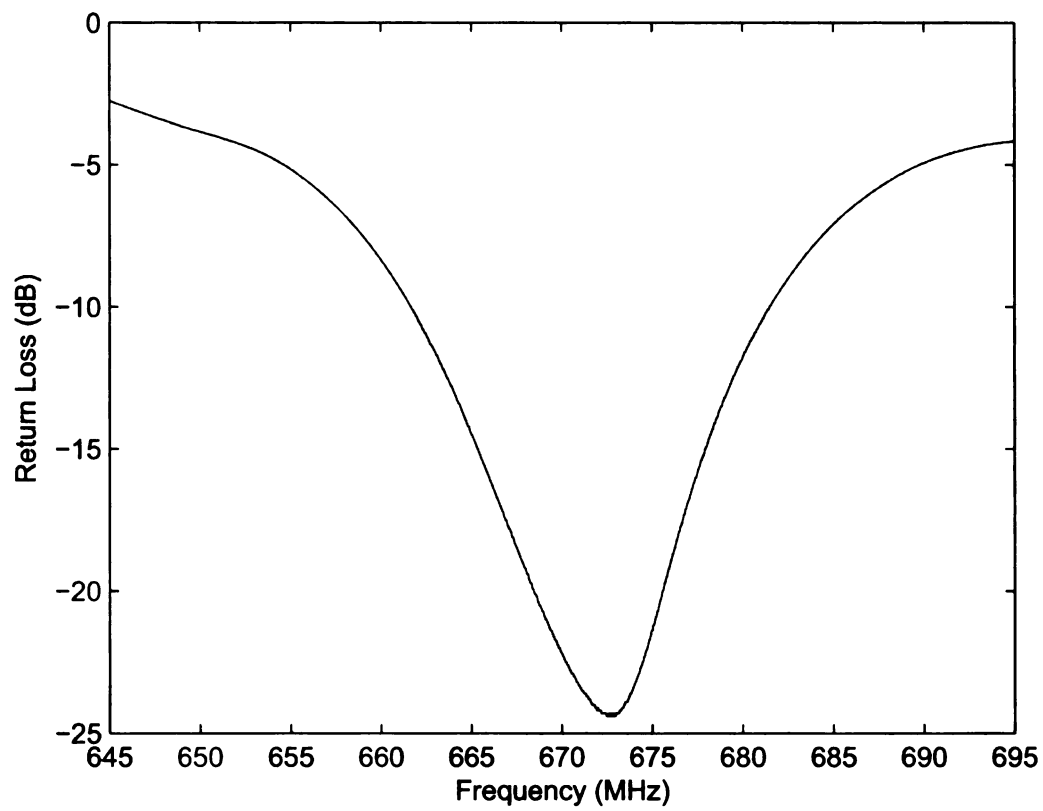


Figure 4.60. Return loss for a state with VSWR of 1.027 at 670 MHz.

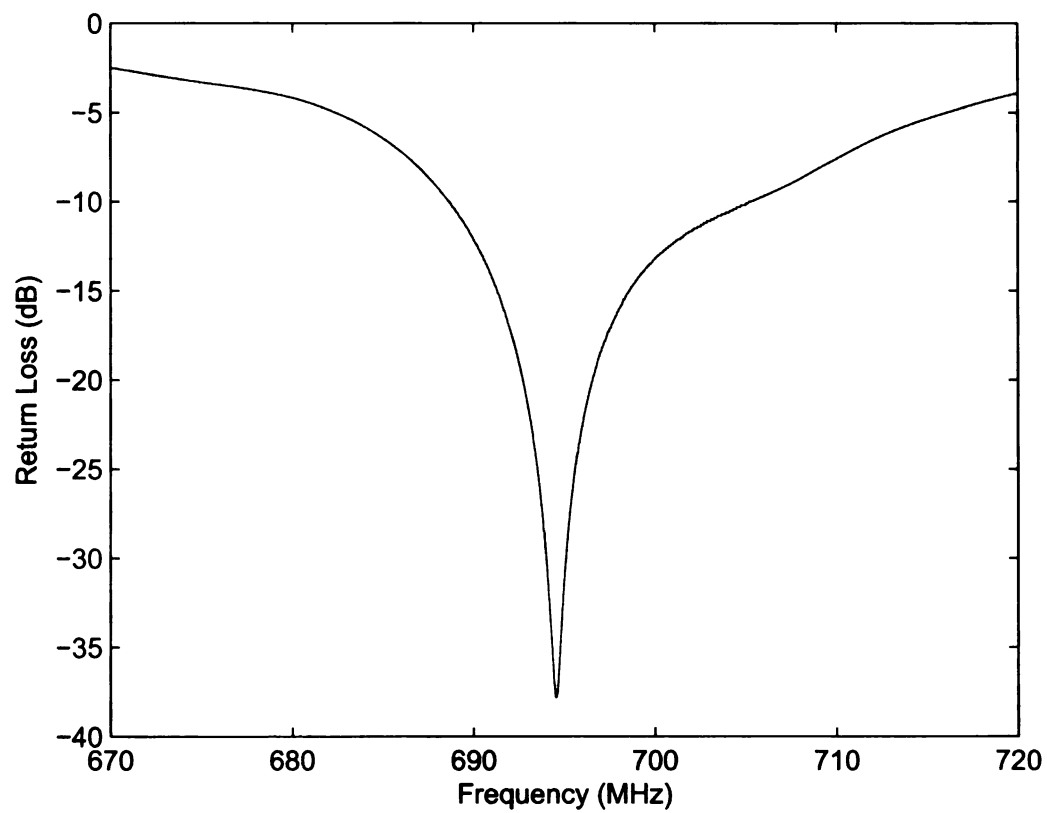


Figure 4.61. Return loss for a state with VSWR of 1.0065 at 695 MHz.

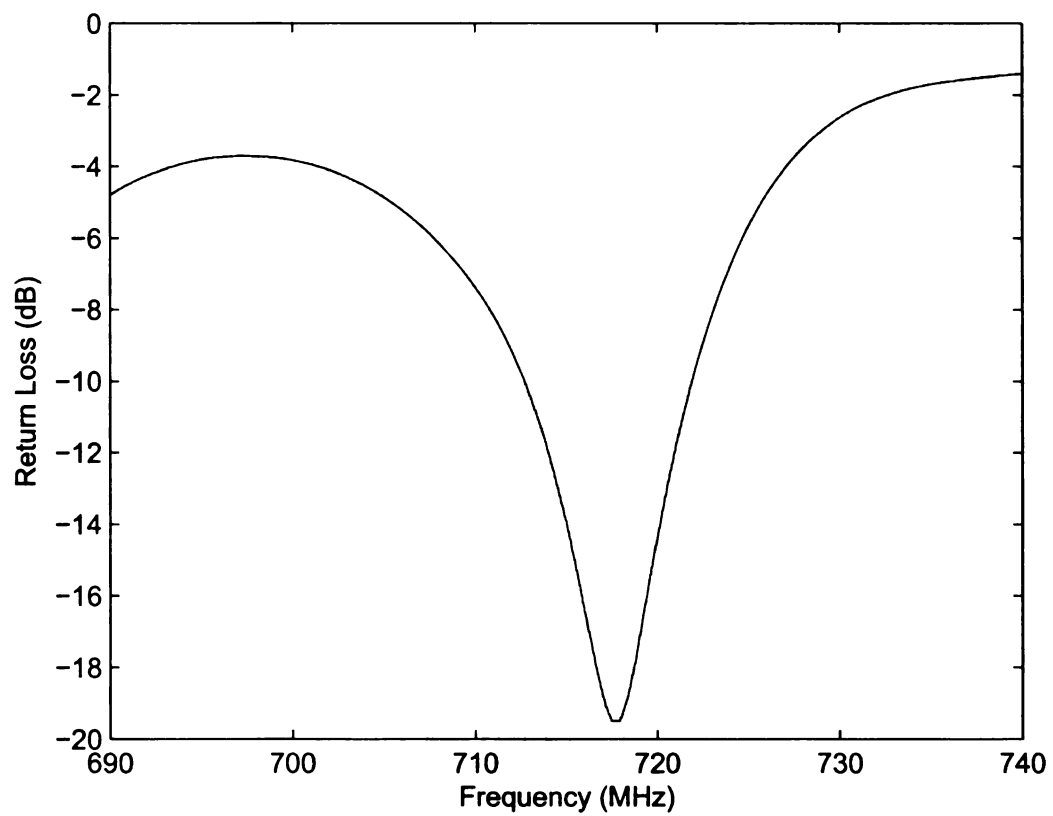


Figure 4.62. Return loss for a state with VSWR of 1.59 at 715 MHz.

Table 4.1. Chromosomes for the best states found in the genetic algorithm searches.

Frequency (MHz)	Chromosome
200	11110011000111000110101101011011
285	01101100100111011100011001000000
330	1111111110111011000001101000101
380	01000000000000000000000001100001
400	10001100000000011000100001110000
417	00001000110010101010011010100101
450	11010010101110010101111101101110
473	11011001010001000100100000010011
513	11101001100000011001011111001101
555	11110110110001111111110011111111
597	00000010000000010000001100000001
670	11111110011111111001110100000100
695	11101111100111000111101110111010
715	11111111010000110111110000001111
840	11111001011011001001110001010110
900	10010001110011100011011101001010

Table 4.2. Bit-to-switch number reference chart.

Bit in Chromosome	Switch Number	Bit in Chromosome	Switch Number
1	32	17	16
2	31	18	15
3	30	19	14
4	29	20	13
5	28	21	12
6	27	22	11
7	26	23	10
8	25	24	9
9	24	25	3
10	23	26	8
11	22	27	7
12	21	28	2
13	20	29	1
14	19	30	6
15	18	31	4
16	17	31	5

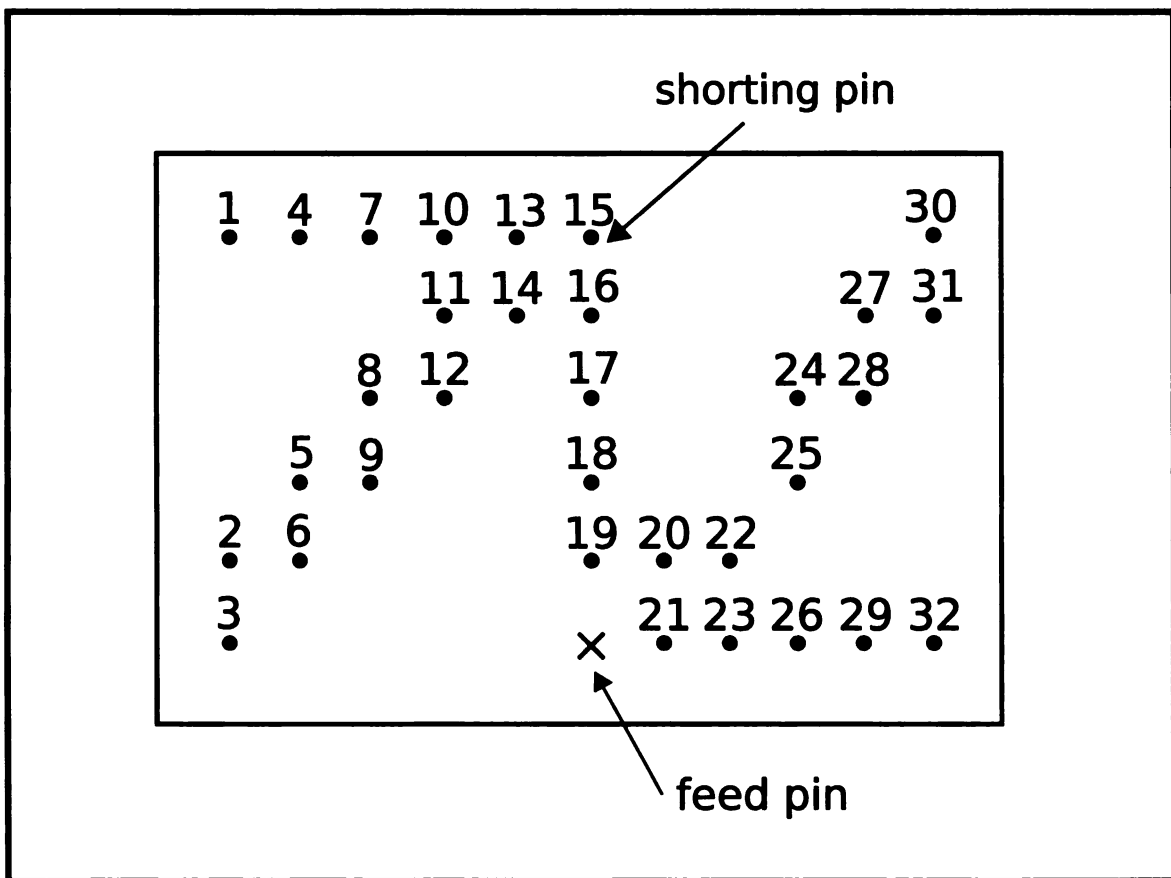


Figure 4.63. Switch numbers on the self-structuring antenna prototype.

Table 4.3. Results of random searches and the genetic algorithm optimizations for the self-structuring patch antenna prototype.

Frequency (MHz)	Random Search VSWR Low	Genetic Algorithm VSWR Low	Measured Resonant Frequency (MHz)	Return Loss (dB)	Bandwidth (%)	Input Impedance (Ω)
200	1.022	1.0088	200.3	-33	3.61	48.5+j1.6
285	3.25	2.588	285	-5.3	-	18.2+j21.6
330	2.81	2.56	330	-7.8	-	24.1+j21.1
380	5.01	7.06	389.1	-19.5	1.9	52.3-j10.7
400	1.036	1.027	400.4	-21.5	1.56	49.2-j8.6
417	1.019	1.013	417.8	-29.9	1.96	49.8-j3
450	1.029	1.0076	450.8	-26.3	2.03	49.1-j5.2
473	1.031	1.0186	473.1	-43.3	1.11	50.6-j3.6
513	1.02	1.008	513.9	-38.6	2.04	49.0-j4.9
555	1.11	1.0094	554.5	-27.6	2	49.0-j4.2
597	1.4	1.624	601.44	-36.3	2.18	50.1+j1.5
630	1.004	-	-	-	-	-
670	1.02	1.027	672.7	-24.1	2.97	51.6+j6.1
695	1.047	1.0065	694.5	-38	2.4	51.1+j0.5
715	1.8	1.59	717.8	-19.4	1.29	50+j10.6
770	2.046	-	-	-	-	-
840	3.529	5.16	840	-3.4	-	60+j100
900	4.968	6.419	900	-4.5	-	99.3+j93.6

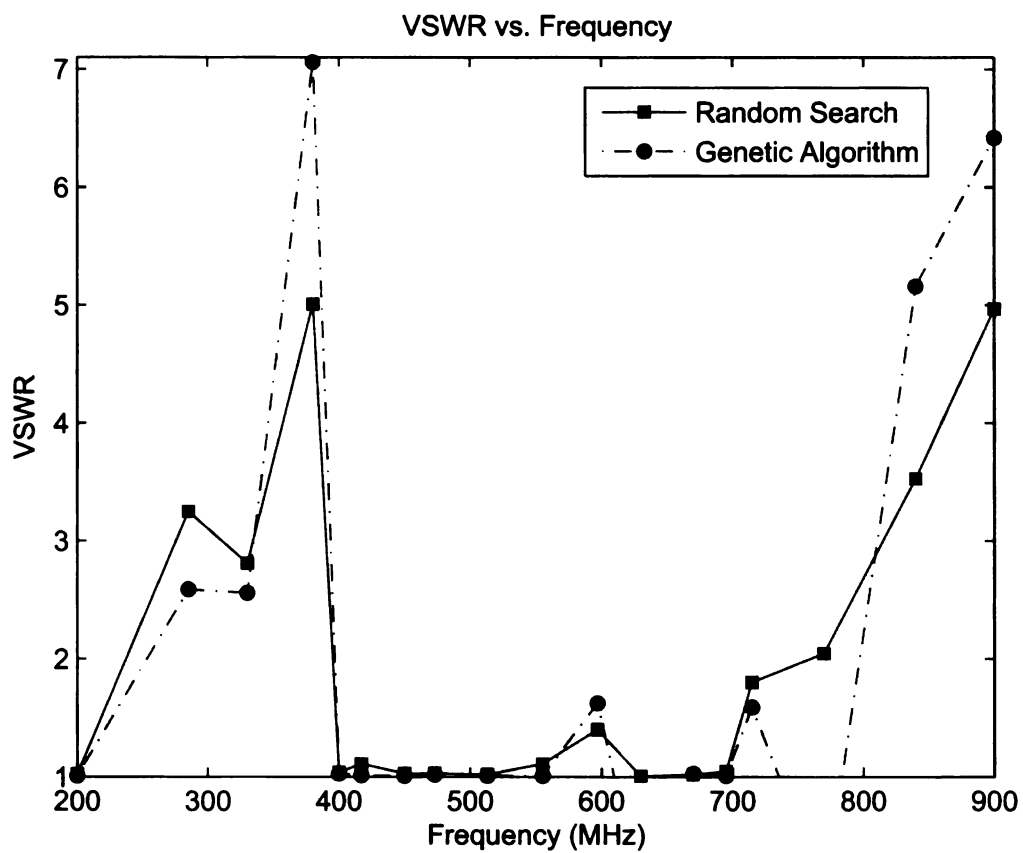


Figure 4.64. Comparison of lowest VSWRs found in the random search and the genetic algorithm optimizations.

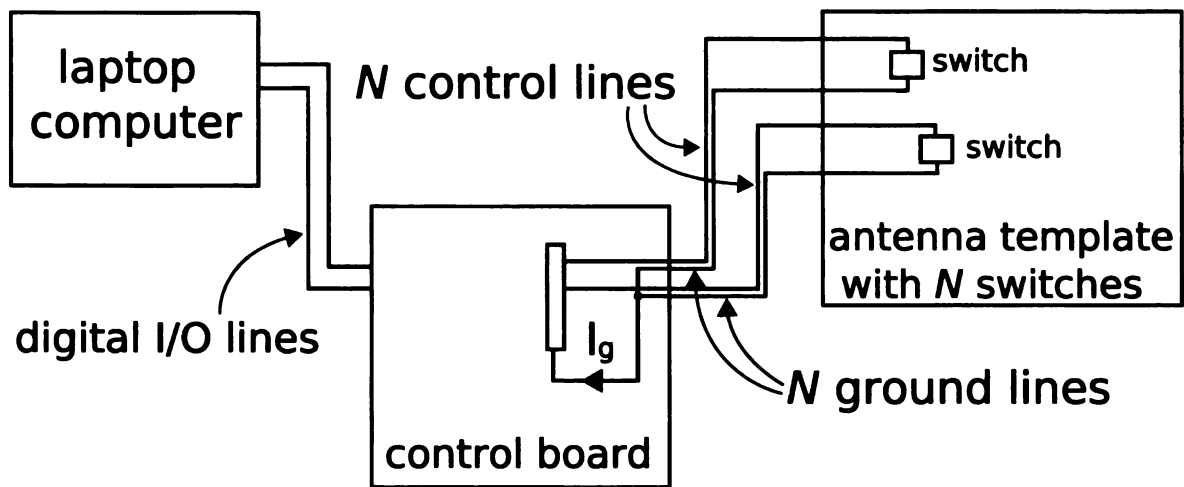


Figure 4.65. Block diagram of experimental setup for electromagnetic compatibility testing.

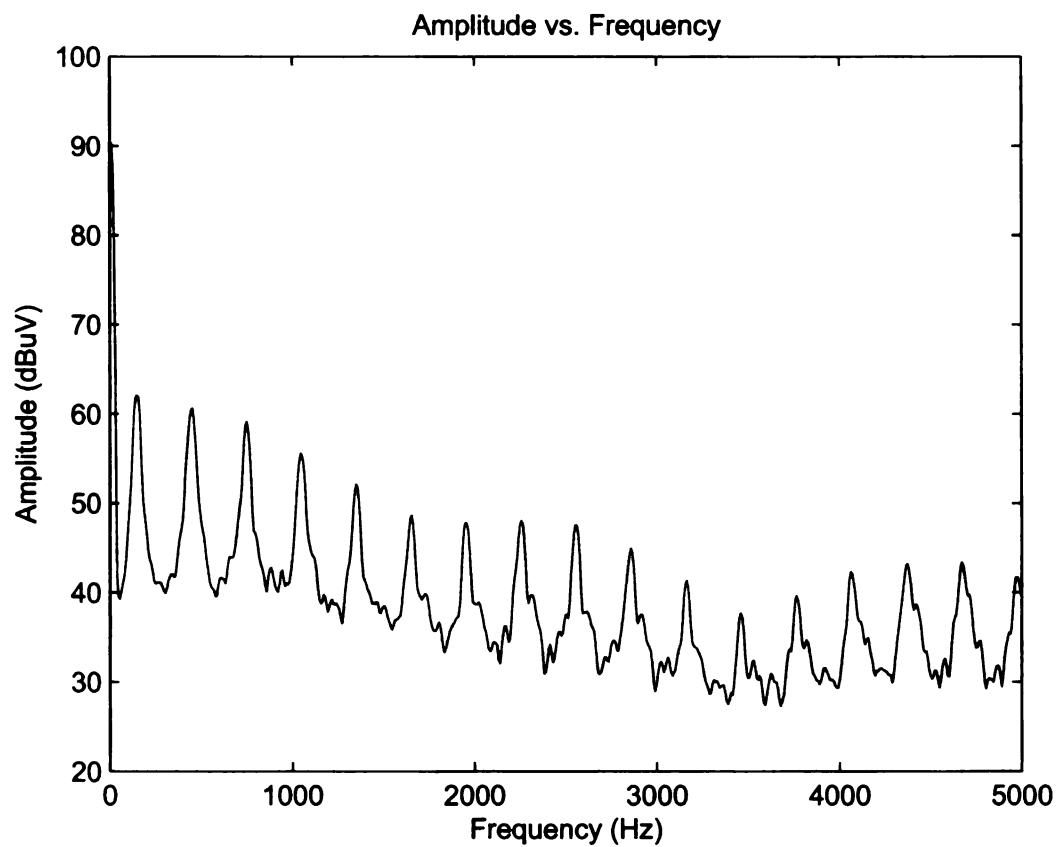


Figure 4.66. Amplitude vs. Frequency of conducted emissions with switching frequency set to 150 Hz.

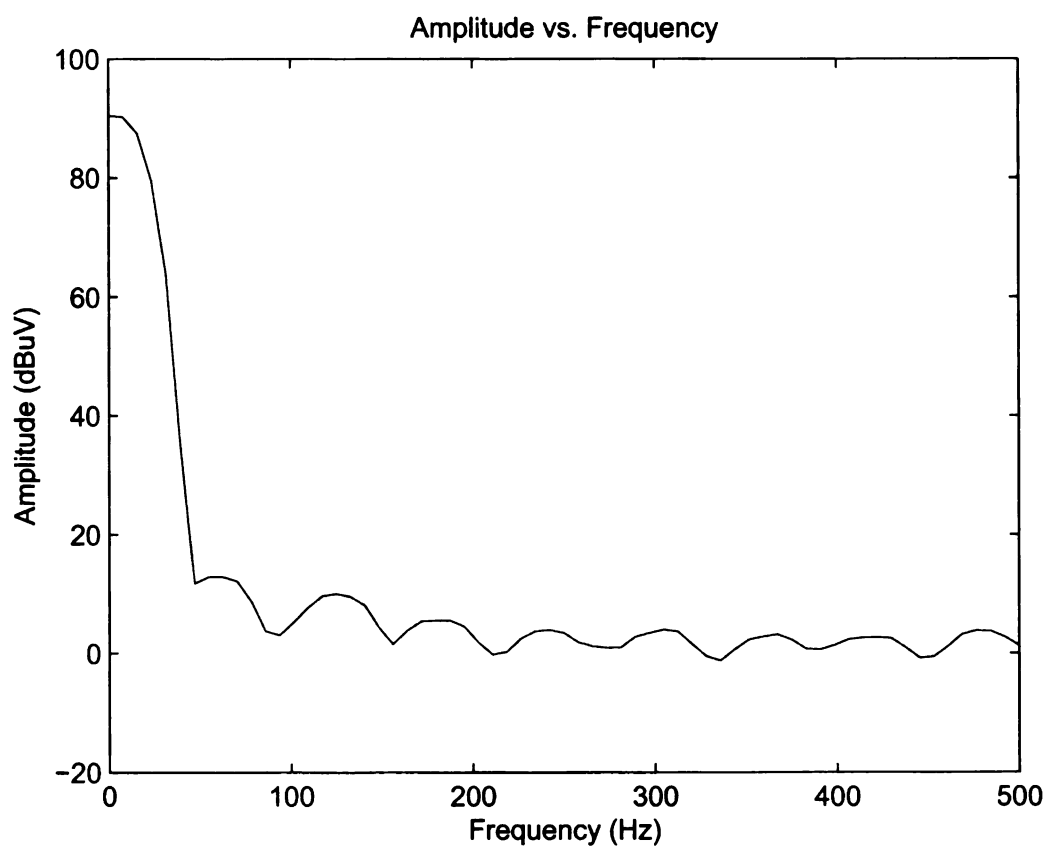


Figure 4.67. Amplitude vs. Frequency of conducted emissions with switches idle.

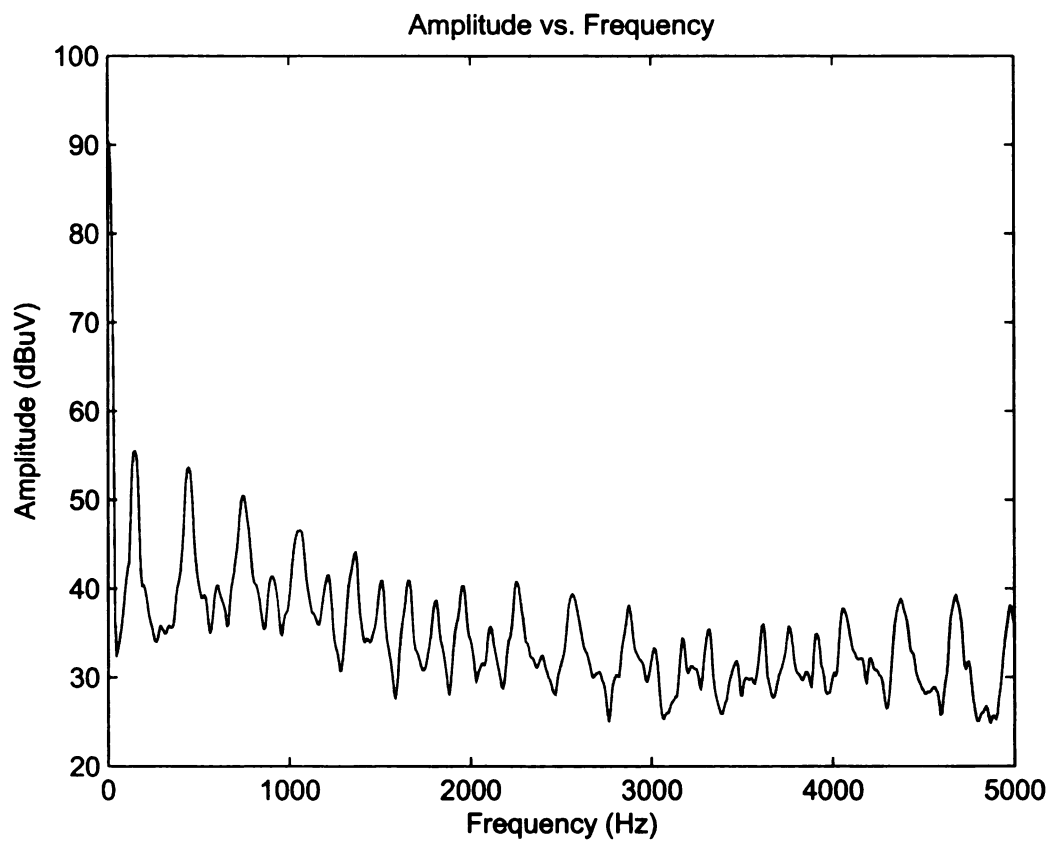


Figure 4.68. Amplitude vs. Frequency of conducted emissions with switching frequency set to 150 Hz and a 455 μ H blocking inductor in series with the ground wire.

CHAPTER 5

CONCLUSIONS

This thesis presents a new type of self-structuring antenna, the self-structuring patch antenna. The background, simulation, and experimental results of the antenna are discussed in Chapters 2, 3, and 4, respectively. Several conclusions can be drawn from the work done in this thesis, as discussed in the following paragraphs.

Many simulations were run for the self-structuring patch antenna, and as such several important conclusions can be made. The self-structuring patch antenna showed frequency tunability for single-frequency operation over a greater than 4:1 frequency band. Some of this frequency band fell below the fundamental resonant frequency of the antenna. When compared to simulations of a traditional microstrip patch antenna, the self-structuring patch antenna showed a better voltage standing wave ratio and return loss while maintaining a nearly identical radiation pattern. While it did show a lower bandwidth under single-frequency operation than the simulated traditional patch antenna, it was still within a similar range as bandwidths found by previous patch antenna researchers.

Simulations of the self-structuring patch antenna also showed that it has the ability to operate at multiple frequencies at once. It has shown capability of operating at up to four distinct frequencies at one time. When these frequencies are moved closer together, the resonances at each frequency combine into one larger resonance, which exhibits a broader bandwidth than one resonance alone. This has potential to be a very useful feature since one of the major drawbacks of a traditional microstrip patch antenna is its narrow bandwidth due to its highly resonant structure.

A prototype of the self-structuring patch antenna was then constructed to verify the results of the simulations. The first experiments that were run on the prototype

were random searches of 75,000 states of the antenna at various frequencies. Since these searches were able to find states with a voltage standing wave ratio (VSWR) of less than 1.1 at the majority of the frequencies searched, one can conclude that many good states exist for the self-structuring patch antenna at the specified frequencies. It then becomes a matter of finding these good states.

The next experiments that were run on the self-structuring antenna prototype were genetic algorithm optimizations at the same frequencies that the random searches were run. In general, the genetic algorithm was able to find states with lower VSWR values than the random searches in far less looks. At frequencies far from the fundamental resonant frequencies of the antenna, the genetic algorithm did not show an improvement over the lowest VSWR value found in the random searches. Once a good state was found using the genetic algorithm, the bandwidth of that state was investigated. Some brief electromagnetic compatibility investigations were also done with the number of switching cycles per second set very high.

Due to time constraints, there are many aspects of the self-structuring patch antenna that were not investigated. This provides many opportunities for future work. To this date, no measurements of the radiation pattern of the self-structuring patch antenna have been made. It would be interesting to set the switches to a known good state at a particular frequency and see if the radiation pattern is similar to that of a traditional patch antenna. Perhaps the most promising area of future work for this self-structuring patch antenna is that of bandwidth enhancement. With equipment capable of optimizing the antenna at multiple frequencies at once, investigations can be done into just how far the bandwidth can be broadened. Another possibility for future work is applying the self-structuring antenna concept to other traditional patch antenna geometries, such as circular patches, cavity-backed patches, and conformal patches.

The lessons learned during the research presented in this thesis can be very useful

to those looking to improve upon the design of this antenna in the future. Many opportunities exist to further this research, and these conclusions can be used as a springboard to better self-structuring patch antenna designs.

APPENDICES

APPENDIX A

VISUAL BASIC CODE: RANDOM SEARCHES OF STATES OF THE SELF-STRUCTURING PATCH ANTENNA

This Visual Basic code was originally written by Raoul Ouedraogo for use with this self-structuring patch antenna and in any future self-structuring antenna research at Michigan State University.

```
Dim StopProcess As Boolean
Dim FilePath As String
Dim OUFilePath As String
Dim Data As String
Dim n As String
Dim Iter As String
Dim Volt_Out() As Double
Dim Vm As String
Dim Ref As String
Dim SWR As String
Dim Vsc As String
```

```
Private Sub cmdDIOSet_Click()
    Set8PinIO txtDIOSet.Text
End Sub
```

```
Private Sub GetData(VoltAvg)
    Dim BinaryCodes As Variant
    Dim Voltages As Variant
    CWA11.AcquireData Voltages, BinaryCodes, 5
    VoltAvg = CWStat1.Mean(Voltages)

    DoEvents
    CWGraph1.PlotY Voltages
End Sub
```

```

Private Sub Set24PinIO(Byte0, Byte1, Byte2)
    CWDIO2.Ports.Item(0).SingleWrite Byte0
    CWDIO2.Ports.Item(1).SingleWrite Byte1
    CWDIO2.Ports.Item(2).SingleWrite Byte2
    StopProcess = True
End Sub

Private Sub Set8PinIO(Byte0)
    CWDIO1.Ports.Item(0).SingleWrite Byte0
End Sub

Private Sub ConfigureCWA11()
    CWA11.Configure
End Sub

Private Sub cmdSetState_Click()
    StopProcess = True
    ' OPEN INPUT FILE
    FilePath = InputBox("Is this the correct path of the file to be read?",
        "Binary File", _"C:\07-08 team\binary1.txt")
    Open FilePath For Input As #1

    'OPEN OUTPUT FILE
    OUFilePath = InputBox(" File to be written to?", "Output SWR File", _
        "C:\07-08 team\Voltage_Output.txt")
    Open OUFilePath For Output As #2

    ' COUNTER
    Iter = 1
    'START LOOP
    Do Until Iter = 75001
        Line Input #1, Data '(vbTab)
        txtByte0.Text = VbCrLf & Data
        Line Input #1, Data
        txtByte1.Text = VbCrLf & Data
        Line Input #1, Data
        txtByte2.Text = VbCrLf & Data
    
```



```

Line Input #1, Data
txtByte3.Text = VbCrLf & Data

Set8PinIO txtByte0.Text
Set24PinIO txtByte1.Text, txtByte2.Text, txtByte3.Text

'WAIT FOR SWITCHES TO SETTLE
For ii = 1 To 9000000
Next ii

'DISPLAY NUMBER OF ITERATIONS
txtCounter.Text = Iter

'READ VOLTAGE
Dim VoltAvg As Variant
Dim i As Integer
ConfigureCWA11
GetData VoltAvg

Vm = 10 ^ (VoltAvg / 0.667)      'calibration equation for Vm
Vsc = 705.2093498               'sample measured short circuit voltage
Ref = Vm / Vsc                  'calculate reflection coefficient
If Ref = 1 Then                 'this loop is to get rid of states that
SWR = 888888                    'make no sense
Else
SWR = (1 + Abs(Ref)) / (1 - Abs(Ref)) 'compute VSWR
End If
If SWR < 1 Then
SWR = 999999
End If
txtShowVolt.Text = Str$(SWR)
'WRITE VOLTAGE TO FILE "C:\07-08 team\Voltage_Output.txt"
Print #2, SWR
'n = n + 1
Iter = Iter + 1
Loop

```

```
'CLOSE FILES
```

```
Close #1
```

```
Close #2
```

```
End Sub
```

```
Private Sub cmdEndProgram_Click()
```

```
    Set8PinIO 0
```

```
    Set24PinIO 0, 0, 0
```

```
End Sub
```

APPENDIX B

VISUAL BASIC CODE: GENETIC ALGORITHM FOR THE SELF-STRUCTURING PATCH ANTENNA

This Visual Basic code was written for the original self-structuring antenna and modified by Raoul Ouedraogo for use with the self-structuring patch antenna and in any future self-structuring antenna research at Michigan State University.

```
Dim NewPop(1000, 64) As Boolean
Dim OldPop(1000, 64) As Boolean
Dim StateToSet(64) As Boolean
Dim BestinPop(64) As Boolean
Dim WorstinPop(64) As Boolean
Dim Plotit(200) As Boolean
Dim Fitness(1000), SWR(1000) As Single
Dim BigFit(200) As Single
Dim GenBest(100) As Single
Dim AvgFitness, MaxFitness, MinFitness, TotalFitness, BestFitness,
WorstFitness As Single
Dim igenno As Integer
Dim BitLength, NGen, IMaxFitness As Integer
Dim ifirst As Integer
Dim ProbCross, ProbMut, PopSize, Xmin, Xmax, X, Bi, kk, ShowSWR
As Single
Dim N0, N1, N2, N3 As String
Dim B0, B1, B2, B3, BinDigit, BestChrome As String
```

```
Private Sub cmdDIOSet_Click()
    Set8PinIO txtDIOSet.Text
End Sub
```

```
Private Sub cmdRunAcquisition_Click()
    Dim VoltAvg As Variant
    Dim i As Integer
    ConfigureCWA11
    GetData VoltAvg
```

End Sub

Private Sub GetData(VoltAvg)

Dim BinaryCodes As Variant

Dim Voltages As Variant

 CWA11.AcquireData Voltages, BinaryCodes, 5

 VoltAvg = CWStat1.Mean(Voltages)

 DoEvents

End Sub

Private Sub Set8PinIO(Byte0)

 CWDIO1.Ports.Item(0).SingleWrite Byte0

End Sub

Private Sub ConfigureCWA11()

 CWA11.Configure

End Sub

Private Sub cmdSetIO24_Click()

 Set24PinIO txtODIO24.Text, txt1DIO24.Text, txt2DIO24.Text

End Sub

Private Sub Set24PinIO(Byte0, Byte1, Byte2)

 CWDIO2.Ports.Item(0).SingleWrite Byte0

 CWDIO2.Ports.Item(1).SingleWrite Byte1

 CWDIO2.Ports.Item(2).SingleWrite Byte2

 StopProcess = True

End Sub

Private Sub cmdRunGa_Click()

 Call RunGA

End Sub

Private Sub RunGA()

 Best_StateFilePath = InputBox(" File to write Best State to?",
 "Best Switch State File", _

 "C:\Documents and Settings\rothwell\Desktop\Best_Sate-Output.txt")

 Open Best_StateFilePath For Output As #1

Dim p As String

```

    BitLength = 32

p = InputBox("Enter population size (<=1000)")
PopSize = CInt(Val(p))
    ProbMut = 1 / PopSize
ProbMut = txtMute.Text
    ProbCross = 0.7
    p = InputBox("Enter number of generations")
    NGen = CInt(Val(p))
    Randomize
Vsc = txtVsc.Text
    Call InitPop

    ifirst = 1
    For igenno = 1 To NGen
        txtGenNo.Text = igenno
        txtGenNo.SetFocus
        Call EvaluateFitness
        Call FitStats
        Call SelectPop
        Call CrossPop
        Call MutatePop
        Print #1, BestChrome
    Next igenno
    For j = 1 To 32
        StateToSet(j) = BestinPop(j)
    Next j
    Call SetState
    Close #1
End Sub

Sub InitPop()
'Initializes the population to random values

    For i = 1 To PopSize
        For j = 1 To BitLength

```

```

        If Rnd() > 0.5 Then
            OldPop(i, j) = True
        Else
            OldPop(i, j) = False
        End If
    Next j
Next i

End Sub
,,,,,,,,,,,,,,,,,,,,,,,,,,,,,,,,,,,,,,,,,,,,,,,,,,,,,,,,,,,,,,,,,,,,,,,,,,,,,

Sub EvaluateFitness()
Dim VoltAvg As Variant

For i = 1 To PopSize

    For j = 1 To 32
        StateToSet(j) = OldPop(i, j)
    Next j

    Call SetState

    'wait while state settles

    For ii = 1 To 1000000
        Next ii
        Vsc = txtVsc.Text

    'read voltage
    ConfigureCWA11
    GetData VoltAvg
    Fitness(i) = 0.5712 - VoltAvg
    Vm = 10 ^ ((VoltAvg - 0.244) / (0.165))
    Ref = Vm / Vsc
    SWR(i) = (1 + Abs(Ref)) / (1 - Abs(Ref))
Next i

```

```

End Sub

Sub FitStats()
Dim sum As Single
Dim i As Integer

'Calculates the statistics of the population fitness

If ifirst = 1 Then
    For k = 1 To BitLength
        BestinPop(k) = OldPop(1, k)
    Next k
    BestFitness = Fitness(1)
    WorstFitness = Fitness(1)
    Fmax = Fitness(1)
    Fmin = Fitness(1)
    ifirst = 0
End If
sum = 0
IMaxFitness = 1
Fmax = BestFitness
Fmin = WorstFitness

For i = 1 To PopSize
    sum = sum + Fitness(i)
    If Fitness(i) > BestFitness Then
        BestChrome = ""
        IMaxFitness = i
        Fmax = Fitness(i)
        ShowSWR = SWR(i)
        BestFitness = Fitness(i)
        For j = 1 To BitLength
            BestinPop(j) = OldPop(i, j)
            If BestinPop(j) Then
                BestChrome = 1 & BestChrome
            Else: BestChrome = 0 & BestChrome
        
```

```

End If
Next j
End If

If Fitness(i) < WorstFitness Then
    Fmin = Fitness(i)
    WorstFitness = Fitness(i)
    For k = 1 To BitLength
        WorstinPop(k) = OldPop(i, k)
    Next k
End If

```

```
Next i
AvgFitness = sum / PopSize
MaxFitness = Fmax
MinFitness = Fmin
TotalFitness = sum
GenBest(igenno) = MaxFitness
txtBest.Text = MaxFitness
txtBest.SetFocus
txtWorst.Text = MinFitness
txtWorst.SetFocus
txtGenAvg.Text = AvgFitness
txtGenAvg.SetFocus
txtBestIndividual.Text = BestChrome
txtXValue.Text = ShowSWR
CWGraph1.PlotY GenBest
```

```
Sub SelectPop()  
Dim NNew, NSelect, Nallocate, i, j, k As Integer
```



```

'Selects the population for the next generation
'First select by expected allocation
NNew = 0
For i = 1 To PopSize
    Nallocate = Int(Fitness(i) / AvgFitness)
    If Nallocate > 4 Then
        For j = 1 To Nallocate
            NNew = NNew + 1
            For k = 1 To BitLength
                NewPop(NNew, k) = OldPop(i, k)
            Next k
        Next j
    End If
Next i

'Now fill the rest randomly
Do While NNew < PopSize
    NSelect = Int(1 + PopSize * Rnd())
    ratio = Fitness(NSelect) / AvgFitness
    n = Int(ratio)
    prob = ratio - n
    test = Rnd()
    If prob > test Then
        NNew = NNew + 1
        For k = 1 To BitLength
            NewPop(NNew, k) = OldPop(NSelect, k)
        Next k
    End If
Loop

'replace last with best result so far
For k = 1 To BitLength
    NewPop(PopSize, k) = BestinPop(k)
Next k

End Sub

```

```

Sub CrossPop()
Dim breed1(64), breed2(64) As Boolean
'performs cross over of breeding population'

ncross = PopSize
For i = 1 To PopSize Step 2

    i1 = Int(1 + Rnd() * ncross)
    For k = 1 To BitLength
        breed1(k) = NewPop(i1, k)
    Next k
    If i1 < ncross Then
        For j = i1 To ncross
            For k = 1 To BitLength
                NewPop(j, k) = NewPop(j + 1, k)
            Next k
        Next j
    End If
    ncross = ncross - 1

    i1 = Int(1 + Rnd() * ncross)
    For k = 1 To BitLength
        breed2(k) = NewPop(i1, k)
    Next k
    If i1 < ncross Then
        For j = i1 To ncross
            For k = 1 To BitLength
                NewPop(j, k) = NewPop(j + 1, k)
            Next k
        Next j
    End If
    ncross = ncross - 1

    test = Rnd()
    If ProbCross > test Then

```

```

    i1 = Int(1 + (BitLength / 2) * Rnd())
    i2 = i1 + 1 + Int(1 + (BitLength / 2) * Rnd())
    For k = 1 To i1
        OldPop(i, k) = breed1(k)
        OldPop(i + 1, k) = breed2(k)
    Next k
    For k = i1 + 1 To i2
        OldPop(i, k) = breed2(k)
        OldPop(i + 1, k) = breed1(k)
    Next k
    For k = i2 + 1 To BitLength
        OldPop(i, k) = breed1(k)
        OldPop(i + 1, k) = breed2(k)
    Next k
Else
    For k = 1 To BitLength
        OldPop(i, k) = breed1(k)
        OldPop(i + 1, k) = breed2(k)
    Next k
End If

Next i

End Sub

Sub MutatePop()

For i = 1 To PopSize
    For k = 1 To BitLength
        test = Rnd()
        If ProbMut > test Then
            OldPop(i, k) = Not (OldPop(i, k))
        End If
    Next k
Next i
End Sub

```

```

Sub SetState()

' create bytes to set switch states
B0 = 0
  For j = 1 To 8
    If StateToSet(j) Then
      B0 = B0 + 2 ^ (j - 1)
    End If
  Next j
B1 = 0
N1 = 1
  For j = 9 To 16
    If StateToSet(j) Then
      B1 = B1 + 2 ^ (N1 - 1)
    End If
    N1 = N1 + 1
  Next j
B2 = 0
N2 = 1
  For j = 17 To 24
    If StateToSet(j) Then
      B2 = B2 + 2 ^ (N2 - 1)
    End If
    N2 = N2 + 1
  Next j
B3 = 0
N3 = 1
  For j = 25 To 32
    If StateToSet(j) Then
      B3 = B3 + 2 ^ (N3 - 1)
    End If
    N3 = N3 + 1
  Next j
'set switch states
txtByte0.Text = B0
txtByte1.Text = B1

```

```
txtByte2.Text = B2  
txtByte3.Text = B3
```

```
Set8PinIO B0  
Set24PinIO B1, B2, B3
```

```
End Sub
```

BIBLIOGRAPHY

BIBLIOGRAPHY

- [1] C.M. Coleman, E.J. Rothwell, J.E. Ross, and L.L. Nagy, "Self-Structuring Antennas," IEEE Antennas and Propagation Magazine, vol. 44, no. 3, pp.11-22, June 2002.
- [2] C.M. Coleman, *Self-Structuring Antennas*, Ph.D. Dissertation, Dept. of Electrical and Computer Engineering, Michigan State University, East Lansing, MI, 2002.
- [3] B.T. Perry, *A Self-Structuring Antenna Prototype*, M.S. Thesis, Dept. of Electrical and Computer Engineering, Michigan State University, East Lansing, MI, 2002.
- [4] C.M. Coleman, E.J. Rothwell, and J.E. Ross, "Self-Structuring Antennas," IEEE AP-S International Symposium and URSI Radio Science Meeting, Salt Lake City, Utah, July 16-21, 2000.
- [5] C. Coleman, B. Perry, E. Rothwell, L. Kempel, J.E. Ross, and L. Nagy, "A Study of Simple Self-Structuring Antenna Templates," IEEE AP-S International Symposium and URSI Radio Science Meeting, San Antonio, Texas, June 16-21, 2002.
- [6] J.E. Ross, E.J. Rothwell, C.M. Coleman, and L.L. Nagy, "Numerical Simulation of Self-Structuring Antennas Based on a Genetic Algorithm Optimization Scheme," IEEE AP-S International Symposium and URSI Radio Science Meeting, Salt Lake City, Utah, July 16-21, 2000.
- [7] C.M. Coleman, E.J. Rothwell, J.E. Ross, and L.L. Nagy, "Application of Two-Level Evolutionary Algorithms to Self-Structuring Antennas," IEEE AP-S International Symposium and URSI Radio Science Meeting, Boston, Massachusetts, July 8-13, 2001.
- [8] B.T. Perry, E.J. Rothwell, L.L. Nagy, and J.E. Ross, "Self-Structuring Antenna Concept for FM-band Automotive Backlight Antenna Design," IEEE AP-S International Symposium and URSI Radio Science Meeting, Washington, D.C., July 5-9, 2005.
- [9] J.E. Ross, E.J. Rothwell, and S. Preschutti, "A Complimentary Self-Structuring Antenna for Use in a Vehicle Environment," IEEE AP-S International Symposium and URSI Radio Science Meeting, Monterey, California, June 21-25, 2004.

- [10] B.T. Perry, E.J. Rothwell, and L.L. Nagy, "Analysis of Switch Failures in a Self-Structuring Antenna System," *IEEE Antennas and Wireless Propagation Letters*, vol. 4, pp. 68-70, 2005.
- [11] B. Perry, C. Coleman, E. Rothwell, L. Kempel, J. Ross, and L. Nagy, "Effect of Switch Failure on the Performance of a Self-Structuring Antenna," *IEEE AP-S International Symposium and URSI Radio Science Meeting*, San Antonio, TX, June 16-21, 2002.
- [12] B.T. Perry, C.M. Coleman, B.F. Basch, E.J. Rothwell, J.E. Ross, and L.L. Nagy, "Self-Structuring Antenna for Television Reception," *IEEE AP-S International Symposium and URSI Radio Science Meeting*, Boston, Massachusetts, July 8-13, 2001.
- [13] J. Jessberger, *Investigation of the Near Field Properties of the Self-Structuring Antenna*, Thesis, Dept. of Electrical and Computer Engineering, Michigan State University, East Lansing, MI, 2005.
- [14] R.A. Fenner, *Bandwidth Extension of a Body Worn Antenna Vest*, M.S. Thesis, Dept. of Electrical and Computer Engineering, Michigan State University, East Lansing, MI, 2007.
- [15] J. Watkins, "Circular Resonant Structures in Microstrip," *Electronics Letters*, vol. 5, no. 21, pp. 524-525, 1969.
- [16] J. Howell, "Microstrip Antennas," *IEEE Group on Antennas and Propagation International Symposium*, Williamsburg, Virginia, 1972.
- [17] J. Howell, "Microstrip Antennas," *IEEE Transactions on Antennas and Propagation*, vol. 23, no. 1, pp. 90-93, 1975.
- [18] Y.T. Lo, D. Solomon, and W.F. Richards, "Theory and Experiment on Microstrip Antennas," *IEEE Transactions on Antennas and Propagation*, vol. 27, no. 2, pp. 137-145, 1979.
- [19] D.H. Schaubert, F.G. Farrar, A. Sindoris, and S. Hayes, "Microstrip Antennas with Frequency Agility and Polarization Diversity," *IEEE Transactions on Antennas and Propagation*, vol. AP-29, no. 1, pp. 118-123, January 1981.
- [20] S.S. Zhong and Y.T. Lo, "Single-Element Rectangular Microstrip Antenna for Dual-Frequency Operation," *Electronics Letters*, vol. 19, no. 8, pp. 298-300, April 1983.

- [21] B. Wang and Y.T. Lo, "Microstrip Antennas for Dual-Frequency Operation," IEEE Transactions on Antennas and Propagation, vol. 32, no. 9, pp. 938-943, September 1984.
- [22] G. Lan and D.L. Sengupta, "Frequency Agile Circular Microstrip Antennas," International Microwave Symposium Digest, vol. 85, no. 1, pp. 693-695, June 1985.
- [23] R. Waterhouse, "Small Microstrip Patch Antenna," Electronics Letters, vol. 31, no. 8, pp. 604-605, 13 April 1995.
- [24] F. Zavosh and J. Aberle, "Improving the Performance of Microstrip-Patch Antennas," IEEE Antennas and Propagation Magazine, vol. 38, no. 4, pp. 7-12, August 1996.
- [25] R.B. Waterhouse, S.D. Targonski, and D.M. Kokotoff, "Design and Performance of Small Printed Antennas," IEEE Transactions on Antennas and Propagation, vol. AP-46, pp. 1629-1633, 1998.
- [26] T. Chakravarty and A. De, "Design of Tunable Modes and Dual-Band Circular Patch Antenna Using Shorting Posts," IEE Proceedings on Microwaves, Antennas and Propagation, vol. 146, no. 3, pp. 224-228, June 1999.
- [27] H.K. Kan and R.B. Waterhouse, "A Small Printed Antenna for Wireless Communication Handset Terminals," Proceedings of the Asia-Pacific Microwave Conference, 2000, pp. 723-726, 3-6 December 2000.
- [28] J. Zhao and S. Raman, "Design of 'Chip-Scale' Patch Antennas for 5-6 GHz Wireless Microsystems," IEEE AP-S International Symposium and URSI Radio Science Meeting, Boston, Massachusetts, July 8-13, 2001.
- [29] A.K. Shackelford, S. Leong, and K. Lee, "Simulation of a Probe-Fed Notched Patch Antenna with a Shorting Post," IEEE AP-S International Symposium and URSI Radio Science Meeting, Boston, Massachusetts, July 8-13, 2001.
- [30] S. Fang, J. Zheng, and X. Luan, "A Novel Multi Arc Slot Antenna for WLAN Applications," IEEE International Workshop on Antenna Technology: Small Antennas and Novel Metamaterials, pp. 209-212, 7-9 March 2005.
- [31] H.K. Kan, R.B. Waterhouse, A.Y.J. Lee, and D. Pavlickovski, "Variations of the Shorted Patch Antenna," IEEE AP-S International Symposium and URSI Radio Science Meeting, Washington, D.C., July 5-9, 2005.

- [32] D. Bonefacic, J. Bartolic, and M. Germ, "Shorted Patch Antenna with PIN Diode Operating Band Switching," Proceedings of the 36th European Microwave Conference, 2006, pp. 862-865, 10-15 September 2006.
- [33] FEKO, Suite 5.0, EM Software and Systems-S.A. Ltd., Stellenbosch, South Africa.
- [34] W.L. Stutzman and G.A. Thiele, *Antenna Theory and Design*, Second Edition, John Wiley and Sons, Hoboken, New Jersey, 1998.
- [35] J.D. Kraus and R.J. Marhefka, *Antennas: For All Applications*, Third Edition, McGraw Hill, New York, New York, 2002.

MICHIGAN STATE UNIVERSITY LIBRARIES



3 1293 02956 8296